Modelling of muscular force induced by non-isometric contraction

by

Natalia Kosterina

May 2012
Technical Reports from
Royal Institute of Technology
Department of Mechanics
SE-100 44 Stockholm, Sweden

Typeset in $\mathcal{AMS}$-LaTeX

TRITA-MEK Technical report 2012:03
ISSN 0348-467X
ISRN KTH/MEK/TR–12/03–SE
ISBN 978-91-7501-339-8

Akademisk avhandling som med tillstånd av Kungliga Tekniska högskolan i Stockholm framlägges till offentlig granskning för avläggande av teknologie doktorsexamen torsdagen den 31 maj 2012 kl 10.00 i E2, Kungliga Tekniska högskolan, Lindstedtsvägen 3, entréplan, Stockholm.

Tryck: Universitetsservice US–AB, Stockholm 2012

Modelling of muscular force induced by non-isometric contraction

Natalia Kosterina
Department of Mechanics, Royal Institute of Technology
SE-100 44 Stockholm, Sweden

Abstract

The main objective of the study was to investigate and simulate skeletal muscle force production during and after isometric contractions, active muscle lengthening and active muscle shortening. The motivation behind this work was to improve the dominant model of muscle force generation based on the theories of Hill from 1938. Effects of residual force enhancement and force depression were observed after concentric and eccentric contractions, and also during stretch-shortening cycles. It was shown that this force modification is not related to lengthening/shortening velocity, but instead the steady-state force after non-isometric contractions can be well described by an initial isometric force to which a modification is added. The modification is evaluated from the mechanical work performed by and on the muscle during length variations. The time constants calculated for isometric force redevelopment appeared to be in certain relations with those for initial isometric force development, an observation which extended our basis for muscle modelling.

A macroscopic muscular model consisting of a contractile element, and parallel and series elastic elements was supplemented with a history component and adopted for mouse soleus muscle experiments. The parameters from the experiment analysis, particularly the force modification after non-isometric contractions and the time constants, were reproduced by the simulations. In a step towards a general implementation, the history modification was introduced in the muscluloskeletal model of OpenSim software, which was then used for simulations of full body movements.

Keywords: Skeletal muscle; Muscular force; Concentric contractions; Eccentric contractions; History effect; Force modification; Muscle model; Musculoskeletal model

Preface

This thesis studies skeletal muscle force production during and after non-isometric contractions and implements a consideration of the effects in two muscle models. In the first part an introduction to the field, a short description of the experimental part and modelling are presented. The second part consists of the following papers:

Paper 1. KOSTERINA N., WESTERBLAD H., LÄNNERGREN J. AND ERIKSSON A., 2008
"Muscular force production after concentric contraction", Journal of Biomechanics 41, 2422–2429

Paper 2. KOSTERINA N., WESTERBLAD H. AND ERIKSSON A., 2009
"Mechanical work as predictor of force enhancement and force depression", Journal of Biomechanics 42, 1628–1634

Paper 3. YAMADA, T., PLACE, N., KOSTERINA, N., ÖSTBERG, T., ZHANG, S.-J., GRUNDTMAN, C., ERLANDSSON-HARRIS, H., LUNDBERG, I.E., GLENMARK, B., BRUTON, J.D. AND WESTERBLAD, H., 2009
"Impaired Myofibrillar Function in the Soleus Muscle of Mice With Collagen-Induced Arthritis", Arthritis & Rheumatism 60(11), 3280–3289

Paper 4. KOSTERINA N., WESTERBLAD H. AND ERIKSSON A., 2011
"History effect and timing of force production introduced in a skeletal muscle model", Biomechanics and Modeling in Mechanobiology, Accepted 8 December 2011, DOI: 10.1007/s10237-011-0364-5

Paper 5. KOSTERINA N., WANG R., ERIKSSON A. AND GUTIERREZ-FAREWIK E.M., 2012
"Force enhancement and force depression in a modified muscle model used for muscle activation prediction", Journal of Biomechanics, Submitted April 2012

Division of work between authors
The research project was initiated by Anders Eriksson (AE) who also acted as supervisor and project leader for the VR (Swedish Research Counsil) funding of the work. AE, Håkan Westerblad (HW) and Natalia Kosterina (NK) have continuously discussed the progress of the project during the course of the work. Ruoli Wang (RW) and Elena M. Gutierrez-Farewik (EGF) made the concluding project feasible.

Paper 1 and Paper 2
The experimental paradigm was developed by AE, NK and HW. The experiments were performed by NK and AE under supervision of HW, with a technical support from Jan Lännergren and Shi-Jin Zhang at Karolinska Institutet. The analysis of the results was done by NK with feedback from AE and HW. The papers were written by NK with inputs from AE and HW.

Paper 3
The study was initiated at Karolinska Institutet and involved 11 authors. The major role of NK was in experimental setup and muscular force data acquisition, NK participated in data analysis. Takashi Yamada (TY), the corresponding author, and HW made the largest impact in the project. The paper was written by TY and then discussed, revised and approved by all authors.

Paper 4
The data analysis and code development were done by NK with feedback from AE and HW. The experimental results were taken from the experiments performed for Papers 1 and 2. The paper was written by NK with inputs from AE and HW.

Paper 5
The experimental paradigm was developed by NK and RW. Data were collected by NK, RW and EGF. The code was developed by NK, the simulations were done by NK with help from RW. The paper was written by NK with inputs from RW, AE and EGF.

Contents

Part I

CHAPTER 1

Introduction

The importance of skeletal muscles cannot be overestimated. The basic muscle role is creating force after neural stimulation which in turn causes movements through muscle contraction. All creatures locomote owing to muscles' ability, and humans would be weak or feeble without properly functioning muscles. An accurate description of muscle function makes it possible to reproduce various muscle contractions and simulate dynamic movements of a whole body represented as a musculoskeletal system.

The first description of a contracting and expanding organ providing movement belongs to Aristotle (384-322 B.C., De Motu Animalium). Galen (129-201 A.D., De Tremore) characterised muscle as a true organ and can therefore be considered as founder of the science of muscles, or myology. Vesalius (1543, De Numano Corporis Fabrica) described muscle components and discovered that muscle implicates the contractile power. Swammerdam (1663, c.f. Needham (1971)) demonstrated consistency of muscular volume with an elementary experiment. Croone (1664, De Ratione Motus Musculorum) first found a cause of muscle contraction, which is a neural signal. In the past century, possibilities to perform advanced experiments led to revolutionary discoveries; some of them will be discussed below in detail. New techniques of the last three decades allow measurements at the molecular level and are used regularly by many groups (Nigg and Herzog 1999). However, there are some unexplained phenomena, providing a basis for future studies. In particular, reasonable descriptions for use in numerical modelling of a whole body or body parts are needed.

1.1. Anatomy and physiology of skeletal muscle

Muscle is a highly organized and structured organ. Each muscle component is associated with a specific function. There are three muscle types: skeletal, cardiac, and smooth, or non-striated. They have significant differences in structure and functioning. This thesis deals with skeletal muscles which are controlled voluntarily but not by the autonomic nervous system. Skeletal muscle is attached by tendons to bones at the origin and insertion points. Each organ is made up of skeletal muscle tissue, connective tissue, nerve tissue, and blood or vascular tissue. The entire muscle is covered by a connective tissue sheath called the epimysium (Fig. 1.1a). Muscle is divided into compartments, fascicles, surrounded by the perimysium. These bundles consist of a number of cells called muscle fibres (Nigg and Herzog 1999; Herzog 2000; Hamill and Knutzen 2008).

The connective tissue covering muscle fibres, i.e., endomysium, protects the delicate cells and provides pathways for the passage of blood vessels and nerves. Muscle

fibre consists of myofibrils arranged in a parallel way, making skeletal muscle striated. Myofibrils are made of repetitive contractile units called sarcomeres (Fig. 1.1b).

Sarcomeres are connected in series, separated by the Z-band and composed of three filament systems playing a major role in muscle contraction. The thick filaments are located in the middle of each sarcomere, and are composed of myosin protein connected to Z-disc by titin to give stability and structure to the sarcomere. A globular heads or myosin heads are located along the thick filaments. The thin filaments consist of actin proteins, which surround each myosin molecule by six parallel entities at both ends.

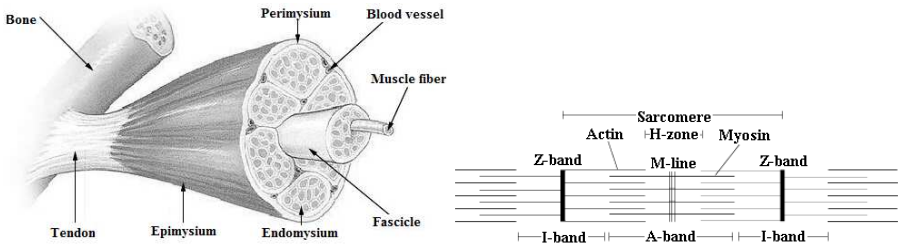

(a) (b)

FIGURE 1.1. Schematic illustration of (a) skeletal muscle and (b) sarcomere structures. Reproduced from Hamill and Knutzen (2008), the textnotes modified.

Sliding filament theory

A theory explaining muscle force production was suggested independently by Huxley and Niedergerke (1954) and Huxley and Hanson (1954). Later Huxley (1957) developed the cross-bridge theory, which has became a basic concept for muscular force production and has been essentially maintained since. The idea lies in the sliding of thin and thick filaments along one another. The myosin heads interact with the actin filaments using ATP (Adenosine triphosphate) and bend to pull the actin, thus shortening the sarcomeres while the filament lengths do not change (Nigg and Herzog 1999). The chemical bonds formed between actin and myosin during the contraction are called cross-bridges.

A lengthened sarcomere is able to form a limited number of cross-bridges in an active state, while a shortened sarcomere has interference of thin filaments as they start to overlap. As a result, muscle fibres produce forces dependent on sarcomere lengths (Gordon et al. 1966; Hamill and Knutzen 2008). A muscle length giving maximum tetanic isometric force is called the optimal muscle length. It is essential to consider the maximum force, the optimal length, and the range of muscle lengths when describing the contractile properties of the muscle. These parameters are shown on the length-tension curves (Fig. 1.2). Each curve actually represents the results of many experiments plotted on the same graph (Lieber and Fridén 2000).

Pennation angle

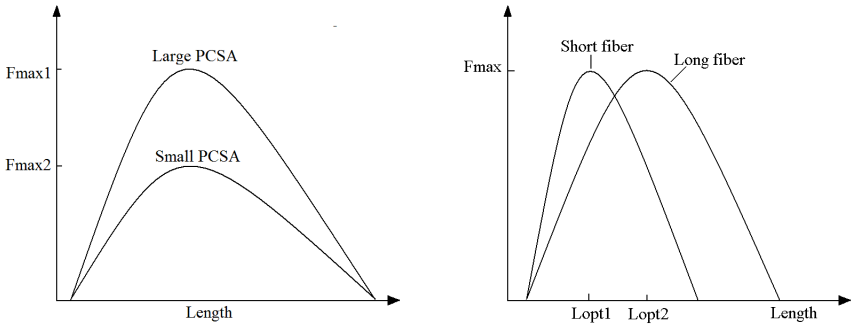

(a) (b)

FIGURE 1.2. Schematic illustration of force-length relations of skeletal muscles with identical pennation angle and (a) fibre length or (b) PCSA. Muscles with a large PCSA produce higher force. Longer muscles have a wider range of possible lengths. Re-drawn from Lieber and Fridén (2000).

As was described above, force production is a result of protein-filament interaction occurring in sarcomeres, but it also depends on the fibre arrangement within the muscle, Fig. 1.3. A fusiform muscle contains fibres lying essentially parallel to the line connecting distal and proximal tendons. These muscles are more flexible than pennate ones, for which fibres run at a certain (pennation) angle to the line of action, making them suitable for stabilization and force production (Nigg and Herzog 1999; Hamill and Knutzen 2008).

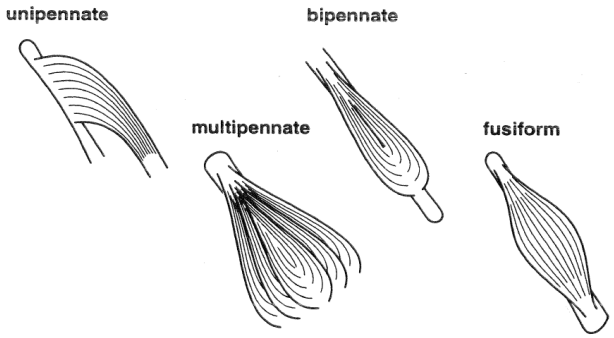

FIGURE 1.3. Classification of muscles depending on the fibres arrangement within a muscle. Reproduced from Nigg and Herzog (1999).

Cross sectional area and fibre length

The contractile properties of a muscle are also dependent on optimal fibre length and a representative physiological cross sectional area ('PCSA'). Muscles with a larger

PCSA promote larger force production (Nigg and Herzog 1999; Lieber and Fridén 2000), Fig. 1.2a. Practically, PCSA can be obtained as the ratio between the muscle volume and the fibre length:

$$PCSA = m \cdot \cos\alpha / (\rho \cdot l_f) \tag{1.1}$$

where m is the muscle weight, α is the pennation angle, ρ is the muscle density, equal to $1056\,\mathrm{kg/m^3}$, and l_f is the fibre length (Hamill and Knutzen 2008). It is commonly assumed that the maximum force in a muscle is proportional to its PCSA.

In two muscles with different optimal lengths but the same PCSA, pennation angle, and the maximum force, the range of possible muscle lengths will differ (Lieber and Fridén 2000), Fig. 1.2b. During a motion, the body segments move when muscles connecting them shorten and lengthen in a prescribed scope of lengths, changing the joint angle.

Fiber types

Another criterion influencing muscle strength is ratio of different fibre types composing the muscle (Hill 1970). Skeletal muscle fibres are commonly classified into 4 types: Type I (slow twitch oxidative), Type IIA (fast twitch oxidative glycolytic), Type IIX/D (fast twitch glycolytic) and Type IIB (fastest twitch glycolitic, does not exist in humans) (Peter et al. 1972; Scott et al. 2001). The determinant factor is the myosin heavy chain isoform, or, as a consequence, maximum shortening velocity of the fibres (Nigg and Herzog 1999; Scott et al. 2001). In the case of repeated contractions, the fast twitch fibres lose their ability to produce relatively large maximum isometric force rapidly, while the slow twitch fibres maintain this ability for a longer period of time. All skeletal muscles include fibres of different types (Fry et al. 1994). Of the main ankle-affecting muscles, the soleus muscle is almost exclusively composed of slow twitch fibres, while the extensor digitorum longus ('EDL') and extraocular muscles consist dominantly of fast twitch type fibres. The ratio of the fibre types changes with age: the number of slow fibres increases, and that of fast fibres decreases (Hirofuji et al. 1992). The ratio of fibre types can also change over time in an individual due to muscle activity (Wernig et al. 1990). The EDL muscles are more susceptible to fatigue than soleus (Burke and Edgerton 1975). The fibre composition in each muscle is optimised for its function, e.g. the soleus plays an important role in maintaining an erect posture in standing, and the EDL is an extensor of the toes and ankle (Palastanga et al. 2002).

1.2. Muscle contraction

As mentioned above, skeletal muscle is controlled by the central nervous system, which includes the brain and the spinal cord. Voluntary muscle contractions are initiated in the brain. The signals in the form of action potentials pass through the nervous system to the specialized cell (motor neuron) and cause a series of chemical reactions and an ion exchange through the fibre membrane in a specialised junction, called the synapse (Fig. 1.4). The transient change in membrane potential is the action potential. This condition promotes the release of Ca^{2+} ions, which invoke cross-bridge formation and innervate the muscle fibres. The cross-bridge cycle repeats itself as long as

the action potential exists. When the stimulation stops, Ca^{2+} ions return into the sarcoplasmic reticulum, preventing cross-bridge formation in the relaxed state (Nigg and Herzog 1999; Hamill and Knutzen 2008).

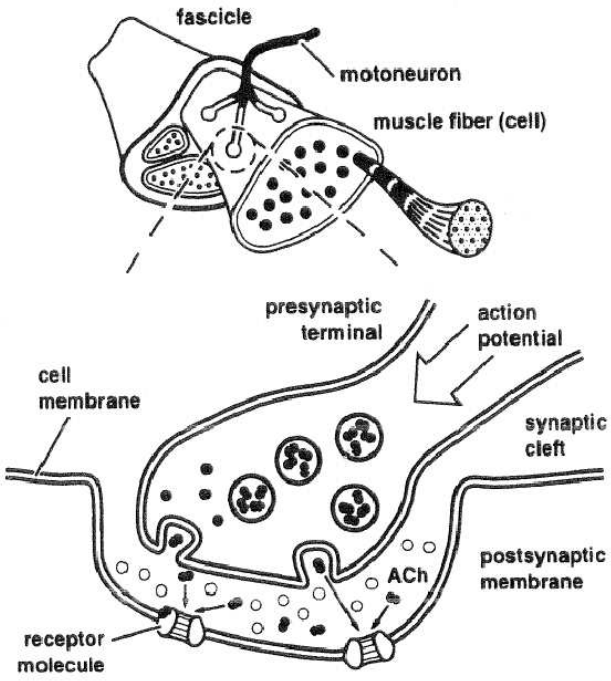

FIGURE 1.4. Schematic illustration of transferring action potential to the muscle fibre. To perform any movement the brain sends a signal through the nervous system towards the muscle. When the signal reaches the muscles, it divides into small branches and delivers the action potential to the fibres. This causes a series of chemical reactions and an ion exchange through the fibre membrane in the synapse. Reproduced from Nigg and Herzog (1999), the textnotes modified.

1.2.1. *Muscle stimulation*

Skeletal muscles are able to produce varying levels of contractile force under neural control *in vivo*. Contractile responses by the muscle must be provoked to perform experiments on skeletal muscle *in vitro*. To deliver electrical charge *in vitro*, single pulses or pulse trains are provided by specialised devices. A muscle response to a stimulus depends on some parameters such as the strength and the frequency of the pulses, the muscle length, the velocity of muscle lengthening/shortening, and the fibre composition of the muscle (Chaffin and Andersson 1991).

Only some of the fibres in the muscle can be recruited by a weak signal. With increasing voltage, additional units are activated and the force becomes larger via multiple fibre summation. The muscle attains a maximally stimulated state when the twitch amplitude reaches its maximum (Hamill and Knutzen 2008).

A single twitch invokes a muscle contraction and a subsequent relaxation. If another twitch is delivered before the muscle relaxes, a greater force will be produced. Increasing the frequency of action potentials sent to the muscle fibres leads to a frequency summation phenomenon (Chaffin and Andersson 1991), Fig. 1.5. A muscle is *maximally stimulated* or tetanic when increasing of signal strength and frequency beyond certain level will not lead to muscular force growth (Hamill and Knutzen 2008).

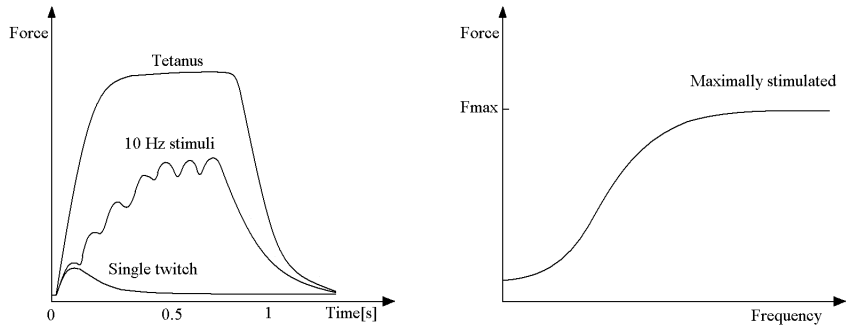

(a) (b)

FIGURE 1.5. (a) Schematic illustration of force-time traces for a single twitch, 10 Hz stimuli and a tetanus applied to a muscle. The muscle force rises with each stimulus and reaches a tetanic plateau. The plateau becomes smoother and the tetanic force increases with increasing frequency until a force limit is approached. (b) Schematic illustration of force-frequency relationship. The tetanic force increases with stimulation frequency until it reaches a limit and the muscle becomes maximally stimulated. Figure (a) is re-drawn from Nurhussen (2006), (b) is based on experimental results on soleus muscle.

1.2.2. *Muscle force and types of contractions*

Understanding force-length relations is essential for performing tests on skeletal muscles (Fig. 1.6). When the muscle is not stimulated, it produces a passive force, which is close to zero for muscle lengths below a certain level, a slack length. This length is usually close to the optimal muscle length. Stretching the un-stimulated muscle beyond the slack length leads to a rapid force increase induced by connective tissue resistance to the stretch. The research suggests titin and myofibrils as the origins of the passive muscle tension (Yoshioka et al. 1986; Horowits and Podolsky 1987; Funatsu et al. 1990).

The force produced during activation due to cross-bridge formation is called an active muscle force. The maximum active force is produced at the optimal muscle length (Nigg and Herzog 1999; Hamill and Knutzen 2008), this has been described above (Section 1.1). Active force is obtained under isometric contractions and maximum stimulation. Combined, the passive and active forces make a strong resistance to lengthening, far beyond the peak of active force (Nigg and Herzog 1999). Though the active force component is the most important in the studies, it is possible to measure only the total and passive muscle forces during experiments. The active force is defined as the difference between these components.

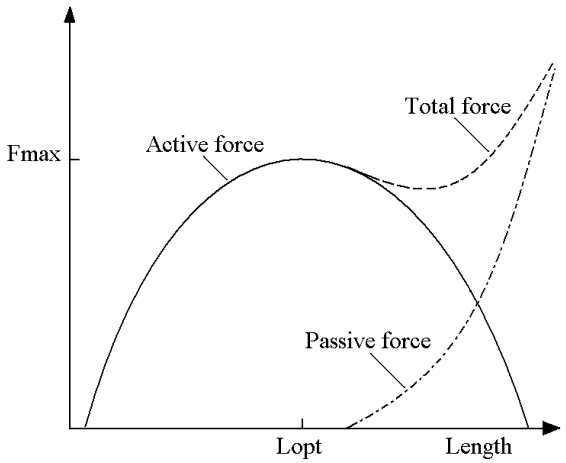

FIGURE 1.6. Schematic illustration of force-length relations. The dash-dotted line shows the passive force, dashed line - total force, and solid line - active muscle force. Re-drawn and modified from Hamill and Knutzen (2008).

To define the dynamic properties during muscle contraction, the force-velocity relationship is used. The muscle shortens at a certain velocity against a constant load, Fig. 1.7. The resistive force decreases in a hyperbolic fashion asymptotically to zero when the shortening velocity increases (Nigg and Herzog 1999; Lieber and Fridén 2000; Hamill and Knutzen 2008). This is intuitively obvious as when lifting two unequal loads; the lighter load can be moved much more quickly.

Another important characteristic is the muscle power (Fig. 1.7). Defined as the product of force and velocity, the power can be integrated over a specific time period. The muscle power diminishes at zero load and very high load (no velocity). The optimal muscle shortening occurs at approximately one-third of maximum shortening velocity (Hill 1938; Nigg and Herzog 1999; Lieber and Fridén 2000).

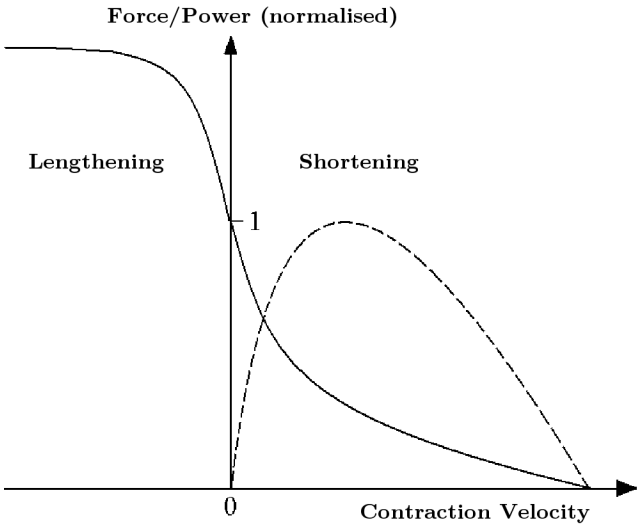

FIGURE 1.7. Schematic illustration of force - velocity (solid line) and power - velocity (dashed line) relations. The mark '1' corresponds to the isometric contraction at the optimal length. Redrawn and modified from Nigg and Herzog (1999) and Hamill and Knutzen (2008).

The term 'muscle contraction' can be misleading, as muscles can generate force while shortening, lengthening, or at a constant length. The contraction type is governed by interaction of the muscle with the surrounding system (Hamill and Knutzen 2008).

A muscle contraction is called *isometric* if the muscle length remains constant while in tension. Contractions under isometric conditions are used for defining the optimal length, maximum isometric force and force-length relations, Fig. 1.8.

During a *concentric contraction* the muscle shortens while generating force, and thereby normally changes the angle of the joint - or joints - where the muscle is attached.

An *eccentric contraction* occurs when the muscle lengthens in an active state. This happens while an opposing force is greater than the force generated by the muscle.

1.2.3. *History effect*

It has been shown experimentally that the steady-state force at an isometric state following a concentric contraction does not reach the maximum isometric force associated with an initially isometric contraction at the final length. This phenomenon is called *residual force depression* (Abbott and Aubert 1952; Edman et al. 1978;

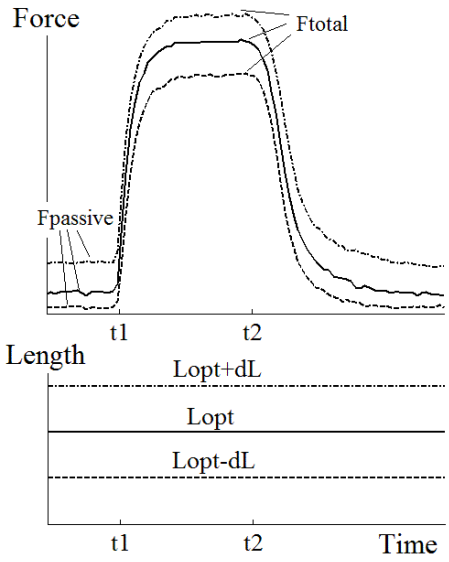

FIGURE 1.8. Examples of force-time traces for a mouse soleus muscle electrically stimulated at different muscle lengths. The stimulation was applied between times t_1 and t_2. When the stimulation stops, force drops down to the initial passive force, i.e. related to the muscle length. Active force is maximum at optimal length (solid line). Both passive and total forces are lower at sub-optimal length (dashed line, Length= $L_{opt} - dL$). Passive force increases with stretch, but the active force decreases (dash-dotted line, Length= $L_{opt} + dL$).

Marechal and Plaghki 1979; Herzog and Leonard 1997), Fig. 1.9a. There is similar phenomenon induced by active muscle lengthening called *residual force enhancement*; the redeveloped force is larger than the isometric force (Schachar et al. 2002; Rassier and Herzog 2002; Bagni et al. 2005; Herzog 2005; Herzog et al. 2006; Morgan 2007), Fig. 1.9b. Moreover, there is a force change following lengthening-shortening and shortening-lengthening cycles (Epstein and Herzog 1998). These phenomena are usually referred to as history dependence of the active force production, and were first described by Abbott and Aubert (1952). The history effect is observed in experiments but is not accurately explained (Herzog and Leonard 2005; Morgan 2007; Herzog et al. 2008). The muscular force consists of active and passive components, and both active and passive force modifications occur with active shortening or lengthening (Bagni et al. 2002; Rassier and Herzog 2002; Joumaa et al. 2008; Herzog et al. 2008). Interesting observations were made by Julian and Morgan (1979) and Morgan et al. (2000). They have noticed that a short stimulation interruption eliminates the history effect after non-isometric contractions.

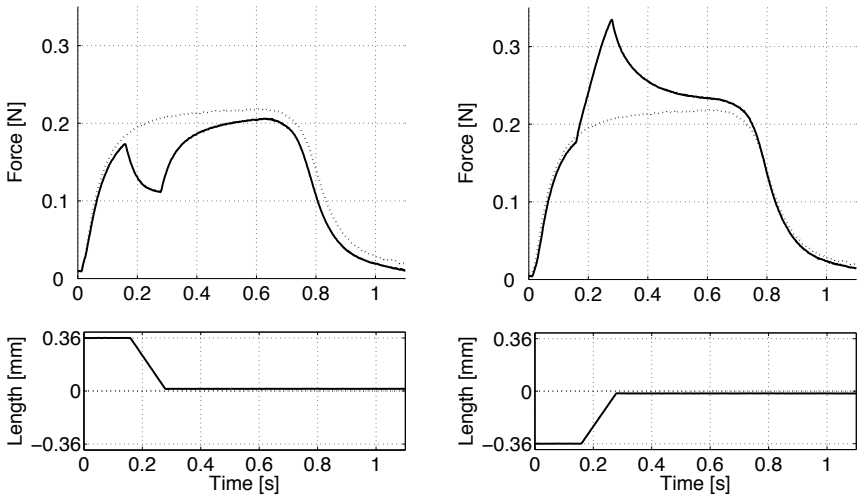

FIGURE 1.9. Examples of force production during (a) concentric and (b) eccentric contractions (solid lines), performed by soleus mouse muscle. The stimulation was applied between times 0 and 0.6. Isometric contraction at the optimal length is shown as a dotted line. Length is expressed as deviation from the optimal length. Force grows when the stimulation starts. After the force almost reached its maximum value, the muscle was (a) shortened or (b) lengthened thus leading to a rapid force fall/rise until the end of the length ramp. While the length was held at the optimal value, the force redeveloped to a new steady-state value, different from the isometric force level. This difference is called the force modification.

Some recent studies aimed to investigate the force depression and force enhancement phenomena in voluntary contractions by humans (Hahn et al. 2007; Altenburg et al. 2008; Seiberl et al. 2012). During non-isometric contractions the brain sends a corrected signal to the motor neurons resulting in a proper movement instead of muscle force changes leading to unexpected movements. For example, when the muscle is lengthening, a smaller action potential is delivered to the muscle to decrease metabolic cost of the contraction. On the contrary, to shorten the muscle, a larger signal should be sent.

There have been many attempts to explain the mechanisms of force modification. Some of them have been disproved by later investigations, while others have led to new questions. Sarcomere length non-uniformities were proposed by Marechal and Plaghki (1979) as a possible mechanism of force depression after shortening. The results by Edman et al. (1978, 1993) support the structural non-uniformities as the underlying mechanism of force depression, but Granzier and Pollack (1989) disproved

this idea by specific experiments. The force depression is associated with a decrease in the muscle stiffness or cross-bridge cycling (Sugi and Tsuchiya 1988; Razumova et al. 1999; Lee and Herzog 2003). For many decades, it has been generally accepted that the active force depression is influenced by shortening magnitude (Abbott and Aubert 1952; Herzog and Leonard 1997; Lou et al. 1998; Schachar et al. 2004; Bullimore et al. 2007) and speed of shortening (Marechal and Plaghki 1979; Sugi and Tsuchiya 1988; Herzog and Leonard 1997; Morgan et al. 2000; Lee and Herzog 2003). The study presented in Paper 1 has shown that these descriptions are true only for a certain experimental paradigm.

The mechanism of force enhancement invoked by eccentric contractions is poorly understood in comparison to force depression. In a recent review, Morgan (2007) stated that these observations might be explained by non-uniformity of half-sarcomere lengthening, but the muscle experiments suffer from various problems. At the same time this theory was not certified by Herzog et al. (2008), but they suggested a calcium-dependent increase in titin stiffness as a cause of the passive force component. Herzog et al. (2006) suggested that the active component of force enhancement is associated with changes in the cross-bridge kinetics that might be reflected in decreased detachment rates following active muscle lengthening. Edman et al. (1978) proposed that the tetanic force enhancement after a lengthening can be described as a parallel elastic element that is formed, reorganized or re-aligned during activation.

The present results show that from a macro-description viewpoint the mechanical work is a good predictor of force modification following active lengthening, shortening, and lengthening-shortening cycle despite the different mechanisms underlying these phenomena, Paper 1 and Paper 2. This observation might provoke a debate in the explanation of physiological aspects, but it serves as general description of force modification due to history effect and a source for improving skeletal muscle models.

1.3. Skeletal muscle modelling

Theoretical models of skeletal muscle differ considerably depending on the structural level and the problem to be solved. The main interest in biomechanics is to estimate and predict forces of the entire muscle. The first significant findings were made by Hill (1938), when he described an experimental relation between muscular force and contraction velocity:

$$(V + b) \cdot (F + a) = b \cdot (F_0 + a), \tag{1.2}$$

where F is the transient muscle force, F_0 is the maximum muscle force, V is the contraction velocity, a and b are specific constants. The Hill-type muscle models have been dominant for a long time and play a major role in musculoskeletal simulations of varying complexities. The original Hill-type muscle element consisted of a contractile element that has force-velocity properties according to the Eq. (1.2).

In order to improve the muscle model, parallel or series elastic elements, viscous dampers, and other passive elements were considered in addition to the contractile element (Zajac et al. (1986); van Soest and Bobbert (1993) and many others). These components represent tendons connecting the muscle with the bones and connective tissue surrounding the entire muscle and the muscle fibres. A rheological muscle

model by Günther et al. (2007) based on Hill element uses the activation level and the length-velocity values as an input. Damping elements significantly improved the muscular force description, though the history effect after non-isometric contractions was not considered. Forcinito et al. (1998) developed a supplement for a common muscle model, with an 'elastic rack', or a step-wise parallel elasticity, which engages upon muscle activation to give a simple muscle memory. Similarly, the force modification component was added to the muscle model.

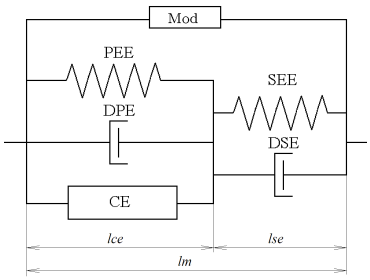

FIGURE 1.10. Schematic representation of the muscular model. The muscle-tendon model consists of two main components: the contractile element (CE) with parallel damped elastic element (PEE, D_{PE}), both of the same length, and the serial damped elastic element (SEE, D_{SE}). In total they form a whole muscle-tendon complex of length l_m, the sum of l_{CE} and l_{SE}. Force modification element (Mod) is placed parallel to CE and SE components.

Numerical description of muscular force production consists in predicting experimental muscle force data by a set of equations and constraints using available parameters such as instant muscle length and stimulation level. The active isometric force immediately following a transient-length contraction, or a modified force, can be described by an asymptotic, i.e., theoretical long-term steady-state force value. This value was compared to the asymptotic force for a pure isometric contraction, where the muscle was held at constant length from the start of stimulation. Such quantities were evaluated from the force-time trace by curve-fitting. With experimental length variations according to Fig. 1.9, the curve fitting considered the isometric phases before and after a length variation. A good numerical fit was generally obtained with exponential function of the form:

$$F(t) = F_\infty + (F_a - F_\infty) \cdot e^{-(t-t_a)/\tau} \tag{1.3}$$

where the force F at a time t goes from a value F_a at time t_a to a steady-state asymptotic value F_∞ through an exponential function with a time constant τ. The conclusion from Paper 1 was that the time constant τ_r for an isometric phase following shortening was –for practical purposes– well predicted by the one, τ_o, for an initial isometric contraction.

The results show that the transient force production in an isometric phase of a contraction following muscle length variation can be well predicted by introduction of a force modification, considering the history through the work quantity, and the initial time constant being a typical parameter for a muscle individual. The force modification is an addition, with its sign positive or negative, and is here seen as a difference to the force obtainable at an isometric contraction at the corresponding length.

The experiments performed also allow analysis of the transient-length phases of contraction, and these phases can, on a macroscopic level, be described by similar expressions. The mathematical analysis of force-time traces is inspired by the experience from fitting Eq. (1.3) to isometric phases. From a mechanical viewpoint, the contents of the equation would indicate the presence of a viscous damper in series with the force generator in the muscle. This can be seen by identifying the equation as an evolution process, where the time differential of the force is described by:

$$\dot{F}(t) \equiv \frac{d\,F}{dt} = \frac{1}{\tau}\left(F_\infty - F(t)\right) \tag{1.4}$$

where F_∞ is the asymptotic force, and the superposed dot denotes a time differential, i.e., the slope of the force-time trace. The expression emphasizes that the force is constantly approaching the asymptotic value, in each time interval reducing the distance by the same ratio.

A common way to consider an evolution expression like the one in Eq. (1.4) is through the state-space, where $F(t)$ and $\dot{F}(t)$ are seen as the axes in a plane diagram, and where an expression of the form in Eq. (1.4) will come out as a straight line, with a slope of $-\frac{1}{\tau}$, and coming to $\dot{F} = 0$ for $F = F_\infty$. Such a state-space visualization of experimental time-data confirmed that the measured muscular force is realistically described by a function like the one in Eq. (1.3) during some phases of the interval, and the asymptotic value is a constant attractor; see Paper 4. The non-isometric parts of the force-trace cannot be described by an exponential function, as the changing length in itself implicates differences in the isometric force.

A macroscopic muscular model based on Günther et al. (2007) was developed and the memory effect described above was included as a force modification component, Figure 1.10, Paper 4. The parameters obtained from the experiment analysis, particularly the force modification during and after non-isometric contractions and the time constants, were reproduced by the simulations. The numerical muscle model is applicable for solving an optimization problem (Eriksson and Svanberg 2011).

1.4. Musculoskeletal modelling

Skeletal muscles and bones are the main elements of the locomotor systems which allow humans and animals to move. Motion of this musculoskeletal system is a result of transforming electrical signals passing through the muscles into muscular forces, leading to coordinated movement of the body. Modelling of this complex system is possible when physiological processes in the muscles can be well described by asymptotic equations. Muscular forces acting on the skeletal system will then indicate a movement according to the dynamics laws (Winters 1995).

A number of different numerical modeling techniques is available depending on the aim of the study. Multibody system models are constructed with rigid body parts that are connected at joints and by discrete spring-damper elements. They are used to study kinematics, muscle dynamics, and joint-forces. Due to the complexity of musculoskeletal modelling, specialised software are usually employed, e.g. AnyBody (AnyBody Technology A/S, Aalborg, Denmark), SIMM (Musculographics Inc., Santa Rosa, CA, USA; Delp and Loan (1995)), and OpenSim (Delp et al. 2007). Applications for biomechanical modelling and computer simulations provide geometry of the system with individual fitting feasibility, and tools for simulations of dynamic movements.

With growing computer capacity, the level of detail and size of the numerical models may increase to include more complex material formulations and more detailed geometries. This improved capacity has also called for more detailed models of the skeletal muscles. The musculoskeletal system was in the present work refined by implementing the force history effect in a muscle model in the open-source software OpenSim. For this, an application programming interface (API) was used, which allows users to extend capabilities of the software by adding newly developed tools. It was noted that modifying all aspects of OpenSim to take the history into account was not feasible, but certain modifications were performed in Paper 5.

A series of experiments on human movement was conducted to test the effects of the modified muscle model. A musculoskeletal model with a certain number of segments, degrees-of-freedom and musculotendon actuators is usually used to evaluate muscular forces and activations using joint kinematics and ground reaction forces through the built-in inverse optimisation. The set of muscle forces that satisfies dynamic equilibrium is not unique, therefore static optimisation is used in the included Compute Muscle Control algorithm to minimise a cost function at every timestep t for the set of N muscles (Thelen et al. 2003):

$$J(t) = \sum_{i=1}^{N} V_{\mathrm{i}} \left[A_{\mathrm{i}}\left(t\right)\right]^2, \tag{1.5}$$

where V_{i} is the volume of muscle i and $A_{\mathrm{i}}(t)$ is the activation of muscle i at time t (Happee 1994; Thelen and Anderson 2006).

Current techniques are limited in muscle force measurements (Schuind et al. 1992; Finni et al. 1998; Lee et al. 1999). To estimate muscle force, the torque can be measured (Svantesson et al. 1994; Lee et al. 1999; Hahn et al. 2007; Altenburg et al. 2008) and the load sharing problem solved, though the solution will depend on the optimisation design and criteria. Our model contains 96 musculotendon actuators and would therefore be computationally demanding to estimate load sharing. Moreover, torque measuring techniques are not applicable in tested movements. In such cases, a muscle model is generally validated by comparing calculated muscle activation with the electromyography signal (McGill 1992; Lloyd and Besier 2003). In OpenSim, the muscle activations are calculated from formula suggested by Thelen et al. (2003):

$$A = \left(\frac{F}{\cos(\alpha)} - F_{\mathrm{passive}}(l)\right) \cdot \frac{1}{F_{\mathrm{lv}}(l, \dot{l})}, \tag{1.6}$$

where F is a muscle force, A the activation, F_{lv} the active force-length-velocity surface, F_{passive} the passive force, and α the pennation angle at the steady-state muscle length l for a given muscle; the superposed dot denotes time differentiation.

Method presented in Paper 5 is based on the validity of necessary approximation in Eq. (1.6). The musculoskeletal system model was refined by implementing the history effect in a muscle model and verified by simulation of some experiments on human movement.

1.5. Thesis outline

The thesis is composed of five studies. The first one, published as Paper 1, uses a series of concentric contraction experiments and investigates the force depression. The second study, Paper 2, consists of an expanded series of experiments for the purpose of force modification examination after various combinations of active lengthening and shortening. The third part is an investigation of contractile properties of muscles of mice with collagen-induced arthritis, which used the same basic experimental paradigm. Paper 3 diverges from the main project, but gives improved general understanding of muscle contractions. Paper 4 deals with analysis of the second series of experiments, aiming at a macroscopic interpretation of the force production. It provides a muscle model improved by a history component and adopted for mouse soleus and EDL muscles. The final study, Paper 5, investigates a muscle history modification introduced in a musculoskeletal model for dynamic simulations of human movements.

These articles are presented in Part II of the thesis. A review of the experiments, mathematical analysis and modelling procedures are given in Chapter 2. A selection of main results are given in Chapter 3, and the main conclusions are discussed in Chapter 4. Chapter 5 gives some overall conclusions form the collection of papers, and gives an outlook on possible and desirable continuations of the current work.

CHAPTER 2

Methods

The project is based on extensive series of experiments on mouse skeletal muscles, Section 2.1. Analysis of the first series of experiments, force depression following concentric contractions, has been presented in Paper 1. Paper 2 is based on contractions with various stretches and shortenings as well as their combination. Force modification, and their prediction were the quantities of interest. Contractions of soleus muscles from mice with collagen-induced arthritis (CIA) were performed to study rheumatoid arthritis, presented in Paper 3.

The force-time traces as the main product of muscle experiments were analysed using methods presented in Section 2.2. A numerical muscle model was then developed based on the improved description of muscular force generation.

The last part of the project involved experiments on human movement, Section 2.3. A full body model was created in a special-purpose software, then simulations of the movements were performed and improved by adding the history effect in the muscle model, Section 2.4.

2.1. Experiments on mouse soleus and EDL muscles

2.1.1. *Muscle preparation*

Muscles of adult male NMRI strain mice were used. The white mice were housed at room temperature with 12/12-hours light/dark cycle for at least 8 weeks. Animals were given food and water *ad libitum*. Their weight was $\sim$30 g. Animals were euthanised by rapid cervical dislocation and thereafter EDL and soleus muscles were dissected. The Stockholm North local ethical committee approved the experimental procedures.

The soleus is a powerful flat muscle on the posterior side of the lower leg. It runs from the upper posterior surfaces of the tibia and fibula to the calcaneus, Fig. 2.1a. The soleus muscle is responsible for plantarflexion of the ankle joint (Murray et al. 1976). The EDL is a pennate muscle, situated at the lateral anterior part of the leg. It originates at the superior anterior surface of the fibula, passes anteriorly over the ankle joint, and divides into four tendons which run to the lateral four toes, Fig. 2.1b. The EDL provides dorsal extension of the toes and ankle (Palastanga et al. 2002; Hamill and Knutzen 2008).

Soleus muscle contains about 80% slow type fibres (Asmussen and Maréchal 1989; Wernig et al. 1990). The EDL muscle has at least 95% of fast twitch fibres, both type IIA and IIB (Wernig et al. 1990). The mixture of the fibres depends on the

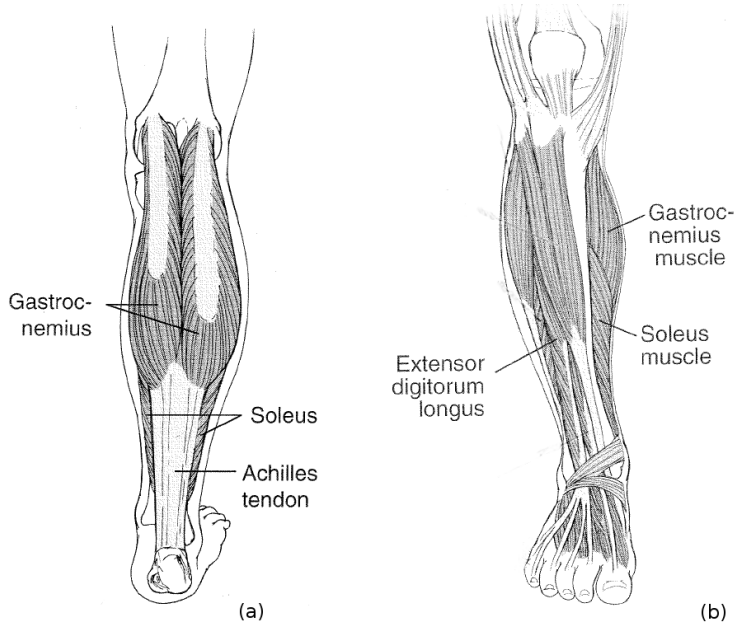

FIGURE 2.1. Schematic illustration of soleus and EDL muscles in the human body. Reproduced from Hamill and Knutzen (2008)

animal age and activity (Hirofuji et al. 1992; Wernig et al. 1990). In the performed experiments, the soleus muscle reached a steady state 0.3 s after the isometric maximal stimulation began. For EDL this time was about 0.15 s. The EDL is very sensitive to lengthening, and experiments on this muscle therefore usually take more time and effort (Burke and Edgerton 1975).

Muscle preparation and solution, supporting the ability of the muscle to contract, are described in detail in Paper 1, Section 2.2 and Paper 2, Section 2.2.

2.1.2. *Experimental design*

The muscle was mounted between an adjustable holder from one side and a length controlling system and a force transducer from the other side. The stimulation was applied through two plate electrodes placed along the muscle (Fig. 2.2). Stimulation, length and muscle force were controlled and recorded via a computer and the Spike2 software (CED, Cambridge, UK). Detailed description of the experimental setup is presented in Paper 1, Section 2.3.

2.1.3. *Testing paradigm*

Isometric contractions have been initially performed to define the individual optimal muscle length, and after experiments to verify the ability of the muscle to produce the maximum isometric force.

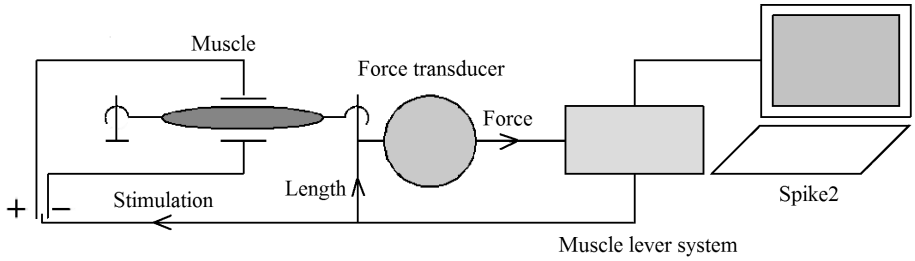

FIGURE 2.2. Schema of the experimental apparatus. The muscle was mounted between an adjustable holder from one side (left on the figure) and a length controlling system and a force transducer from another side. The stimulation was applied through two plate electrodes placed along the muscle. Stimulation, length and muscle force were controlled and recorded via computer and the Spike2 software (CED, Cambridge, UK).

The first series of experiments consisted of concentric contractions with various shortenings and ramp times, performed on soleus and EDL muscles. The experiments were divided into three groups depending on the final muscle length, i.e. the muscle length after active shortening. The isometric force redevelopment at optimal ($l_{fin} = l_o$), suboptimal ($l_{fin} = l_0 - 0.72$mm) and superoptimal ($l_{fin} = l_0 + 0.72$mm) muscle lengths was preceded by the same set of ramps. The extensive description of the concentric contraction experiments can be found in Paper 1, Section 2.4.

The second stage of the project consisted in expanded sets of ramps applied on soleus and EDL muscles. The final muscle length, l_{fin}, was equal to the optimal, l_o in most tests. All the experiments can be divided into four groups depending on the character of the ramps. These are 'Shortening', 'Lengthening', 'Lengthening-Shortening' and 'Long Shortening'. Examples of force-time traces are presented in Fig. 2.3. The extensive description of the second series of experiments can be found in Paper 2, Section 2.4.

2.1.4. *Mice with collagen-induced arthritis*

Female DBA/1 mice, weighing 18-22 grams, were supplied for induction end evaluation of CIA. Type II collagen was obtained from bovine nasal cartilage and mixed in a collagen emulsion (Kokkola et al. 2003). The emulsion was injected subcutaneously into the base of the tail of the DBA/1 mice. On day 28, the mice received a booster injection. Control mice were treated by saline on both occasions. When the arthritis developed in the animals and the whole paws were inflamed, the mice were euthanised and the muscles were then dissected for the experiments.

The time to peak force, half-relaxation time of the twitch and the force-frequency relationship were determined by evoking tetani using the above described procedure, Section 2.1.2. The shortening velocity at zero load was measured with slack tests

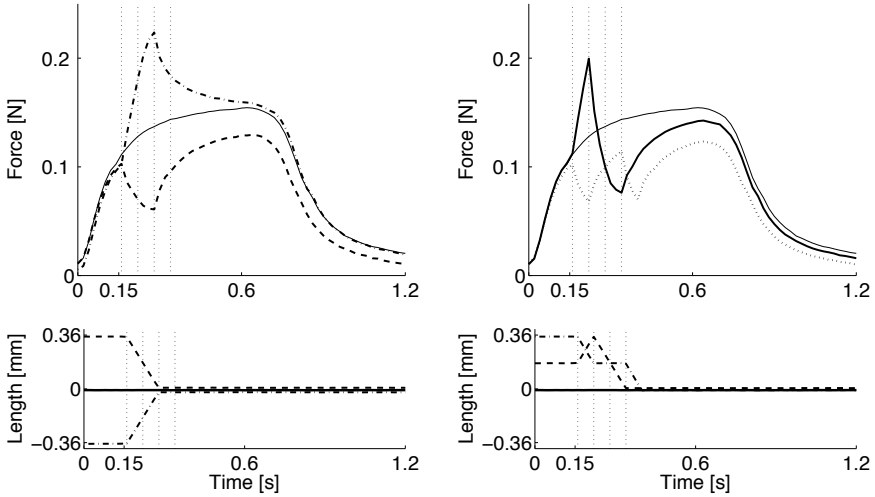

FIGURE 2.3. Examples of force-time traces on mouse soleus muscles from Paper 2. Thin solid lines correspond to isometric contractions. Transient-length contractions: (a) dash-dot line - lengthening and dashed line - shortening on 0.36 mm in 0.12 s, (b) dotted line - two-step shortening on 0.18 mm in 0.06 s each with 0.12 s delay between them, thick solid line - lengthening-shortening cycle. All experiments end at the optimal length of the muscle. Time t=0 denotes start of stimulation, Length=0 the individual optimal length.

(Lännergren 1978). Rapid releases of at least 5 different amplitudes were applied during tetani of 1-minute intervals in a similar experimental setup.

To measure myoplasmic free Ca^{2+} concentration ($[Ca^{2+}]_i$), intact single fibres were dissected from the soleus muscle, microinjected with the Ca^{2+} indicator and stimulated at an optimal fiber length.

Muscle samples were fractionated into myofibrillar and cytosolic fractions (Fagan et al. 1999). Protein concentrations of muscle fractions were measured using the Bradford technique (Bradford 1976). The relative content of myosin heavy chain and actin in total myofibrillar proteins and distribution of various isoforms were evaluated densitometrically using ImageJ (National Institute of Health, Bethesda, MD; http://www.rsb.info.nih.gov/).

An immunologic method, immunoblotting, for identifying, locating and quantitatively measuring immunoreactive substances (proteins) is based on the ability of the proteins to bind to specific antibodies (Magi and Liberatori 2005). The immunoblotting was performed on unstimulated muscle samples, to avoid the complication of

changes that could result from contractile activity. The redox modification was assessed with densitometry, involving measurement of the total density in a box covering the width and length of each lane, with results analyzed using ImageJ. In addition, for S-nitrosocysteine, the density of myosin heavy chain and troponin I was measured. The extensive description of the testing procedure described in Paper 3, Section 2.

2.2. Muscle modelling

The experimental data was analyzed to evaluate parameters for an extensive description of muscle force during contraction. The force-time traces have been fitted by exponential functions during isometric phases. This fit is generally used and shows a good agreement with the experimental data (Hancock et al. 2004; Corr and Herzog 2005). The force level reachable after various length regimes was evaluated and the difference from the isometric force, obtained from pure isometric test at the corresponding muscle length, was calculated. This force modification appeared to be linearly related to the mechanical work produced by and on the muscle during lengthening and shortening ramps. The mechanical work was calculated by integrating the force multiplied by ramp velocity, over the ramp period. The extensive description of the evaluation procedure for the isometric steady-state force, active and passive force modification, and the mechanical work performed by or on the muscle can be found in Paper 1, Section 2.5 and Paper 2, Section 2.5.

A state-space visualization of the experimental dynamic parameters was used to evaluate the timing constants of the muscular force production. All experimental data were filtered by a second-order Butterworth lowpass filter with a cutoff frequency of 60 Hz and plotted in state-space diagrams, with $F(t)$ as ordinate and $\dot{F}(t)$ as abscissa. The borderlines between the different iso-kinetic parts of the curves were marked, and each such segment treated separately. As examples, the state-space diagrams corresponding to isometric and eccentric contractions are given in Fig. 2.4.

Simulation of muscular force generation was based on work done by Günther et al. (2007) and van Soest and Bobbert (1993) and was implemented in Matlab. A muscle-tendon complex was represented as a contractile element (CE) in parallel with an elastic element (PEE) and connected to a series elastic element (SEE), Fig. 1.10. Both elastic elements contain a damping components (D_{PE}, D_{SE}) in order to avoid high frequency oscillations which might occur in impact (Günther et al. 2007; Rode et al. 2009b). In our work, a force modification component (Mod) is added in parallel to both CE and SEE.

The activation dynamics of a muscle is modelled as described by Ebashi and Endo (1968) and Hatze (1977), where the isometric force F_{CE} is scaled by the activation A, which in turn represents the Ca^{2+} concentration of the muscle (Günther et al. 2007). The contraction dynamics derived by van Soest and Bobbert (1993) was based on the Hill equation (Hill 1938). The force equilibrium equation was solved at each timestep for CE length velocity. Then a history effect was introduced as the force modification addition to the total force:

$$dF_{\mathrm{mod}} = K_{\mathrm{hist}} \cdot W \cdot A, \tag{2.1}$$

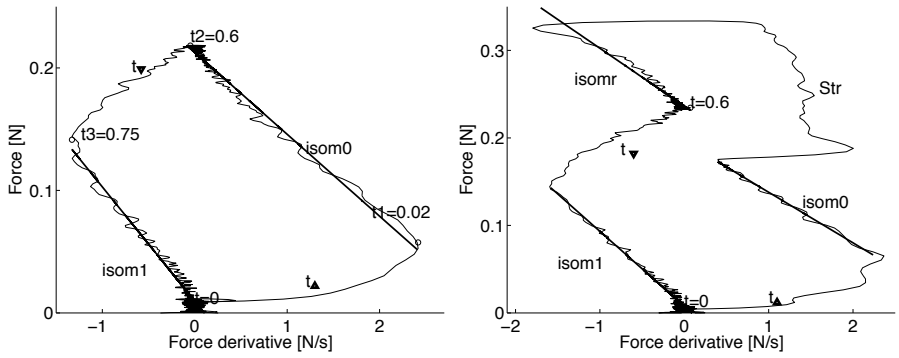

FIGURE 2.4. State-space plot of an example from Paper 4: (a) isometric and (b) lengthening tests performed on mouse SOL muscle, showing the relation between current force and force time differential values over experimental time. Time $t_0 = 0$ denotes start of stimulation, the force time differential, $\dot{F}(t)$, increases during $t_\triangle$ until reaching a maximum value at time t_1. Then the force, $F(t)$, rises exponentially and reaches a steady-state value when the $\dot{F}(t)$ drops to zero. After the stimulation terminates at time $t = 0.6\,\mathrm{s}$, force and force derivative start to decrease. $\dot{F}(t)$ drops to its minimum value during $t_\triangledown$ (until time t_3), then the force decays exponentially to its passive level. The straight lines are regression fits of the isometric phases of muscle contractions: 'isom0' - initial force development, 'isomr' - force redevelopment after stretching, 'isom1' - force decay after destimulation. 'Str' denotes the active stretch phase.

where K_{hist} is the history coefficient, and $W = \sum F \cdot \dot{l} \cdot \Delta t$ is the mechanical work performed by and on the muscle during the dynamic movement (described by the sign of W). F and $\dot{l}$ are quantities in the time series of intervals Δt.

To adjust the model for the soleus and EDL mouse muscles, 20 parameters were varied. The modelling parameters are presented in Table 1. Full set of equations can be found in Paper 4, Section 2.4 and in the mentioned references.

2.3. Experiments on human movement

Healthy adults were tested in the 3D gait analysis laboratory at Astrid Lindgren's Children's Hospital, Stockholm, Sweden. The subjects were examined using an 8–camera motion capture system (Vicon MX40, Oxford, UK) and two force-plates (Kister, Winterthur, Switzerland). Sixty-four reflective markers (9mm) were placed bilaterally on bony landmarks based on a conventional full-body marker set (Vicon Plug-in-Gait), plus a multi-segment foot model marker set (Stebbins et al. 2006). The electromyography (EMG) signals of four muscles (rectus femoris (RecFem), tibialis anterior

(TibAnt), medial head of the gastrocnemius muscle (MedGas) and soleus (Sol)) were measured on skin surface bilaterally (Motion Laboratory System, Baton Rouge, LA, U.S.A.) according to the SENIAM protocol (www.seniam.org, Hermens et al. (1999)).

The maximal voluntary isometric contraction test was performed by the volunteers to estimate a maximum strength of each muscle for EMG scaling (Örtqvist et al. 2007). The participants performed a squat and a standing heel-raise (rise up and down on toes) with a 3 second delay in the raised position. One subject performed an additional set of squats both slow and quick, and both with and without an additional load of 40 kg, held at the shoulders.

2.4. Musculoskeletal modelling

A generic musculoskeletal model with 14 segments, 23 degrees-of-freedom and 96 musculotendon actuators was used to generate the simulation in OpenSim 2.4 (Delp et al. 1990; Anderson and Pandy 1999; Delp et al. 2007). A subject-specific simulation of heel-raise and squat was generated. Computed muscle control (CMC) (Thelen et al. 2003) with the pre-defined constraints on muscle excitation was used to find a set of actuator excitations, A, implicitly using the activation-force relation, Eq. (1.6), from Thelen et al. (2003):

$$F = \Big(A \cdot F_{\mathrm{lv}}(l, \dot{l}) + F_{\mathrm{passive}}(l)\Big) \cdot \cos(\alpha), \tag{2.2}$$

where F is a steady-state muscle force, A the activation, F_{lv} the active force-length-velocity surface, F_{passive} the passive force, α the pennation angle at the steady-state muscle length l for a given muscle, and $\dot{l}$ is time derivative of muscle length.

Modification of activation was proposed to supplement the muscle model with the history effect as follows:

$$A_{\mathrm{mod}} = \left(\frac{F - dF_{\mathrm{mod}}}{\cos(\alpha)} - F_{\mathrm{passive}}(l)\right) \cdot \frac{1}{F_{\mathrm{lv}}(l, \dot{l})} = A - dA_{\mathrm{mod}}, \tag{2.3}$$

where activation modification could be expressed through force modification:

$$dA_{\mathrm{mod}} = \frac{dF_{\mathrm{mod}}}{\cos(\alpha) \cdot F_{\mathrm{lv}}}. \tag{2.4}$$

The force modification was evaluated as in Eq. (2.1). The new functionality was added to the general OpenSim software as a plug-in written in C++ using the application programming interface.

Due to lack of information about the history coefficient for human muscles, considering $K_{\mathrm{hist}} = -3\mathrm{m}^{-1}$ and $-4\mathrm{m}^{-1}$ for mouse extensor digitorum longus and soleus, respectively, we employed the value $K_{\mathrm{hist}} = -10\mathrm{m}^{-1}$ for all studied muscles. The decision was based on the amount of force modification which lies in a range between -30 and $+20\%$ of maximum isometric force, MVIC (Ruiter et al. 1998; Lee and Herzog 2003; Oskouei and Herzog 2005), and the tested movements are not very demanding.

CHAPTER 3

Results

The main result of the experimental studies is the finding that there exists a relation between the force history modification and the mechanical work performed by and on the muscle during the contractions. This description of the history effect along with experimentally obtained parameters has been applied in a numerical muscle model and a musculoskeletal model. The modified models have indicated the possibility for better prediction of muscular force and activation, even if exact parameters for the effect have not been verified.

3.1. Force depression and force enhancement

The results of the series of concentric contractions have shown a clear correlation between the force depression and the mechanical work performed by the muscle, Figure 3.1(a2,b2), and disproved a generally adopted relation of force depression and the velocity of shortening, Figure 3.1(a1,b1). The extended series of experiments shows a negative linear correlation between the force modification and the mechanical work produced on or by the muscle, Figure 3.2. The linear fits show that this correlation exists within each set of experiments (shortening, long shortening, lengthening, lengthening-shortening). A corresponding modification of the passive force component following each stimulation was also observed.

3.2. Impaired contractile function

The tetanic force per cross-sectional area was markedly decreased in the soleus muscle of mice with CIA, and the change was not due to a decrease in the amplitude of $[Ca^{2+}]_i$ transients. The reduction in force production was accompanied by slowing of the twitch contraction and relaxation, and a decrease in the maximum shortening velocity. Immunoblot analyses showed a marked increase in neuronal nitric oxide synthase expression but not in inducible or endothelial NOS expression, which, together with the observed decrease in superoxide dismutas 2 expression, favors peroxynitrite formation. These changes were accompanied by increased 3-nitrotyrosine, carbonyl, and malondialdehyde adducts content in myofibrillar proteins from the muscles of mice with CIA. Moreover, there was a significant increase in S-nitrosocysteine content in myosin heavy-chain and troponin I myofibrillar proteins from the soleus muscle of mice with CIA.

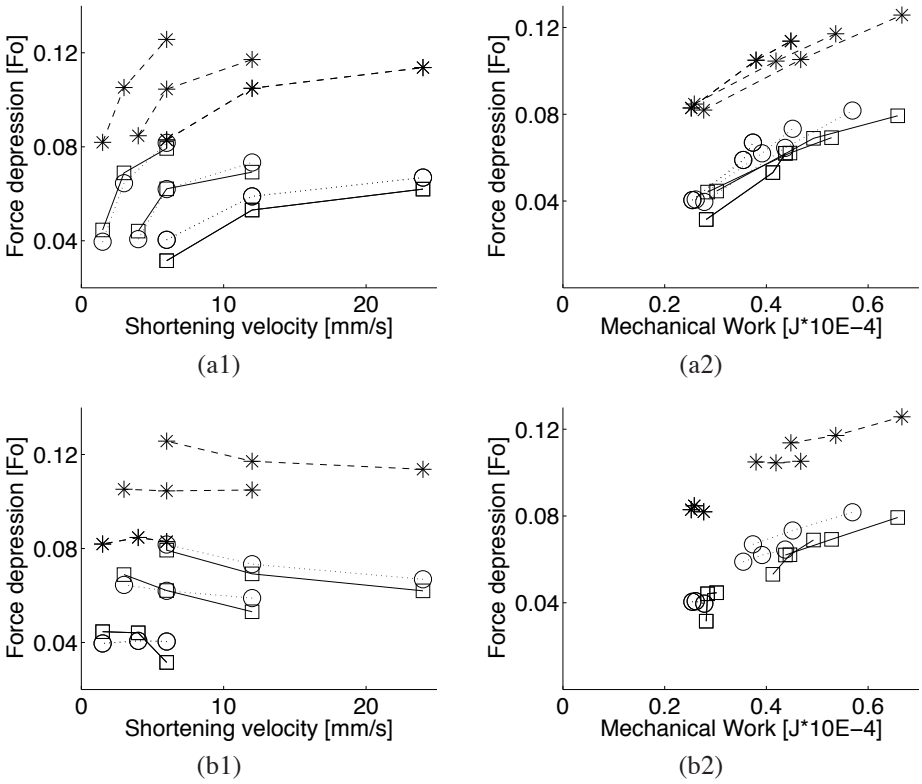

FIGURE 3.1. Steady-state force depression as a function of (1) shortening velocity and (2) mechanical work. Lines connect groups of experiments with the same a) shortening time, t_r, and b) shortening length, l_r. Square, circle and asterisk markers correspond to experiments with optimal, superoptimal and suboptimal final muscle lengths: $l_{\text{fin}} = 0, +0.72, -0.72$ mm, respectively. Average values for group of 5 SOL muscles.

3.3. Hill-type muscle model

The timing aspects of muscular force production, such as time constants, activation time and deactivation time, have been investigated using the state-space diagrams. The exponential nature of force development was confirmed. Moreover, the isometric phase for the force redevelopment after the muscle length variation appeared to be exponential as well and related to the time constant of initial force development at the corresponding muscle length. The parameters from the experimental analysis were used for a macroscopic muscular model. Simulations of the muscle contractions reproduced the force generation including the history effect, see Figure 3.3.

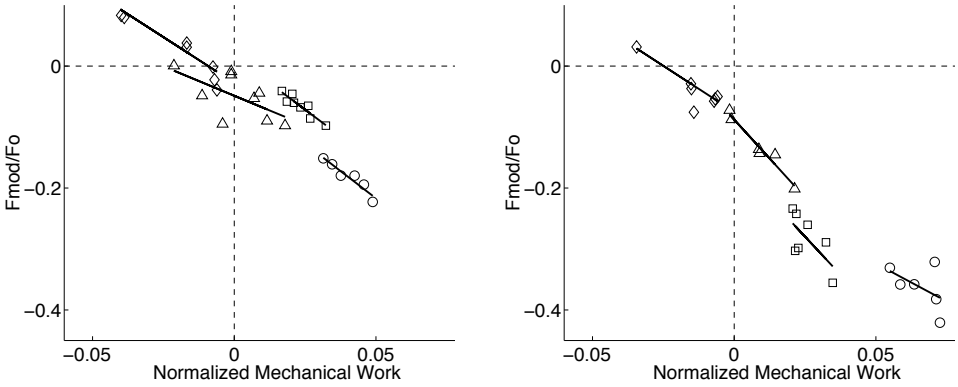

(a) (b)

FIGURE 3.2. Steady-state force modification as a function of normalized mechanical work of mouse (a) SOL and (b) EDL muscles. Data points represent mean values for four groups: Shortening - squares, Stretch - diamonds, Long Shortening - circles, Stretch-Shortening - triangles. Average value for group, maximum standard deviations for mechanical work are about 3%, for force modification are about 9% for both SOL and EDL.

3.4. Musculoskeletal model

Experimental data for squat and heel-raise were analysed in OpenSim, then activation was modified according to Eq. (2.3). The original and modified activations were compared with the measured and normalised EMG signal, Figure 3.4a. The modified activation gave a better match with the experimental measurements for most of the studied muscles, therefore indicating a reliability of the method even if the testing protocol was not sufficient for exact evaluation of the history parameters. Muscular force evaluated in OpenSim was also modified to demonstrate the impact of the history effect on the force, Figure 3.4a. Simulations of the pilot tests have shown that the history effect is more evident during fast and loaded movements than during slow movements without load.

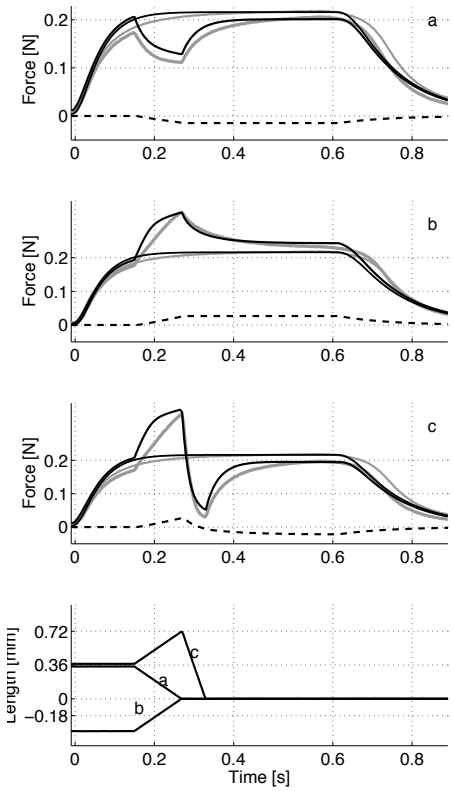

FIGURE 3.3. Simulations (*black*) and experiments (*grey*) of non-isometric contractions: shortening (**a**), stretching (**b**) and stretch-shortening (**c**), in each case compared to isometric contraction at the final length. Force modification is plotted as *dashed line*. The length regime is plotted below the force curves. SOL muscle.

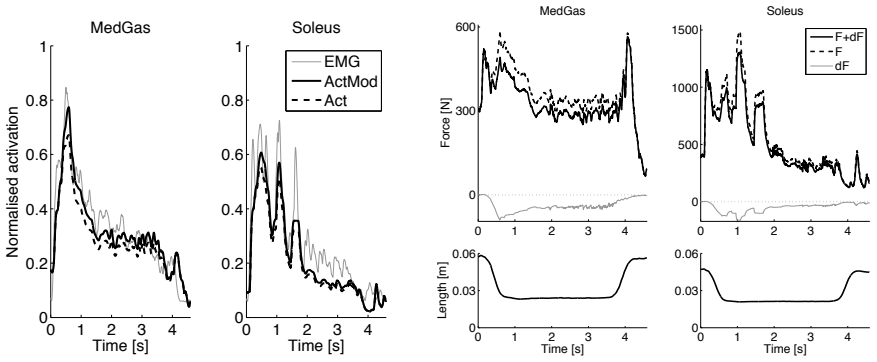

FIGURE 3.4. Simulation of one heel-raise cycle with ≈ 3 seconds delay in the upper position. The results are given for MedGas and Sol muscles. (a) Normalised EMG signal - *thin grey line*, muscle activation - *dashed black line*, modified muscle activation - *solid thick black line*. (b) Muscle force (*dashed black line*) and modified muscle force (*solid black line*) are plotted above, traces of normalized muscle length plotted below.

CHAPTER 4

Discussion

4.1. Experiments on skeletal muscle

The thesis aimed at investigating skeletal muscle history effects and extending a general muscle model by introducing the phenomenon present in every movement.

The study was initiated by a set of concentric contractions, where shortenings of different length magnitudes and velocities lead to depression of the isometric force following the active length change. The investigation disproved the generally accepted relation between the force depression and the velocity or amount of muscle shortening (Sugi and Tsuchiya 1988; Josephson and Stokes 1999; Herzog et al. 2000). Force depression showed positive correlation with the shortening velocity for a fixed shortening time but not for a fixed amount of shortening, Figure 3.1(a1,b1). The mechanical work done by the muscle during active shortening was suggested as a new predictive parameter for the force depression, Figure 3.1(a2,b2). This measure has been associated with force depression in several studies, (Ruiter et al. 1998; Granzier and Pollack 1989), but the first systematic investigation of the possible relationship was performed by Herzog et al. (2000).

Motivated by the initial results, a wider investigation was conducted. A variety of lengthening and shortening ramps and combinations of those indicated the mechanical work produced by and on the muscle to be a good predictor for both force depression after shortening and force enhancement after lengthening. The mechanical work depends on both magnitude and velocity of the length variation. This measure accumulates during all kinds of movements and this history effect exists in all non-isometric muscle contractions.

The study gives a basis for improvement of the muscular force description used in the muscle models. A majority of the models compute the muscular force using only the current parameters and omit the feature of the muscle to reflect the preceding length variations in the resulting force. The history effect can be easily added to the Hill-type model as the mechanical work W scaled with a muscle-specific coefficient K_{hist} and the current muscle activation level A.

Besides the modelling goal, the findings are important in explaining the mechanisms underlying the history phenomena. Herzog et al. (2000) suggested that mechanical work needed for actin filament deformation during shortening is related to the evoked force depression. They also stated that the rate of cross-bridge cycling and hence ATP consumption is higher during shortening than during isometric contraction, pointing at the metabolic nature of the history effect (Herzog et al. 2000; Allen

et al. 2008). When testing maximally stimulated soleus and EDL muscles, a scaling coefficient K_{hist} appeared to be about 2 times larger for EDL than for soleus. This observation confirms the hypothesis of the metabolic nature of the force modification because the ATP consumption during contractions is remarkably faster in EDL than in soleus muscles (Barclay et al. 1993).

The passive force modification observed after the contractions seems to be explained by the muscle fiber structure rather than by the metabolism because it is not related to the velocity of contraction nor to the mechanical work, Fig. 5 in Paper 1 and Fig. 5 in Paper 2 (Joumaa et al. 2008). Passive force modification was not considered for modelling in this thesis.

To create a basis for a numerical muscle model, the timing aspects of force production were obtained from an exponential fitting of the force-time traces and the state-space diagrams (Paper 4). Both methods gave similar time constants, thereby confirming the exponential nature of force development (Stein et al. 1982; Hancock et al. 2004; Corr and Herzog 2005). Soleus muscle reaches tetanus in twice the time as the EDL muscle, corresponding to the main characteristics of slow and fast muscle fibers composing the studied muscles (Luff 1981; Ranatunga 1982; Stein et al. 1982; Brooks and Faulkner 1988).

The time constants of isometric force development were similar ($\pm 30\%$) to the ones of force redevelopment after shortening and lengthening. This observation can be explained by a relatively fast process of muscle activation, or Ca^{2+} uptake, preceding force development in pure isometric contraction. The state-space diagrams make it possible to evaluate times for the muscle force rate rise and fall, i.e. times between the stimulation change (0/100%) and the beginning of an exponential phase for the force. These time intervals can be related to muscle activation and deactivation aspects.

In the study of mice with rheumatoid arthritis, a marked decrease in muscle force per cross-sectional area was shown for mice muscles with CIA. The shortening velocity at zero load also decreased for CIA muscles, reflecting the cycling rate of the cross-bridges. The contractile dysfunction was not accompanied by decrease in sarcoplasmic reticulum $[Ca^{2+}]_i$ release, but rather by $[Ca^{2+}]_i$ uptake thereby demonstrating the impaired cross-bridge function. Higher redox modifications in myofibrillar proteins of CIA muscles are most likely the consequence of increased peroxynitrite production. Overall, these results suggest a harmful effect of peroxynitrite-derived radicals on cross-bridge function in the soleus muscle of mice with CIA.

A previous study showed that treatment with a metalloporphyrin, which has peroxynitrite-scavenging activity, ameliorates septic contractile dysfunction in the diaphragms of rats (Nin et al. 2004). Interestingly, it has been reported that peroxynitrite scavenging markedly reduces both arthritis incidence and severity in murine CIA (Mabley et al. 2002), but further studies are required to reveal whether this treatment also improves muscle function.

4.2. Modelling of skeletal muscle

The main application of the results obtained from experimental studies is modelling of human musculoskeletal movements (Zajac 1989). Modelling of this complex system

requires assumptions and simplifications regarding geometric architecture, cell and tissue mechanics (Winters 1995). However, modern technologies allow the research to consider more details and features thereby bringing the field of biomechanics to a higher level, and making the applications widely applicable in medicine (Arnold et al. 2001; Wang et al. 2010; Wang and Gutierrez-Farewik 2011), sport (Seyfarth et al. 2002), ergonomics (Christensen et al. 2003) and robotics (Duysens et al. 2002; Haeufle et al. 2011). Solving optimisation problems is computationally time-consuming and the muscle models are therefore often very simple (Ren et al. 2007; Eriksson 2008; Pettersson et al. 2010; Eriksson and Svanberg 2011). Improvements of the muscle models should be described by very simple formulas to retain models suitable for solving optimisation problems with a detailed geometry.

Beginning with the muscle-tendon complex, the force is seen as the muscle response to variation of the length and the excitation induced by motor units. The principal muscle model by Günther et al. (2007) was adapted for soleus mouse muscle and enhanced with the history component. The force enhancement and force depression phenomena lead to isometric force change up to 10% in non-vulnerable contractions and can last for several seconds (Gielen and Houk 1987). With this impact on the force generation, the phenomena should be accounted for. Due to the simple formula used to describe this complex phenomenon, the modification has not prolonged the required simulation time significantly, where instantaneous postures were analysed.

The simulated force generation showed a good similarity with the experimental traces of both isometric and non-isometric contractions. Due to a notable variance in the results for active lengthening and peculiarity of eccentric contractions, simulation of a stretch phase diverges the most from the experiments. However, a specific mechanism of eccentric force simulation based on a recruitable elastic titin spring was proposed (Till et al. 2008; Rode et al. 2009a). Twenty parameters were required to be adjusted for the model. The subset of muscle-specific values was reduced to a number of four. It is interesting that many of the parameters fitted for piglet plantar flexors by Günther et al. (2007) could be unchanged for mouse soleus and EDL muscles. This fact demonstrates a wide applicability of this and similar muscular models. However, additional experiments and precise adjustment of the parameters will of course refine the model.

In the whole body model, interaction of the muscle excitation and the muscle force dominates. The history phenomena in voluntary contractions is not merely force depression or force enhancement; the activation modification arises as a response to alterations in metabolic processes. When modelling musculoskeletal movements, the system is represented by actuators (muscles) and places of action (attachment points on bones). To reproduce a specific movement, a quasi-static dynamic equilibrium is solved to follow kinematics data, and an optimal set of forces is then computed by optimising muscle activations.

An open-source software OpenSim was used for simulations of a squat and a standing heel-raise. The forces and preliminary activations were solved using built-in functions. The history phenomena could not be added to the muscle forces because they would lead to an incorrect movement. The muscle activations were therefore

modified to reflect the subtraction of an approximate force modification term. The modified activations have shown a better fit with the recorded EMG data, suggesting the correctness of the method.

Inversely, assuming that the activations are valid, the force modification was added to the output forces to illustrate the possible effect of the history phenomena if the neural system does not predict it. For the chosen history coefficient, the force changed up to 15% and the modification was consistent with the knowledge acquired (Ruiter et al. 1998; Lee and Herzog 2003; Oskouei and Herzog 2005).

Modifications of muscular force and activation were proposed in Paper 5 to supplement the muscle model with the history effect as follows:

$$F + (1 - c) \cdot dF_{\mathrm{mod}} = \Big((A - c \cdot dA_{\mathrm{mod}}) \cdot F_{\mathrm{lv}}(l, \dot{l}) + F_{\mathrm{passive}}(l) \Big) \cdot \cos(\alpha), \quad (4.1)$$

where $c \in [0, 1]$ defines a balance between force modification dF_{mod} and activation modification dA_{mod} induced by active muscle length variations and motor control. In the current study we assumed that $c = 1$, i.e. the brain has full control of the force generation and adjusts the activation level so that the force is not influenced by the length variations. In fact, $c = 1$ had to be used in the current study since it was not possible to apply the modified equation in the computed muscle control analysis. An example of $c = 0$ is when the central nervous system does not consider the history effect, for instance when *in vitro* stimulation at a constant activation is performed. Referring to study by Seiberl et al. (2012) wherein both activation and force were modified after active stretch, we speculate that coefficient c might possess any value between 0 and 1 depending on the extent to which the brain predicts and responds to the active muscle length variation leading to the history effect.

CHAPTER 5

Conclusion

5.1. Conclusion

Performed studies confirm the presence of active and passive force modification following contraction with various length changes. The results show that muscular force does not only depend on length and its time differential. The steady-state force also takes into account the accumulated length history, as shown in transient-length contractions. Our results indicate that the mechanical work produced by or on the muscle during length variation is a good general predictor for the steady-state force modification induced by transient-length contractions. The experimental analysis allowed us to specify the time constants of the exponential functions describing isometric force redevelopment after non-isometric contractions. The muscle activation times calculated from the state-space diagrams were in agreement with the generally accepted muscle properties, thereby demonstrating the reliability of the method.

The results from the physiological experiments served as a basis for an improved description of the muscular force production, with respect to both attainable force level and timing aspects. A Hill-type model was implemented and enhanced with a history component representing the effect of muscular force modification following non-isometric contractions. The history effect has also been added in inverse dynamic evaluations of musculoskeletal motions. The distinctive feature of the history phenomena to be reflected on both force and activation of the muscle was presented and discussed in the final study.

5.2. Outlook

The widely used numerical muscular models do not take several important aspects into account. A more precise formulation of the muscle force production is required for modelling force development under different stimulation and length regimes. More accurate muscle models will particularly contribute to human movement analysis techniques. A precise musculoskeletal model considering significant muscle phenomena lends confidence to using computer techniques for treatment of patients with locomotor disorders, e.g. surgery planning and postoperative supervision. Optimisation techniques may benefit body movement simulations if an extensive muscle model is employed. Accurate musculoskeletal models can help to understand and to discover a more effective performance in sport biomechanics.

The history modification investigated and applied in muscle models during this doctoral study requires the history coefficient as a muscle-specific parameter. The

history coefficient was evaluated for mouse soleus and EDL muscles during *in vitro* experiments, Papers 2 and 4. Due to limitations of the available techniques, the same method should probably be used for identifying the history coefficients of different human muscles accurately. It would be interesting to study whether this coefficient can be unique after scaling to muscle fiber composition, PCSA, optimal length and/or force, and if one constant is valid between individuals and species.

The inclusion of the modified muscle model in real dynamic simulations will surely benefit the outcome, but the performance might be affected. The history demands work evaluation at every timestep. Moreover, an additional parameter should be transmitted to the next step. Choosing the initial conditions will then affect the result, so the simulations should begin when the muscles are deactivated or have not performed active movements after a relaxation state. Some modelling techniques require optimisation through the whole time period, in which cases evaluating and transferring the modification component depending on current muscle force and activation may prolong total calculation. An optimistic fact is the growing computer capacity which enables complicated computations.

Concerning motor control, which was not studied in detail in this thesis, a relation between muscle activation and muscle force should include the history. As was discussed above, the history effect may affect both the excitation and the resulting force. In voluntary contractions the motor control system can respond to preceding contractions into account and regulates the signal in order to achieve the desired movement. Based on this supposition, the optimised movement, i.e. absolutely controlled, should introduce history in activation only.

If the motor control system does not totally consider the gained 'memory', the prospective motion will be in some way awkward. Smoothness in performance of the movements could be a measure of motor control quality. Perhaps in some situations the brain does not adjust the neural signal accurately, for instance, when a performed movement is new or sudden, with an increased load or velocity, or under the influence of the circumstances.

Summary of Papers

Paper 1

A series of concentric contraction experiments on mice muscles was performed. The results show that the steady-state muscular force following active shortening does not reach the maximum isometric force associated with the final muscle length. Isolated mouse extensor digitorum longus and soleus muscles were used to investigate the force generation. The muscles were pre-stimulated at fixed lengths, shortened and then held isometrically to give maximum post-shortening forces, before de-stimulation. The mechanical work during active shortening was evaluated by integrating the product of force and shortening velocity over the shortening period. The main finding is a positive relation between the force depression and the mechanical work, whereas the force depression was not correlated to the velocity of shortening. Depression of the passive force component was also observed following all stimulations. Experiments show that the fully stimulated redevelopment of isometric force following concentric contraction follows a time function similar to the creation of force when isometric muscle is initially stimulated. The conclusion is that the isometric force development after active shortening can be well described by an asymptotic force which depends on the produced work and the initial isometric time constant.

Paper 2

Transient force production during various non-isometric contractions was investigated. Isolated extensor digitorum longus and soleus muscles from mice were used to investigate the force produced by a muscle, and some parameters hypothetically influencing this history-dependent force modification. The muscles were pre-stimulated at a fixed length, then different lengthening/shortening episodes were introduced, whereafter changes of the active force were recorded while the muscles were held isometrically to approach a steady-state force before de-stimulation. The mechanical work during active lengthening and shortening was evaluated by integrating the product of force and ramp velocity over the length-varying period. The results show a negative linear correlation between the force modification and the mechanical work produced on or by the muscle, continuous between shortening and lengthening. A corresponding modification of the passive force component following each stimulation was also observed. The conclusion is that the isometric force attained after lengthening or shortening is well described by an asymptotic force which is determined by the mechanical work.

Paper 3

The study investigates functions of mice soleus muscles with collagen-induced arthritis (CIA) and possible reasons of the disease. Rheumatoid arthritis leads to progressive muscle weakness. Contractile properties of the whole muscle and concentration of free Ca^{2+} in muscle fibers should be examined. The underlying mechanisms of contractile dysfunction were assessed by investigating redox modifications using Western blotting and antibodies against some enzymes and organic compounds. The tetanic force per cross-sectional area was markedly decreased in the soleus muscle of mice with CIA, and the change was not due to a decrease in the amplitude of $[Ca^{2+}]_i$ transients. The reduction in force production was accompanied by slowing of the twitch contraction and relaxation and a decrease in the maximum shortening velocity. Immunoblot analyses showed changes which favor peroxynitrite formation. These findings and other alterations show impaired contractile function in the soleus muscle of mice with CIA and suggest that this abnormality is due to peroxynitrite-induced modifications in myofibrillar proteins.

Paper 4

The study aimed at evaluating muscle parameters for a detailed description of muscular force generation. The experimental data from paper 2 was used to study force production during non-isometric contractions. State-space diagrams were used to investigate the timing aspects of force production, showing a dominant exponential nature of the force development in isometric phases of the contractions. The timing of force production calculated from the state-space diagrams was in agreement with the generally accepted muscle properties, thereby demonstrating the reliability of the new method. A macroscopic muscular model consisting of a contractile element (CE), parallel and series elastic elements (PEE, SEE) was developed and adapted for SOL mouse muscles. The history effect and the timings obtained from the state-space diagrams gave better simulation results for SOL mouse muscles in a variety of length regimes.

Paper 5

The objective of the study was to apply the history effect in a musculoskeletal model. The muscle force modification was added to the open-source software OpenSim using an application programming interface. An improved muscle model depending on the preceding contractile events together with the current parameters was applied in dynamic simulations of heel-raise in upright position and squat movements, using as a basis the activation patterns obtained from the software, with its common implicit activation-force expressions. For the studied movements, the history gives a small but visible effect to the muscular force trace. The modification improves the existing muscle models and is significant especially for simulations of fast movements with load.

Acknowledgements

My deep gratitude to my supervisor Professor Anders Eriksson for leading me through the doctoral studies, for sharing his knowledge, for motivating without demands, for inspirations by being satisfied with any result, for his optimism and guidance. I would thank Professor Håkan Westerblad from Karolinska Institutet for sharing his deepest knowledge in the field of muscle physiology. Thanks to Dr. Elena Gutierrez-Farewik for her never-ceasing energy and ideas.

A special thanks to Ruoli, Zeinab, Eva, Robert, Krishna, Seif and all my colleagues in our research group and at the Mechanics Department for the friendly environment. Thanks to Takashi, Shi-Jin and other colleagues at Karolinska Institutet and Astrid Lindgrens sjukhuset, who made my work there cheerful.

I gratefully acknowledge the Swedish Research Council for the opportunity to fulfil the Doctoral study in Stockholm.

My school math teachers and University lecturers deserve a special mention here for preparing me for the doctoral studies. My appreciation to the dearest S.M. Bauer from SPbSU for being my adviser for many years.

Thanks to all my friends for the joy beyond the studies.

I express my gratitude to my parents for the way you brought me up and educated, otherwise I would never achieve this degree. And finally I thank my husband for his love, delight and support. Thanks to my little son for the pleasure he does for me without realising yet.

Bibliography

Abbott, B., Aubert, X., 1952. The force exerted by active striated muscle during and after change of length. Journal of Physiology 117, 77–86.

Allen, D., Lamb, G., Westerblad, H., 2008. Skeletal muscle fatigue: cellular mechanisms. Physiological Reviews 88, 287–332.

Altenburg, T., Ruiter, C. D., Verdijk, P., Mechelen, W. V., Haan, A. D., 2008. Vastus lateralis surface and single motor unit emg following submaximal shortening and lengthening contractions. Applied Physiology, Nutrition, and Metabolism 33(6), 1086–1095.

Anderson, F., Pandy, M., 1999. A dynamic optimization solution for vertical jumping in three dimensions. Computer Methods in Biomechanics and Biomedical Engineering 2(3), 201–231.

Arnold, A., Blemker, S., Delp, S., 2001. Evaluation of a deformable musculoskeletal model for estimating muscle-tendon lengths during crouch gait. Annals of Biomedical Engineering 29, 263–274.

Asmussen, G., Maréchal, G., 1989. Maximal shortening velocities, isomyosins and fibre types in soleus muscle of mice, rats and guinea-pigs. Journal of Physiology 416, 245–254.

Bagni, M., Cecchi, G., Colombini, B., 2005. Crossbridge properties investigated by fast ramp stretching of activated frog muscle fibres. Journal of Physiology 565(1), 261–268.

Bagni, M., Cecchi, G., Colombini, B., Colomo, F., 2002. A non-cross-bridge stiffness in activated frog muscle fibers. Biophysical Journal 82, 3118–3127.

Barclay, C., Constable, J., Gibbs, C., 1993. Energetics of fast- and slow-twitch muscles of the mouse. Journal of Physiology 472, 61–80.

Bradford, M., 1976. A rapid and sensitive method for the quantitation of microgram quantities of protein utilizing the principle of protein-dye binding. Analytical Biochemistry 72, 248–254.

Brooks, S., Faulkner, J., 1988. Contractile properties of skeletal muscles from young, adult and aged mice. Journal of Physiology 404, 71–82.

Bullimore, S., Leonard, T., Rassier, D., Herzog, W., 2007. History-dependence of isometric muscle force: Effect of prior stretch or shortening amplitude. Journal of Biomechanics 40, 1518–1524.

Burke, R., Edgerton, V., 1975. Motor unit properties and selective involvement in movement. Exercise and sport sciences reviews 3(1), 31.

Chaffin, D., Andersson, G., 1991. Occupational biomechanics. Wiley, New York.

Christensen, S., Siebertz, K., Damsgaard, M., de Zee, M., Rasmussen, J., Paul, G., 2003. Human seat modeling using inverse dynamic musculo-skeletal models. SAE Technical Paper 2003-01-2221.

Corr, D., Herzog, W., 2005. Force recovery after activated shortening in whole skeletal muscle: Transient and steady-state aspects of force depression. Journal of Applied Physiology 99(1), 252–260.

Delp, S., Anderson, F., Arnold, A., Loan, P., Habib, A., John, C., Thelen, E. G. D., 2007. Opensim: open-source software to create and analyze dynamic simulations of movement. IEEE Transactions on Biomedical Engineering 54(11), 1940–1950.

Delp, S., Loan, J., 1995. A graphics-based software system to develop and analyze models of musculoskeletal structures. Computers in Biology and Medicine 25(1), 21–34.

Delp, S., Loan, J., Hoy, M., Zajac, F., Topp, E., Rosen, J., 1990. An interactive graphics-based model of the lower extremity to study orthopaedic surgical procedures. IEEE Transactions on Biomedical Engineering 37(8), 757–767.

Duysens, J., de Crommert, H. V., Smits-Engelsman, B., der Helm, F. V., 2002. A walking robot called human: Lessons to be learned from neural control of locomotion. Journal of Biomechanics 35(4), 447–453.

Ebashi, S., Endo, M., 1968. Calcium ion and muscle contraction. Progress in Biophysics and Molecular Biology 18, 123–166.

Edman, K., Caputo, C., Lou, F., 1993. Depression of tetanic force induced by loaded shortening of frog muscle fibres. Journal of Physiology 466, 535–552.

Edman, K., Elzinga, G., Noble, M., 1978. Enhancement of mechanical performance by stretch during tetanic contractions of vertebrate skeletal muscle fibres. Journal of Physiology 281, 139–155.

Epstein, M., Herzog, W., 1998. Theoretical models of skeletal muscle: biological and mathematical considerations. Wiley, New York.

Eriksson, A., 2008. Optimization in target movement simulations. Computer Methods in Applied mechanics and Engineering 197(49-50), 4207–4215.

Eriksson, A., Svanberg, K., 2011. Optimization in simulations of human movement planning. International Journal for Numerical Methods in Engineering 87(12), 1127–1147.

Fagan, J., Sleczka, B., Sohar, I., 1999. Quantitation of oxidative damage to tissue proteins. The International Journal of Biochemistry & Cell Biology 31, 751–757.

Finni, T., Komi, P. V., Lukkariniemi, J., 1998. Achilles tendon loading during walking: application of a novel optic fiber technique. European Journal of Applied Physiology and Occupational Physiology 77(3), 289–291.

Forcinito, M., Epstein, M., Herzog, W., 1998. Can a rheological muscle model predict force depression/enhancement? Journal of Biomechanics 31(12), 1093–1099.

Fry, A., Allemeier, C., Staron, R., 1994. Correlation between percentage fiber type area and myosin heavy chain content in human skeletal muscle. European Journal of Applied Physiology and Occupational Physiology 68, 246–251.

Funatsu, T., Higuchi, H., Ishiwata, S., 1990. Elastic filaments in skeletal muscle revealed by selective removal of thin filaments with plasma gelsolin. Journal of Cell Biology 110, 53–62.

Gielen, C., Houk, J., 1987. A model of the motor servo: incorporating nonlinear spindle receptor and muscle mechanical properties. Biological Cybernetics 57, 217–231.

Gordon, A., Huxley, A., Julian, F., 1966. The variation in isometric tension with sarcomere length in vertebrate muscle fibers. Journal of Physiology 184, 170–192.

Granzier, H., Pollack, G., 1989. Effect of active pre-shortening on isometric and isotonic performance of single frog muscle fibres. Journal of Physiology 415, 299–327.

Günther, M., Schmitt, S., Wank, V., 2007. High-frequency oscillations as a consequence of neglected serial damping in Hill-type muscle models. Biological Cybernetics 97(1), 63–79.

Haeufle, D., Gunther, M., Blickhan, R., Schmitt, S., 2011. Proof of concept of an artificial muscle: Theoretical model, numerical model, and hardware experiment.

Hahn, D., Seiberl, W., Schwirtz, A., 2007. Force enhancement during and following muscle stretch of maximal voluntarily activated human quadriceps femoris. European Journal of Applied Physiology 100(6), 701–709.

Hamill, J., Knutzen, K., 2008. Biomechanical Basis of Human Movement, 3rd Edition. Lippincott Williams & Wilkins, New York.

Hancock, W., Martin, D., Huntsman, L., 2004. Ca^{2+} and segment length dependence of isometric force kinetics in intact ferret cardiac muscle. Circulation Research 73(4), 603–611.

Happee, R., 1994. Inverse dynamic optimization including muscular dynamics, a new simulation method applied to goal directed movements. Journal of Biomechanics 27(7), 953–960.

Hatze, H., 1977. A myocybernetic control model of skeletal muscle. Biological Cybernetics 25(2), 103–119.

Hermens, H., Freriks, B., Merletti, R., Stegeman, D., Blok, J., Rau, G., Disselhorst-Klug, C., Hägg, G., 1999. European recommendations for surface electromyography. Roessingh Research and Development, Enschede, the Netherlands.

Herzog, W., 2000. Skeletal muscle mechanics: from mechanisms to function. Wiley, New York.

Herzog, W., 2005. Force enhancement following stretch of activated muscle: Critical review and proposal for mechanisms. Medical and Biological Engineering and Computing 43(2), 173–180.

Herzog, W., Lee, E., Rassier, D., 2006. Residual force enhancement in skeletal muscle. Journal of Physiology 574(3), 635–642.

Herzog, W., Leonard, T., 1997. Depression of cat soleus forces following isokinetic shortening. Journal of Biomechanics 30(9), 865–872.

Herzog, W., Leonard, T., 2005. The role of passive structures in force enhancement of skeletal muscles following active stretch. Journal of Biomechanics 38, 409–415.

Herzog, W., Leonard, T., Joumaa, V., Mehta, A., 2008. Mysteries of muscle contraction. Journal of Applied Biomechanics 24(1), 1–13.

Herzog, W., Leonard, T., Wu, J., 2000. The relationship between force depression following shortening and mechanical work in skeletal muscle. Journal of Biomechanics 33(5), 659–668.

Hill, A., 1938. The heat of shortening and the dynamic constants of muscle. Proceedings of the Royal Society of London 126, 136–195.

Hill, A., 1970. First and last experiments in muscle mechanics. Cambridge University Press, Cambridge, U.K.

Hirofuji, C., Ishihara, A., Itoh, K., Itoh, M., Taguchi, S., Takeuchi-Hayashi, H., 1992. Fibre type composition of the soleus muscle in hypoxia-acclimatised rats. Journal of Anatomy 181(2), 327–333.

Horowits, R., Podolsky, R. J., 1987. The postional stability of thick filaments in activated skeletal muscle depends on sarcomere length: evidence for the role of titin filaments. Journal of Cell Biology 105, 2217–2223.

Huxley, A., 1957. Muscle structure and theories of contraction. Progress in Biophysics and biophysical Chemistry 7, 255–318.

Huxley, A., Niedergerke, R., 1954. Structural changes in muscle during contraction; interference microscopy of living muscle fibres. Nature 173, 971.

Huxley, H., Hanson, J., 1954. Changes in the cross-striations of muscle during contraction and stretch and their structural interpretation. Nature 173, 973.

Josephson, R., Stokes, D., 1999. Work-dependent deactivation of a crustacean muscle. Journal of Experimental Biology 202(18), 2551–2565.

Joumaa, V., Rassier, D., Leonard, T., Herzog, W., 2008. The origin of passive force enhancement in skeletal muscle. American Journal of Physiology - Cell Physiology 294(1), C74–C78.

Julian, F., Morgan, D., 1979. The effect on tension of non-uniform distribution of length changes applied to frog muscle fibres. Journal of Physiology 293, 379–392.

Kokkola, R., Li, J., Sundberg, E., Aveberger, A., Palmblad, K., Yang, H., Tracey, K., Andersson, U., Harris, H., 2003. Successful treatment of collagen-induced arthritis in mice and rats by targeting extracellular high mobility group box chromosomal protein 1 activity. Arthritis & Rheumatism 48(7), 2052–2058.

Lännergren, J., 1978. The force-velocity relation of isolated twitch and slow muscle fibres of xenopus laevis. Journal of Physiology 283, 501–21.

Lee, H., Herzog, W., 2003. Force depression following muscle shortening of voluntarily activated and electrically stimulated human adductor pollicis. Journal of Physiology 551, 993–1003.

Lee, H.-D., Suter, E., Herzog, W., 1999. Force depression in human quadriceps femoris following voluntary shortening contractions. Journal of Applied Physiology 87(5), 1651–1655.

Lieber, R., Fridén, J., 2000. Functional and clinical significance of skeletal muscle architecture. Muscle Nerve 23(11), 1647–1666.

Lloyd, D., Besier, T., 2003. An emg-driven musculoskeletalmodel to estimate muscle forces and knee joint moments in vivo. Journal of Biomechanics 36(6), 765–776.

Lou, F., Curtin, N., Woledge, R., 1998. Contraction with shortening during stimulation or during relaxation: How do the energetic costs compare? Journal of Muscle Research and Cell Motility 19(7), 797–802.

Luff, A., 1981. Dynamic properties of the inferior rectus, extensor digitorum longus, diaphragm and soleus muscles of the mouse. Journal of Physiology 313, 161–171.

Mabley, J., Liaudet, L., Pacher, P., Southan, G., Groves, J., Salzman, A., Szabó, C., 2002. Part ii: beneficial effects of the peroxynitrite decomposition catalyst fp15 in murine models of arthritis and colitis. Molecular Medicine 8(10), 581–590.

Magi, B., Liberatori, S., 2005. Immunoblotting techniques. In: Burns, R. (Ed.), Immunochemical Protocols. Vol. 295 of Methods in Molecular Biology. Humana Press, Department of Molecular Biology, University of Siena, Siena, Italy, pp. 227–253.

Marechal, G., Plaghki, L., 1979. The deficit of the isometric tetanic tension redeveloped after a release of frog muscle at a constant velocity. Journal of General Physiology 73(4), 453–467.

McGill, S., 1992. A myoelectrically based dynamic three-dimensional model to predict loads on lumbar spine tissues during lateral bending. Journal of Biomechanics 25, 395–414.

Morgan, D., 2007. Can all residual force enhancement be explained by sarcomere non-uniformities? Journal of Physiology 578(2), 613–615.

Morgan, D., Whitehead, N., Wise, A., Gregory, J., Proske, U., 2000. Tension changes in the cat soleus muscle following slow stretch or shortening of the contracting muscle. Journal of Physiology 522(3), 503–513.

Murray, M., Guten, G., Baldwin, J., Gardner, G., 1976. A comparison of plantar flexion torque with and without the triceps surae. Acta Orthopaedica 47(1), 122–124.

Needham, D., 1971. Machina Carnis. Cambridge University Press, Cambridge, U.K.

Nigg, B., Herzog, W., 1999. Biomechanics of the musculo-skeletal system. Wiley, Chichester, England.

Nin, N., Cassina, A., Boggia, J., Alfonso, E., Botti, H., Peluffo, G., Trostchansky, A., Batthyány, C., Radi, R., Rubbo, H., Hurtado, F., 2004. Septic diaphragmatic dysfunction is prevented by mn(iii) porphyrin therapy and inducible nitric oxide synthase inhibition. Intensive Care Medicine 30, 2271–2278.

Nurhussen, F., 2006. Experimental studies on mouse slow and fast twitch muscles. Lic. thesis, KTH Mechanics, Royal Institute of Technology, Stockholm.

Örtqvist, M., Gutierrez-Farewik, E., Farewik, M., Jansson, A., Bartonek, Å., Broström, E., 2007. Reliability of a new instrument for measuring plantarflexor muscle strength. Archives of Physical Medicine and Rehabilitation 88(9), 1164–1170.

Oskouei, A., Herzog, W., 2005. Observations on force enhancement in submaximal voluntary contractions of human adductor pollicis muscle. Journal of Applied Physiology 98(6), 2087–2095.

Palastanga, N., Field, D., Soames, R., 2002. Anatomy and human movement: structure and function, 4th Edition. Elsevier Health Sciences, New York.

Peter, J., Barnard, R., Edgerton, V., Gillespie, C., Stempel, K., 1972. Metabolic profiles of three fiber types of skeletal muscle in guinea pigs and rabbits. Biochemistry 11(14), 2627–2633.

Pettersson, R., Nordmark, A., Eriksson, A., 2010. Free-time optimization of targeted movements based on temporal FE approximation. Proceedings CST2010, Valencia.

Ranatunga, K., 1982. Temperature-dependence of shortening velocity and rate of isometric tension development in rat skeletal muscle. Journal of Physiology 329, 465–483.

Rassier, D., Herzog, W., 2002. Force enhancement following an active stretch in skeletal muscle. Journal of Electromyography and Kinesiology 12(6), 471–477.

Razumova, M., Bukatina, A., Campbell, K., 1999. Stiffness-distortion sarcomere model for muscle simulation. Journal of Applied Physiology 87, 1861–1876.

Ren, L., Jones, R., Howard, D., 2007. Predictive modelling of human walking over a complete gait cycle. Journal of Biomechanics 40(7), 1567–1574.

Rode, C., Siebert, T., Blickhan, R., 2009a. Titin-induced force enhancement and force depression: A 'sticky-spring' mechanism in muscle contractions? Journal of Theoretical Biology 259(2), 350–360.

Rode, C., Siebert, T., Herzog, W., Blickhan, R., 2009b. The effects of parallel and series elastic components on estimated active cat soleus muscle force. Journal of Mechanics in Medicine and Biology 9(1), 105–122.

Ruiter, C. D., Haan, A. D., Jones, D., Sargeant, A., 1998. Shortening-induced force depression in human adductor pollicis muscle. The Journal of Physiology 507(2), 583–591.

Schachar, R., Herzog, W., Leonard, T., 2002. Force enhancement above the initial isometric force on the descending limb of the force-length relationship. Journal of Biomechanics 35(10), 1299–1306.

Schachar, R., Herzog, W., Leonard, T., 2004. The effects of muscle stretching and shortening on isometric forces on the descending limb of the force-length relationship. Journal of Biomechanics 37(6), 917–926.

Schuind, F., Garcia-Elias, M., Cooney, W., An, K.-N., 1992. Flexor tendon forces: In vivo measurements. The Journal of Hand Surgery 17(2), 291–298.

Scott, W., Stevens, J., Binder-Macleod, S., 2001. Human skeletal muscle fiber type classifications. Physical Therapy 81(11), 1810–1816.

Seiberl, W., Hahn, D., Herzog, W., Schwirtz, A., 2012. Feedback controlled force enhancement and activation reduction of voluntarily activated quadriceps femoris during sub-maximal muscle action. Journal of Electromyography and Kinesiology 22, 117–123.

Seyfarth, A., Geyer, H., Günther, M., Blickhan, R., 2002. A movement criterion for running. Journal of Biomechanics 35(5), 649–655.

Stebbins, J., Harrington, M., Thompson, N., Zavatsky, A., Theologis, T., 2006. Repeatability of a model for measuring multi-segment foot kinematics in children. Gait Posture 23(4), 401–410.

Stein, R., Gordon, T., Shrive, J., 1982. Temperature dependence of mammalian muscle contractions and atpase activities. Biophysical Journal 40(2), 97–107.

Sugi, H., Tsuchiya, T., 1988. Stiffness changes during enhancement and deficit of isometric force by slow length changes in frog skeletal muscle fibres. Journal of Physiology 407, 215–229.

Svantesson, U., Grimby, G., Thomeé, R., 1994. Potentiation of concentric plantar flexion torque following eccentric and isometric muscle actions. Acta Physiologica Scandinavica 152(3), 287–193.

Thelen, D., Anderson, F., 2006. Using computed muscle control to generate forward dynamic simulations of human walking from experimental data. Journal of Biomechanics 39, 1107–1115.

Thelen, D., Anderson, F., Delp, S., 2003. Generating dynamic simulations of movement using computed muscle control. Journal of Biomechanics 36, 321–328.

Till, O., Siebert, T., Rode, C., Blickhan, R., 2008. Characterization of isovelocity extension of activated muscle: A hill-type model for eccentric contractions and a method for parameter determination. Journal of Theoretical Biology 255(2), 176–187.

van Soest, A., Bobbert, M., 1993. The contribution of muscle properties in the control of explosive movements. Biological Cybernetics 69(3), 195–204.

Wang, R., Gutierrez-Farewik, E., 2011. The effect of subtalar inversion/eversion on the dynamic function of the tibialis anterior, soleus, and gastrocnemius during the stance phase of gait. Gait Posture 34(1), 29–35.

Wang, R., Thur, S., Gutierrez-Farewik, E., Broström, E., 2010. One year follow-up after operative ankle fractures: A prospective gait analysis study with a multi-segment foot model. Gait Posture 31(2), 234–240.

Wernig, A., Irintchev, A., Weisshaupt, P., 1990. Muscle injury, cross-sectional area and fibre type distribution in mouse soleus after intermittent wheel-running. Journal of Physiology 428, 639–652.

Winters, J., 1995. How detailed should muscle models be to understand multi-joint movement coordination? Human Movement Science 14(4-5), 401–442.

Yoshioka, T., Higuchi, H., Kimura, S., Ohashi, K., Umazume, Y., Maruyama, K., 1986. Effects of mild trypsin treatment on the passive tension generation and connectin splitting in stretched skinned fibers from frog skeletal muscle. Biomedical Research 7, 181–186.

Zajac, F., 1989. Muscle and tendon: properties, models, scaling, and application to biomechanics and motor control. Critical Reviews in Biomedical Engineering 17(4), 359–411.
Zajac, F., Topp, E., Stevenson, P., 1986. A dimensionless musculotendon model. pp. 601–604.

Part II

Papers

(Papers are given in slightly re-formatted manuscript versions)

1

Paper 1

Muscular force production after concentric contraction

By Natalia Kosterina[1], Håkan Westerblad[2], Jan Lännergren[2] and Anders Eriksson[1]

[1] Department of Mechanics, Royal Institute of Technology, SE-100 44 Stockholm, Sweden
[2] Department of Physiology and Pharmacology, Karolinska Institutet, Stockholm, Sweden

Journal of Biomechanics
7 August 2008 (Vol. 41, Issue 11, Pages 2422–2429)

The steady-state force following active shortening does not reach the maximum isometric force associated with the final length. Isolated extensor digitorum longus and soleus muscles from mice (NMRI strain) were used to investigate the force produced by a muscle, and some parameters hypothetically influencing this shortening-induced force depression. The muscles were pre-stimulated at fixed length, shortened and then held isometrically to give maximum post-shortening forces, before de-stimulation. The shortening magnitude was 0.18 mm, 0.36 mm or 0.72 mm (about 2-7% of optimal length), time of shortening was chosen as 0.03 s, 0.06 s and 0.12 s, and final length as +0.72, 0 and -0.72 mm, related to optimal length. The mechanical work during active shortening was evaluated by integrating the product of force and shortening velocity over the shortening period. The results show a positive correlation between the force depression and the mechanical work, whereas the force depression was not correlated to the velocity of shortening. Depression of the passive force component was also observed following all stimulations. Experiments show that the fully stimulated redevelopment of isometric force following concentric contraction follows a time function similar to the creation of force when isometric muscle is initially stimulated. The conclusion is that the isometric force development after active shortening can be well described by an asymptotic force which is decided by the produced work, and the initial isometric time constant.

Keywords: Mouse muscles; Concentric contractions; Force depression; History dependence; Muscular work

1. Introduction

The main function of the skeletal muscle is to provide force during walking, running and other everyday actions. Muscles generate work during activities and produce movement, and it is important to know the mechanisms underlying such processes as muscle shortening and stretching. In particular, the understanding of transient force production under various length regimes is a necessity for improved description of muscular action in numerical simulations of movement, (Eriksson 2008; Kaphle and Eriksson 2008).

One important aspect is the history dependence in force production. For instance, the steady-state force following concentric contraction does not reach the maximum isometric force associated with the final length. This property is typically referred to as shortening-induced force depression, (Abbott and Aubert 1952). It has been generally accepted that this depression is increasing with increasing shortening magnitude, (Abbott and Aubert 1952; Herzog and Leonard 1997; Lou et al. 1998; Schachar et al. 2004; Bullimore et al. 2007). Furthermore, force depression is long lasting, (Herzog et al. 1998), and is associated with a decrease in the muscle stiffness, (Sugi and Tsuchiya 1988; Razumova et al. 1999; Lee and Herzog 2003). Moreover, it is argued that force depression is directly influenced by the speed of shortening (Marechal and Plaghki 1979; Sugi and Tsuchiya 1988; Herzog and Leonard 1997; Morgan et al. 2000; Lee and Herzog 2003). The latter opinion is based on experiments in which a muscle was shortened by a given magnitude and with a given stimulation, but at different speeds. There is a similar force modification following active stretch of the muscle, as the redeveloped force is higher than the isometric force: force enhancement, (Schachar et al. 2002; Rassier and Herzog 2002; Bagni et al. 2005; Herzog 2005). Muscular force consists of active and passive components, and both active and passive force modification occurs with shortening or stretch.

The present work was motivated by efforts towards numerical modeling of muscular force production, as discussed by Eriksson (2008). In this context, a general description of transient macroscopic muscle force production was seen as:

$$F(t) = \overline{F}(l, \dot{l}, a; t) + dF(h; t), \tag{1}$$

where 'transient' indicates a time-dependence, and 'macroscopic' that the force is seen in an external context, without un-necessary internal phenomenological details. The first term in the equation is thereby the part predicted by, e.g., a Hill-type model. Many such models have been developed, e.g., Günther et al. (2007), but they all lack memory for previous contractions, Forcinito et al. (1998). The aim of the present investigation was to find a basis for creation of the second term, which is a symbolic description of a correction to the force, due to history effects. In Eq. (1), the force F at a time t is related to a force value $\overline{F}$ dependent on the current muscle length l, the current time differential of the length $\dot{l}$, and a stimulation measure a, which is essential but not investigated here. In the force modification dF, the history parameter h reflects parameters for the individual muscle (optimal muscle length, maximum isometric force, etc.) and the context (experimental or live-state description). In the post-shortening isometric situation, the only transient effects in a Hill-type numerical model, which are related to the length variation of the contractile component of the model, disappear, and only the differences shown by the second term remain. After concentric contractions, this is what is commonly denoted as the force depression F_{dep}. In Fig. 1a force depression is seen as the difference between the redeveloped force following active shortening and the force of purely isometric contraction at the same length, both seen in a hypothetical long-term state, neglecting that fatigue effects will reduce the force.

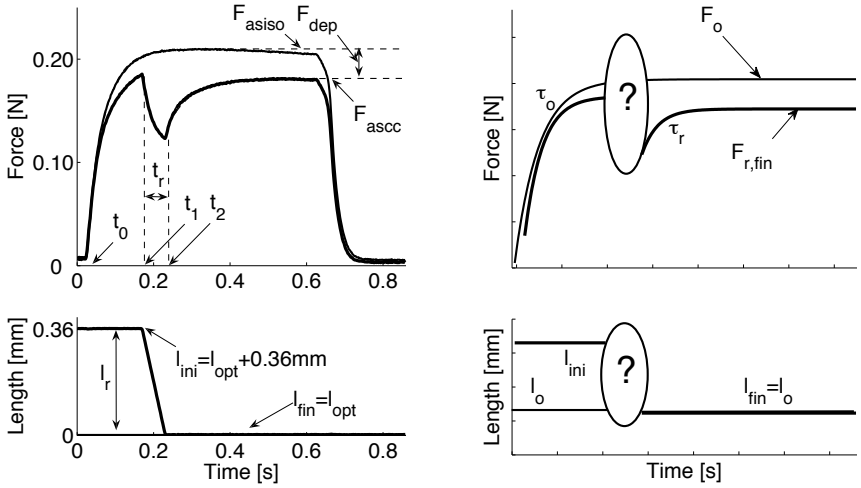

FIGURE 1. Schematic illustration of studied contractions. (a) example of force trace for stimulated mouse EDL muscle held isometrically for 0.6 s; stimulated isometrically for $t_1 - t_0 = 0.15$ s, shortened by $l_\mathrm{r} = 0.36$ mm during $t_\mathrm{r} = t_2 - t_1 = 0.06$ s and then held isometrically for 0.39 s. $\mathrm{F_{asiso}}$ and $\mathrm{F_{ascc}}$ are asymptotic values for the muscular force production after isometric and concentric contractions, respectively. (b) evaluation model for force production in initial and post-shortening isometric phases (shortening phase is not evaluated). $\mathrm{F_o}$ and $\mathrm{F_{r,fin}}$ are values for the muscular force production after isometric and concentric contractions, respectively. τ_o and τ_r are time constants describing force-time relations at length l_o during isometric and post-shortening isometric contractions, respectively. Length expressed as difference to optimal length.

Modeling post-shortening force is, however, not only a question of a steady-state value, as force produced by a muscle will show a time variation essential in a numerical simulation of movement. In the present context, this is visible between the reduced force at the end of a concentric contraction and the steady-state isometric force at the final length. The assumption here was that the time variation can be approximately represented by an asymptotic force and a time evolution function. In the interpretation of experiments, the time function was assumed to be an exponential, described by a time constant, Fig. 1b and Eq. (2).

The objective of the present study was to investigate asymptotic value and time constant for the muscular force production after concentric contractions of different parameters. Representative values for a description of the post-shortening force variation were sought through systematic shortening experiments on mouse muscles, in different muscular length regions.

2. Materials and methods

2.1. *Animals*

Adult male mice (NMRI strain) were housed at room temperature and fed ad libitum. The weight of the mice was about 30 g. Animals were killed by rapid neck disarticulation. The experiments were approved by the Stockholm North local ethical committee.

2.2. *Muscle preparation and mounting*

Experiments were performed on isolated extensor digitorum longus (EDL) and soleus (SOL) muscles. Only one EDL and one SOL muscle was used from each mouse in order to avoid statistical dependence effects, but also due to constraints on experimental time. Small stainless steel hooks were tied, using a thin nylon thread, to the tendons very close (~ 0.1 mm) to the muscle belly. The muscle was then mounted between a force transducer, Dual-Mode Muscle Lever System (Aurora Scientic, Ontario, Canada), and an adjustable holder in a lab-built muscle bath. The muscle was manually stretched by separating the mountings until it began to produce a passive force. This muscle length was thereby close to the optimal length allowing maximum active isometric force.

The weight of the muscle was measured after the experiments. A nominal cross-sectional area was evaluated from tissue density ρ =1056 kg/m^3 and the individual optimal muscle length.

The final results are based on results from n $= 4$ EDL muscles and n $= 5$ SOL muscles, and are given as mean $\pm$ standard deviation. Optimal forces were $F_{\text{opt}} = 0.237 \pm 0.072$ N for EDL and $F_{\text{opt}} = 0.215 \pm 0.028$ N for SOL muscles. Optimal lengths were 11.73 ± 1.14 mm and 11.18 ± 1.12 mm, and cross-sectional areas were 1.11 ± 0.10 mm^2 and 1.37 ± 0.44 mm^2, respectively.

During the experiment, the muscle was bathed in a continuously stirred Tyrode solution of the following composition (all in mM): 121 NaCl, 5 KCl, 0.5 $MgCl_2$, 1.8 $CaCl_2$, 0.4 NaH_2PO_4, 0.1 NaEDTA, 24 $NaHCO_3$, 5.5 glucose. Fetal calf serum (0.2%) was added to the solution. The solution was bubbled with $95\%O_2/5\%CO_2$ (pH 7.4). Experiments were performed at room temperature ($\sim 24°C$); at this temperature the contraction timing of mouse muscles is similar to human muscles at body temperature ($\sim 37°C$).

Testing of each muscle was initiated following at least 30 minutes of rest after mounting, and took about 3 hours, with at least one minute of rest between stimulations.

2.3. *Experimental design, stimulation and registration*

A prescribed length variation scheme was applied to the muscle; the precision in a desired length was ~ 0.01 mm. Stimulations with trains of supramaximal square current pulses (0.5 ms) were applied via platinum plate electrodes at specified frequencies (100 Hz for EDL and 70 Hz for SOL), previously found to give tetanic contraction.

Stimulation patterns and length variations were controlled via computer and the Spike2 software (CED, Cambridge, UK). Records of stimulation, force and muscle length were stored for further analysis in a computer, with sampling frequency 500 Hz.

Isometric tests were first performed to find the optimal muscle length for each specimen. This was done through stretching the muscles by small steps, stimulating it, and noting the maximum force produced and the passive force (1 s after stimulation) at every length, the difference being the active force. The highest active force, F_{opt}, defined an optimum length, l_{opt}, which was used as basis for the length variations in subsequent experiments. It was verified that the isometric force varied approximately parabolically around the optimal length. Lengths l were defined as a difference to individual optimal length.

2.4. *Testing paradigm*

The testing sequence was designed to see force as function of length, rather than vice versa. Force produced by the muscle was therefore measured as function of time, for prescribed variations in specimen length. By choosing suitable final muscle length, l_{fin}, ramp size, l_r, and ramp time, t_r, (Fig. 1a), different combinations of length and velocity were obtained. Isometric contractions are special cases with $l_r = 0$.

The central experiments in the series were the concentric contractions. The muscles were fist passively lengthened to $l_{\text{ini}} = l_{\text{fin}} + l_r$. The EDL and SOL muscles were isometrically stimulated for $t_1 - t_0$ =150 ms and 500 ms, respectively, before shortening, in order to give an almost maximum pre-shortening isometric force. Total stimulation times were 600 ms and 1500 ms, respectively, limited in order to avoid fatigue effects. Passive forces were measured 1 s after stimulation at length l_{fin}. A pure shortening ramp without sudden initial steps was used, in order to show time evolution of force in different length regimes, cf. Barclay and Lichtwark (2007).

Three sets of experiments were performed on all muscles. In the first series, final muscle length was equal to the optimum length $l_{\text{fin}} = 0$, the others used $l_{\text{fin}} = +0.72$ mm and $l_{\text{fin}} = -0.72$ mm, respectively.

Ramp size l_r and ramp times t_r were chosen systematically to allow comparisons of steady-state active force modifications. Thus, l_r was 0.18 mm, 0.36 mm and 0.72 mm, and t_r was 0.03 s, 0.06 s and 0.12 s; all nine combinations were tested creating shortening velocities $1.5 \leq l_r/t_r \leq 24$ mm/s (corresponding to between ~ 0.15 and $\sim 2.4\ l_{\text{opt}}$/s). For each muscle, 27 contractions were therefore recorded, being the combinations of three ramp sizes, three ramp times and three final lengths. Isometric tests were done at optimal length after every nine shortening experiments, to verify that the force output remained stable.

2.5. *Evaluation procedure*

The force-time histories recorded were fitted by exponential functions, through an in-house equal weights least-squares algorithm in Matlab (version R2006a, The MathWorks, Inc., Natick, MA, USA), with a view on the experiments as in Fig. 1b, giving

expressions of the form:

$$F(t) = F_{\text{r,fin}} + (F_{\text{a}} - F_{\text{r,fin}}) \cdot \exp(-1/\tau_r \cdot (t - t_2)), \tag{2}$$

where F_{a}, $F_{\text{r,fin}}$, and $1/\tau_r$ were results from fitting for a phase starting at time t_2. The equation defines an exponential curve for F, starting at $F = F_a$ at time $t = t_2$, and with $F = F_{\text{r,fin}}$ as the long term asymptote as $t \rightarrow \infty$. The redeveloped isometric force-time trace between end of ramp and end of stimulation was considered.

A similar evaluation of force evolution was performed for isometric cases at lengths l_{fin}, until maximum force was reached. Similarly as in Eq. (2), isometric asymptotic forces F_{o}, $F_{\text{o,+}}$ and $F_{\text{o,-}}$ were obtained for the three final lengths, with $F_{\text{o}} \approx F_{\text{opt}}$. Isometric force development gave exponential time constants τ_{o}, $\tau_{\text{o,+}}$, $\tau_{\text{o,-}}$.

From the obtained values, the steady-state force depression was evaluated. In each series of experiments, the force depression F_{dep} was obtained as the difference between the asymptotic redeveloped isometric force following shortening and the asymptotic isometric force for the current final length, Fig 1b, as:

$$F_{\text{dep}} = -(F_{\text{r,fin}} - F_{\text{o}}) - F_{\text{dep,p}}. \tag{3}$$

The active depression of the muscular force was obtained by subtracting the passive parts, measured at the post-stimulation phases at l_{fin}, from $F_{\text{r,fin}}$ and F_{o}. A depression in passive force was evaluated as the reduction in passive force 1 s after stimulation, according to:

$$F_{\text{dep,p}} = -(F_{\text{fin,p}} - F_{\text{o,p}}) \tag{4}$$

where $F_{\text{fin,p}}$ is the passive force 1 s after the concentric contraction, and $F_{\text{o,p}}$ the passive force after isometric contraction.

Mechanical work produced by the muscle during shortening was evaluated by integrating the force multiplied by shortening velocity, over the ramp period:

$$W = \int_{l_{\text{ini}}}^{l_{\text{fin}}} F\, dl \equiv -\int_{t_1}^{t_1+t_r} F(t) \frac{dl}{dt} dt \tag{5}$$

where the second of the equivalent forms was used for evaluation. The integral was evaluated numerically through all recorded force values in the considered interval. Negative work from passive force during initial stretching to l_{ini} was not considered.

3. Results

Examples of total force and length traces in EDL and SOL muscles, for optimal, superoptimal and suboptimal final muscle lengths are given in Fig. 2. The force representing the maximal sustained output was reached or almost reached before shortening was introduced. During active shortening, force rapidly decreased, and once shortening was completed, force recovered and attained a new steady-state value. This new steady-state force was consistently smaller than the corresponding isometric reference force, regardless of the ramp conditions.

The exponential fitting showed good agreement with experimental data for isometric force development and force redevelopment after active shortening ($R^2 > 0.99$) (Hancock et al. 2004; Corr and Herzog 2005).

Figure 3 shows average active force depressions after shortening as functions of shortening velocity. Lines are drawn in the figures to connect experiments with either the same ramp time t_r (a), or the same ramp size l_r, (b). Average force depression is similarly plotted as function of average mechanical work in Fig. 4, showing good correlation in all situations.

The experiments at superoptimal and suboptimal final lengths gave similar relations between force depression, mechanical work and rise time constants as the cases with optimal final length.

Passive force was consistently slightly lower after both isometric and concentric contractions, but redeveloped during the rest between experiments. For concentric cases, the difference was more pronounced, indicating a passive force depression. The average passive force depression, $F_{\text{dep,p}}$, is plotted in Fig. 5 for EDL and SOL muscles with $l_{\text{fin}} = 0$ mm, $l_{\text{fin}} = -0.72$ mm and $l_{\text{fin}} = +0.72$ mm.

4. Discussion

The main objective of this work was to evaluate the reliability of some proposed descriptions for the steady-state force depression, i.e., a modification following concentric contraction. This force depression shows that muscular force is not — even asymptotically — described by only the first term of Eq. (1).

The results show that the shortening velocity is not a good predictor for this depression. This was verified by sets of experiments, where the velocities were produced through different combinations of ramp size and time, but with the same final isometric length. Figures 3a show that the force depression F_{dep} is positively correlated with the shortening velocity l_r/t_r when varying the ramp size, with a constant ramp time, as suggested by Sugi and Tsuchiya (1988); Herzog and Leonard (1997); Josephson and Stokes (1999); Herzog et al. (2000); Leonard and Herzog (2005); Herzog and Leonard (2007). This hypothesis is, however, contradicted by the experiments where different velocities were introduced by varying the ramp time at a constant ramp size. This is consistent with results observed in a variety of other preparations. The conclusion is that not only the shortening velocity but also the shortening magnitude must be an important parameter for the force depression, and the ramp size is not, in itself, a good predictor, as was suggested by Bullimore et al. (2007) with a stress-induced inhibition of crossbridges as explanation.

A measure which considers both magnitude and velocity of shortening is the mechanical work, W, produced by the muscular force during shortening. This measure gives positive correlation with the force depression for performed experiments, as shown by Fig. 4. This relation was also suggested by Josephson and Stokes (1999), and tentatively by Herzog et al. (2000), although the hypothesis in the latter seems to have been later discarded by Bullimore et al. (2007). Although clear for the present experiments, further experiments with other length and stimulation paradigms are needed in order to verify the generality of this correlation.

The motivation for the tentative statement in Herzog et al. (2000), that force-depression was predicted by mechanical work, was related to the amount of work needed in actin filament deformation during shortening. It can also be dependent on

the metabolic changes. For instance, the rate of cross-bridge cycling, and hence the rate of ATP consumption, is higher during shortening than under isometric conditions. This leads to a more rapid breakdown of phosphocreatine during shortening, resulting in an increased concentration of phosphate ions, which tends to decrease isometric force production (Allen et al. 2008).

It is seen from Figures 3 and 4 that the EDL muscles, for all ramp parameters, give a force depression which is considerably larger then the corresponding one for SOL, although the length and force scales are very similar. Introducing a proportional function for the relation between the force depression measure F_{dep}/F_o and the mechanical work, it is seen that the proportionality constant is about 2.5 times higher for EDL than for SOL. This difference fits with the idea that the force depression is caused by metabolic factors, because the rate of ATP consumption during contractions is markedly faster in EDL than in SOL muscles (Barclay et al. 1993).

Figure 5 shows that the passive force depression is essentially independent of the parameters and the mechanical work performed in the concentric contraction experiments. This is clearly different to the active force depression, which depends on the mechanical work. As discussed above, the active force depression is likely to depend on metabolic factors and these factors would then not affect the passive force depression. Titin is a molecular spring that runs from the Z lines of sarcomeres to the M band, and it is the structure responsible for most of the passive force in muscle cells (Joumaa et al. 2008). There is an increase in passive force when contracting muscles are being stretched, i.e. the opposite to what is observed here. Titin has a central role in the stretched-induced enhancement of passive force (Joumaa et al. 2008) and it is possible that titin is also involved in the present passive force depression. Thus, our concentric contractions resulted in a reversible decrease in passive force that seems unrelated to energy metabolism, but the underlying mechanisms remain uncertain.

The rise time constant of redeveloped muscle force, τ_r, is shown to be, for practical simulation purposes, similar to the time constant for initial isometric contractions at optimal length, τ_o (Fig 6). This indicates that when the muscles are stimulated with a high intensity, the rising of the Ca^{2+} level and subsequent activation of the actin filament during the force development phase is a considerably faster process than the cross-bridge cycling leading to increased force. Once fully activated, the increase in force production occurs at the same rates, regardless of whether a shortening has just ended. This statement seems to be verified by both muscle types, but the EDL muscles show a time constant about one-third of that for SOL muscles. Time constants are in the experiments almost independent of isometric length.

The experiments clearly show that a macro expression for transient muscular force such as Eq. (1) must not only take length l and length differential $\dot{l}$ into account. Following concentric contractions, it is obvious that steady-state force also shows a history dependence, which can symbolically be seen as the second term in Eq. (1). With this indication, the functional parameter and dependence remain to be investigated. Whether a common description of the force modification is possible, valid for all contraction histories and expressed in basic muscular macro-parameters

such as optimal length, maximum isometric force and inherent time scales, is an open question.

5. Conclusions

Experiments show that shortening velocity is not a good general predictor for the force modification following concentric contraction. They indicate that steady-state force depression is better predicted by the mechanical work produced by the muscle during active shortening.

The isometric force development after active shortening can be well described by an asymptotic force which is decided by the produced work, and the initial isometric time constant.

Conflict of interest statement

None declared

Acknowledgements

The authors gratefully acknowledge technical support in preparing muscle specimens from Shi-Jin Zhang, and financial support from the Swedish Research Council.

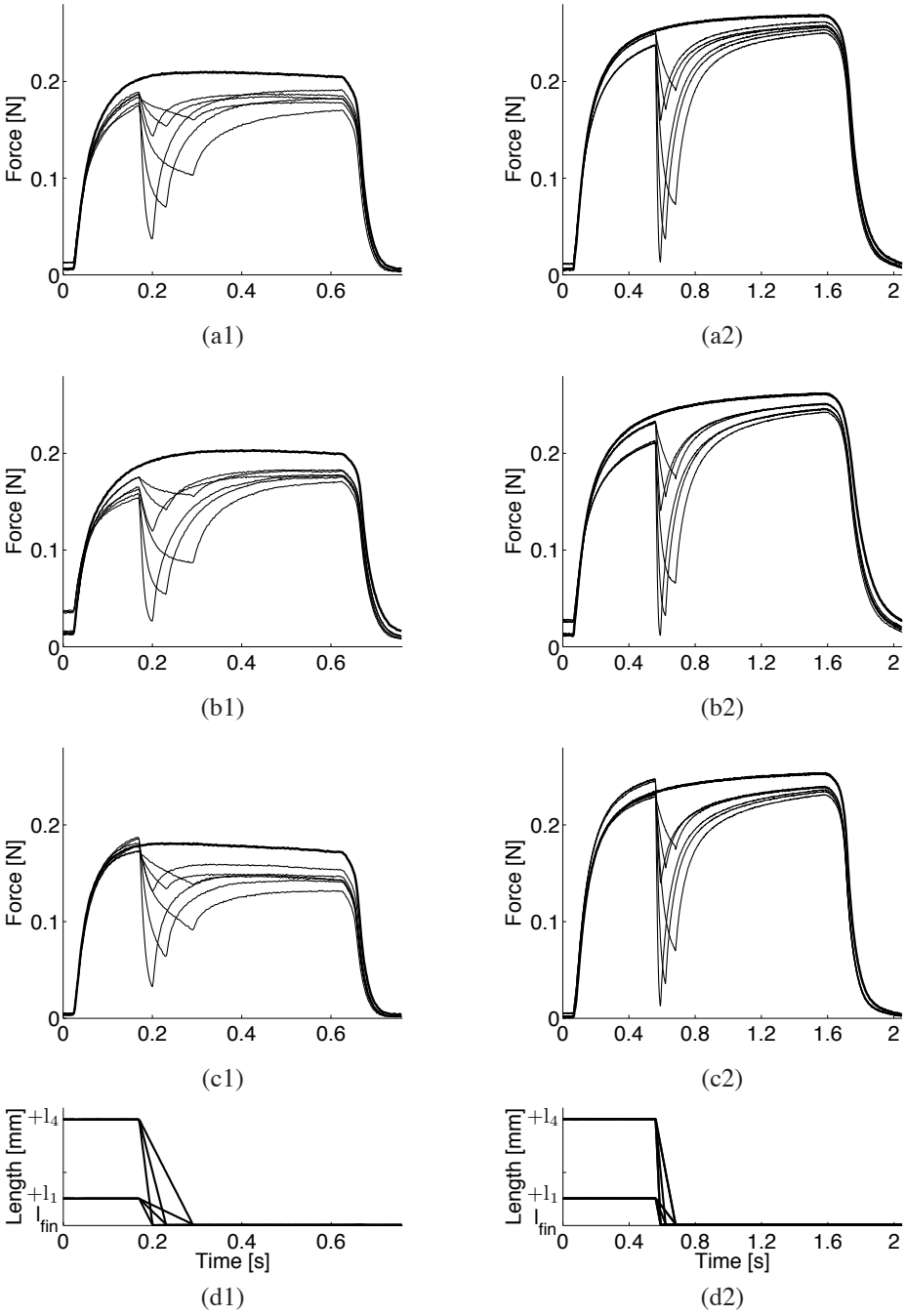

FIGURE 2. Examples of active shortening of mouse EDL (1) and SOL (2) muscles with a) optimal, b) superoptimal and c) suboptimal final muscle length: $l_{\text{fin}} = 0, +0.72, -0.72$ mm, respectively. Shortening lengths $l_{\text{r}} = 0.18, 0.72$ mm, shortening times $t_{\text{r}} = 0.03, 0.06, 0.12$ s.

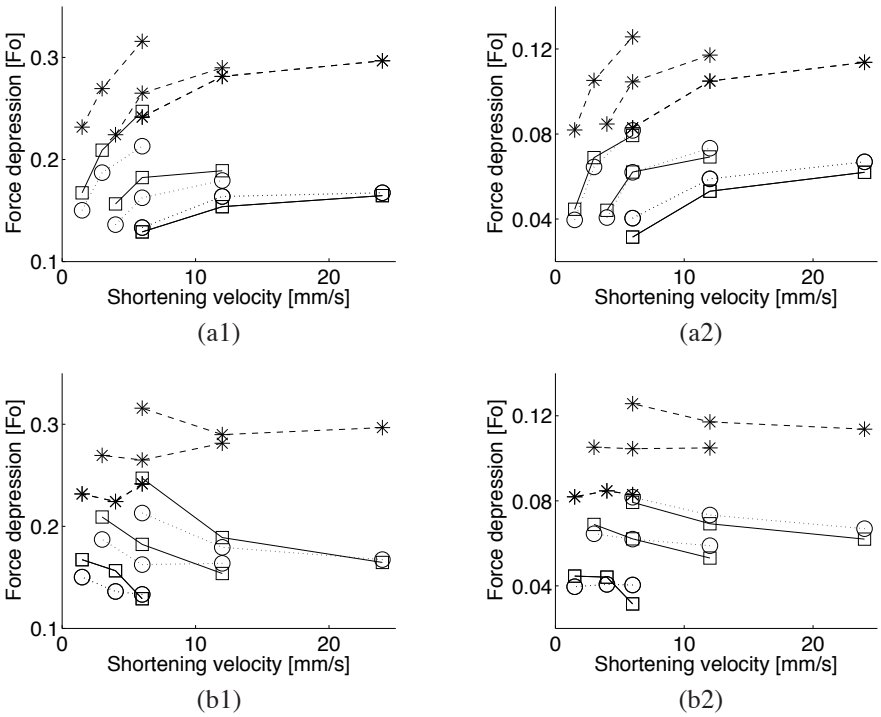

FIGURE 3. Steady-state force depression as a function of shortening velocity of mouse EDL (1) and SOL (2) muscles. Lines connect groups of experiments with the same a) shortening time, t_r, or b) shortening length, l_r. Square, circle and star markers correspond to experiments with optimal, superoptimal and suboptimal final muscle lengths: $l_{\text{fin}} = 0, +0.72, -0.72$ mm, respectively. Average value for group (n_{EDL}=4, n_{SOL}=5).

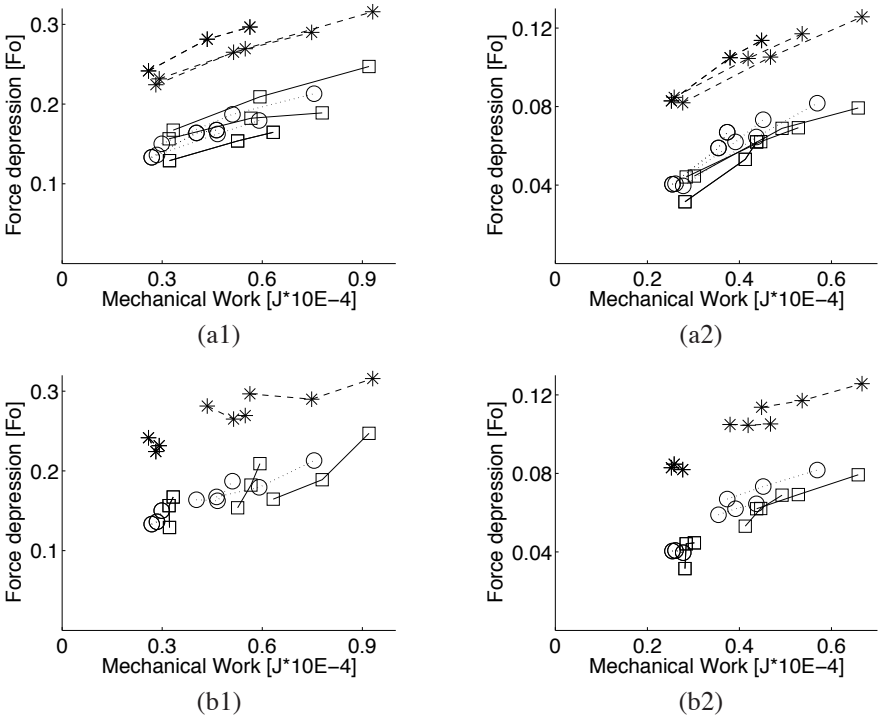

FIGURE 4. Steady-state force depression as a function of mechanical work of mouse EDL (1) and SOL (2) muscles. Lines connect groups of experiments with the same a) t_r, b) l_r. Square, circle and star markers correspond to experiments with optimal, superoptimal and suboptimal final muscle lengths:$l_{\text{fin}} = 0, +0.72, -0.72$ mm, respectively. Average value for group (n_{EDL}=4, n_{SOL}=5).

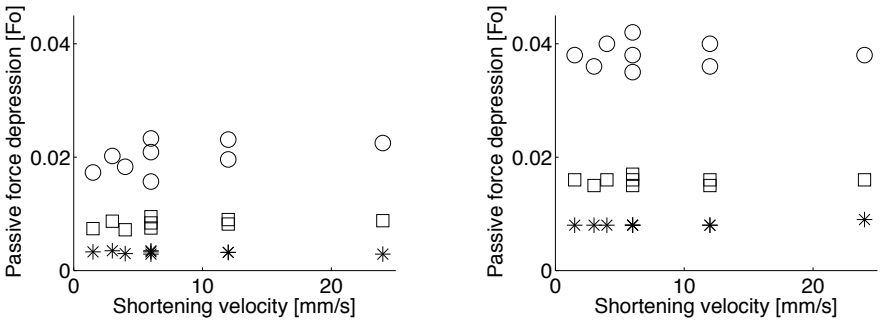

FIGURE 5. Passive force depression $F_{\text{dep,p}}$, $F_{\text{dep,p,+}}$ and $F_{\text{dep,p,}-}$, normalized with respect to active isometric force at a corresponding length, as a function of shortening velocity of mouse EDL (1) and SOL (2) muscles. Square, circle and star markers correspond to experiments with optimal, superoptimal and suboptimal final muscle lengths: $l_{\text{fin}} = 0, +0.72, -0.72$ mm, respectively. Average value for group (n_{EDL}=4, n_{SOL}=5).

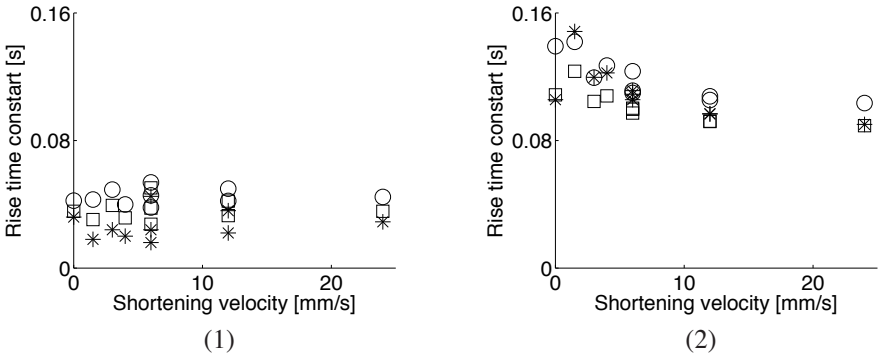

FIGURE 6. Rise time constants for isometric force development, τ_{o}, $\tau_{\text{o,+}}$, $\tau_{\text{o,-}}$ (shortening velocity $= 0$), and post-shortening isometric force redevelopment, τ_r, $\tau_{r,+}$, $\tau_{r,-}$, as a function of shortening velocity of mouse EDL (1) and SOL (2) muscles. Square, circle and star markers correspond to experiments with optimal, superoptimal and suboptimal final muscle lengths: $l_{\text{fin}} = 0, +0.72, -0.72$ mm, respectively. Average value for group (n_{EDL}=4, n_{SOL}=5).

References

Abbott, B., Aubert, X., 1952. The force exerted by active striated muscle during and after change of length. Journal of Physiology 117, 77–86.

Allen, D., Lamb, G., Westerblad, H., 2008. Skeletal muscle fatigue: cellular mechanisms. Physiological Reviews 88, 287–332.

Bagni, M., Cecchi, G., Colombini, B., 2005. Crossbridge properties investigated by fast ramp stretching of activated frog muscle fibres. Journal of Physiology 565 (1), 261–268.

Barclay, C., Lichtwark, G., 2007. The mechanics of mouse skeletal muscle when shortening during relaxation. Journal of Biomechanics 40(14), 3121–3129.

Barclay, C. J., Constable, J. K., Gibbs, C. L., 1993. Energetics of fast- and slow-twitch muscles of the mouse. Journal of Physiology 472, 61–80.

Bullimore, S., Leonard, T., Rassier, D., Herzog, W., 2007. History-dependence of isometric muscle force: Effect of prior stretch or shortening amplitude. Journal of Biomechanics 40, 1518–1524.

Corr, D., Herzog, W., 2005. Force recovery after activated shortening in whole skeletal muscle: Transient and steady-state aspects of force depression. Journal of Applied Physiology 99(1), 252–260.

Eriksson, A., 2008. Optimization in target movement simulations. Computer Methods in Applied mechanics and Engineering(accepted).

Forcinito, M., Epstein, M., Herzog, W., 1998. Can a rheological muscle model predict force depression/enhancement? Journal of Biomechanics 31(12), 1093–1099.

Günther, M., Schmitt, S., Wank, V., 2007. High-frequency oscillations as a consequence of neglected serial damping in hill-type muscle models. Biological Cybernetics 97(1), 63–79.

Hancock, W., Martin, D., Huntsman, L., 2004. Ca2+ and segment length dependence of isometric force kinetics in intact ferret cardiac muscle. Circulation research 73(4), 603–611.

Herzog, W., 2005. Force enhancement following stretch of activated muscle: Critical review and proposal for mechanisms. Medical and Biological Engineering and Computing 43(2), 173–180.

Herzog, W., Leonard, T., 1997. Depression of cat soleus forces following isokinetic shortening. Journal of Biomechanics 30(9), 865–872.

Herzog, W., Leonard, T., 2007. Residual force depression is not abolished following a quick shortening step. Journal of Biomechanics 40, 2806–2810.

Herzog, W., Leonard, T., Wu, J., 1998. Force depression following skeletal muscle shortening is long lasting. Journal of Biomechanics 31, 1163–1168.

Herzog, W., Leonard, T., Wu, J., 2000. The relationship between force depression following shortening and mechanical work in skeletal muscle. Journal of Biomechanics 33(5), 659–668.

Josephson, R., Stokes, D., 1999. Work-dependent deactivation of a crustacean muscle. Journal of Experimental Biology 202(18), 2551–2565.

Joumaa, V., Rassier, D. E., Leonard, T. R., , Herzog, W., 2008. The origin of passive force enhancement in skeletal muscle. American Journal of Physiology - Cell Physiology 294(1), C74–C78.

Kaphle, M., Eriksson, A., 2008. Optimality in forward dynamics simulations. Journal of Biomechanics 41(6), 1213–1221.

Lee, H., Herzog, W., 2003. Force depression following muscle shortening of voluntarily activated and electrically stimulated human adductor pollicis. Journal of Physiology 551, 993–1003.

Leonard, T., Herzog, W., 2005. Does the speed of shortening affect steady-state force depression in cat soleus muscle? Journal of Biomechanics 38(11), 2190–2197.

Lou, F., Curtin, N., Woledge, R., 1998. Contraction with shortening during stimulation or during relaxation: How do the energetic costs compare? Journal of Muscle Research and Cell Motility 19 (7), 797–802.

Marechal, G., Plaghki, L., 1979. The deficit of the isometric tetanic tension redeveloped after a release of frog muscle at a constant velocity. Journal of General Physiology 73(4), 453–467.

Morgan, D., Whitehead, N., Wise, A., Gregory, J., Proske, U., 2000. Tension changes in the cat soleus muscle following slow stretch or shortening of the contracting muscle. Journal of Physiology 522 (3), pp. 522(3), 503–513.

Rassier, D., Herzog, W., 2002. Force enhancement following an active stretch in skeletal muscle. Journal of Electromyography and Kinesiology 12(6), 471–477.

Razumova, M., Bukatina, A., Campbell, K., 1999. Stiffness-distortion sarcomere model for muscle simulation. Journal of Applied Physiology 87, 1861–1876.

Schachar, R., Herzog, W., Leonard, T., 2002. Force enhancement above the initial isometric force on the descending limb of the force-length relationship. Journal of Biomechanics 35(10), 1299–1306.

Schachar, R., Herzog, W., Leonard, T., 2004. The effects of muscle stretching and shortening on isometric forces on the descending limb of the force-length relationship. Journal of Biomechanics 37(6), 917–926.

Sugi, H., Tsuchiya, T., 1988. Stiffness changes during enhancement and deficit of isometric force by slow length changes in frog skeletal muscle fibres. Journal of Physiology 407, 215–229.

2

Paper 2

Mechanical work as predictor of force enhancement and force depression

By Natalia Kosterina[1], Håkan Westerblad[2] and Anders Eriksson[1]

[1] Department of Mechanics, Royal Institute of Technology, SE-100 44 Stockholm, Sweden
[2] Department of Physiology and Pharmacology, Karolinska Institutet, Stockholm, Sweden

Journal of Biomechanics
7 August 2009 (Vol. 42, Issue 11, Pages 1628–1634)

The steady-state force following active muscle shortening or stretch differs from the maximum isometric force associated with the final length. This phenomenon proves that the isometric force production is not only dependent on current muscle length and length time derivative, but depends on the preceding contraction history. Isolated extensor digitorum longus and soleus muscles from mice (NMRI strain) were used to investigate the force produced by a muscle, and some parameters hypothetically influencing this history-dependent force modification. The muscles were pre-stimulated at a fixed length, then different stretch/shortening episodes were introduced, whereafter changes of the active force were recorded while the muscles were held isometrically to approach a steady-state force before de-stimulation. The mechanical work during active stretch and shortening was evaluated by integrating the product of force and ramp velocity over the length-varying period. The results show a negative linear correlation between the force modification and the mechanical work produced on or by the muscle, continuous between shortening and stretch. A corresponding modification of the passive force component following each stimulation was also observed. The conclusion is that the isometric force attained after stretch or shortening is well described by an asymptotic force which is determined by the mechanical work.

Keywords: Mouse skeletal muscles; Transient-length contractions; Force depression; Stretch-shortening cycle; Force enhancement; History dependence; Muscular work

1. Introduction

Skeletal muscles generate work during activities and produce movement, and it is important to know the mechanisms underlying such processes as muscle shortening and stretch. In particular, the understanding of transient force production under various length regimes is a necessity for improved description of muscular action in numerical simulations of movement, (Kaphle and Eriksson 2008; Yamane and Nakamura 2007).

One important aspect is the history dependence of force production. For instance, the steady-state force following concentric contraction does not reach the maximum

isometric force associated with the final length. This property is typically referred to as shortening-induced force depression, (Abbott and Aubert 1952). It has been generally accepted that this depression is influenced by shortening magnitude, (Abbott and Aubert 1952; Herzog and Leonard 1997; Lou et al. 1998; Schachar et al. 2004; Bullimore et al. 2007) and speed of shortening (Marechal and Plaghki 1979; Sugi and Tsuchiya 1988; Herzog and Leonard 1997; Morgan et al. 2000; Lee and Herzog 2003). A previous paper by the authors (Kosterina et al. 2008) has shown that these descriptions are true, but only for a certain experimental paradigm. A more robust predictor of force depression was shown to be the mechanical work produced by the muscle during shortening.

There is a similar force modification following active stretch of the muscle, as the redeveloped force is higher than the isometric force: force enhancement, (Schachar et al. 2002; Rassier and Herzog 2002; Bagni et al. 2005; Herzog 2005; Morgan 2007). Muscular force consists of active and passive components, and both active and passive force modifications occur with shortening or stretch, (Bagni et al. 2002; Rassier and Herzog 2002; Joumaa et al. 2008; Herzog et al. 2008).

The present work was motivated by efforts towards numerical modeling of transient macroscopic muscular force production, Eriksson (2008). 'Transient' here indicates a time-dependence, and 'macroscopic' that the force is seen in an external context, without internal phenomenological details. The history dependence is thereby to be introduced as an additional component in, e.g., a Hill-type model. Many such models have been developed, e.g., Günther et al. (2007), but they normally lack memory for previous contractions, Forcinito et al. (1998). The aim of the present investigation was to find a basis for creation of a numerical description of a correction to the force, due to history effects. This will give a total expression for the force F at a time t, related to the Hill force value $\overline{F}$, which is dependent on the current muscle length l, the current time differential of the length $\dot{l}$, and a stimulation measure a, the latter essential but not investigated here. In the post-shortening and post-stretch isometric situations, the only transient effect in a Hill-type numerical model, which is related to the length variation of the contractile component of the model, disappears. In Fig. 1, force modification is seen as the difference between the redeveloped force following active non-isometric contraction and the force of purely isometric contraction at the same length, both seen in a hypothetical long-term state, neglecting that fatigue effects will reduce the force.

Modeling redeveloped force is, however, not only a question of a steady-state value, as force produced by a muscle will show a time variation. Consideration of this effect is essential in a numerical simulation of movement. In the present context, it is visible between the redeveloped force at the end of a length-modifying contraction and the steady-state isometric force at the final length. The assumption here was that the time variation can be approximately represented by an asymptotic force and a time evolution function. In the interpretation of experiments, the time function was assumed to be an exponential, described by a time constant.

In the present study, we hypothesize that force modification, both depression and enhancement, can be related to the amount of mechanical work performed by or on the

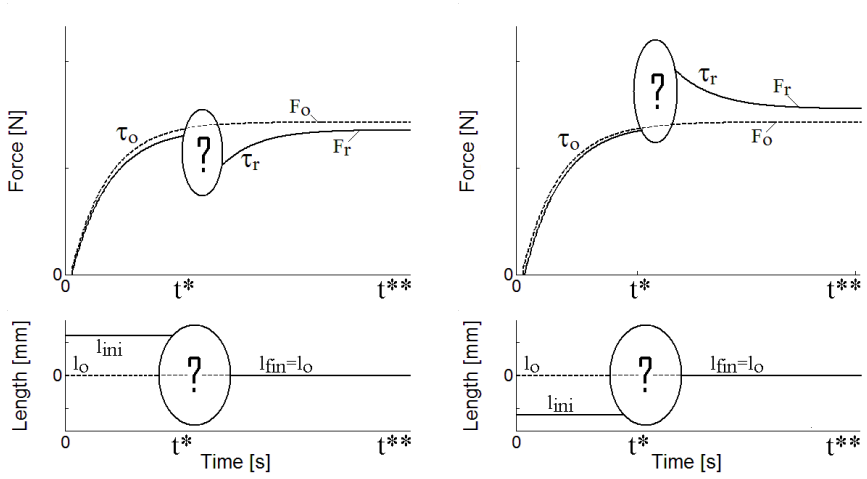

FIGURE 1. Schematic illustration of contractions studied. Evaluation model for force production in initial and (a) post-shortening or (b) post-stretch isometric phases (ramp phase is not evaluated). F_o and F_r are asymptotic values for the muscular force after isometric and transient-length contractions, respectively. τ_o and τ_r are time constants describing force-time relations at length l_o during isometric and post-ramp isometric contractions, respectively. Length expressed as difference to optimal length. The total force modification is the difference between F_r and F_o, consisting of active and passive parts.

muscle during the change of length. This statement is based on previous observations, Kosterina et al. (2008), based on investigations of force depression following concentric contractions. The objective of the present study was to investigate asymptotic values for the muscular force production after more general transient-length contractions of different parameters.

2. Materials and methods

2.1. *Animals*

Adult male mice (NMRI strain) were housed at room temperature and fed ad libitum. The weight of the mice was about 30 g. Animals were killed by rapid neck disarticulation. The experiments were approved by the Stockholm North local ethical committee.

2.2. *Muscle preparation and mounting*

Experiments were performed on isolated extensor digitorum longus (EDL) and soleus (SOL) muscles. Small stainless steel hooks were tied, using a thin nylon thread, to

the tendons very close (~ 0.1 mm) to the muscle belly. The muscle was then mounted between a force transducer, Dual-Mode Muscle Lever System (Aurora Scientic, Ontario, Canada), and an adjustable holder in a lab-built muscle bath. The muscle was manually stretched until it began to produce passive force. This muscle length was thereby close to the optimal length giving maximum tetanic isometric force.

During the experiment, the muscle was bathed in a continuously stirred Tyrode solution of the following composition (mM): 121 NaCl, 5 KCl, 0.5 $MgCl_2$, 1.8 $CaCl_2$, 0.4 NaH_2PO_4, 0.1 NaEDTA, 24 $NaHCO_3$, 5.5 glucose. Fetal calf serum (0.2%) was added to the solution. The solution was bubbled with $95\%O_2/5\%CO_2$ (pH 7.4). Experiments were performed at room temperature ($\sim 24°C$); at this temperature the contraction timing of mouse muscles is similar to human muscles at body temperature ($\sim 37°C$).

Testing of each muscle was initiated following at least 30 minutes of rest after mounting, the muscles were rested at least one minute between stimulations. Each muscle was subjected to a number of the length regimes discussed below; a set of experiments contained all parametric variations for that type of length regime. The sets were introduced in different orders for the specimen.

Isometric tests were done at optimal length after every set of experiments, to verify that the force output remained stable, otherwise data from the last set were discarded. The maximum admissible decrease in optimal force was specified as 10%, and mean final force drop averaged 4% for SOL and 8% for EDL muscles. A total of 10 SOL and 14 EDL muscles were tested, but final results for each set of experiments, as further discussed below, are based on results from n $= 4-6$ EDL muscles and n $= 5-6$ SOL muscles. The results are given as mean $\pm$ standard deviation. Maximum active isometric forces were 0.27 ± 0.073 N for EDL and 0.143 ± 0.054 N for SOL muscles. Optimal lengths were 11.77 ± 1.00 mm and 10.41 ± 0.48 mm, and cross-sectional areas were 1.14 ± 0.14 mm^2 and 1.17 ± 0.12 mm^2, respectively.

The weight of the muscle was measured after the experiments. A nominal cross-sectional area was evaluated from tissue density ρ =1056 kg/m^3 and the individual optimal muscle length.

2.3. *Experimental design, stimulation and registration*

A prescribed length variation scheme was applied to the muscle; the precision in a desired length was ~ 0.01 mm. Stimulations with trains of supramaximal square current pulses (0.5 ms) were applied via platinum plate electrodes at specified frequencies: 100 Hz for EDL and 70 Hz for SOL.

Stimulation patterns and length variations were controlled via computer and the Spike2 software (CED, Cambridge, UK). Records of stimulation, force and muscle length were stored for further analysis in a computer, with a sampling frequency of 500 Hz.

Isometric tests were first performed to find the optimal muscle length for each specimen. This was done through stretching the muscles by small steps, stimulating it, and noting the maximum force produced and the passive force (1 s after stimulation) at every length, the difference being the active force. The highest active force defined

an optimum length, l_{opt}, which was used as basis for the length variations in subsequent experiments. It was verified that the active isometric force varied approximately parabolically around the optimal length. Lengths (l) were defined as a difference to individual optimal length l_{opt}.

2.4. *Testing paradigm*

The testing sequence was designed to study force as a function of length, rather than vice versa. Force produced by the muscle was therefore measured as a function of time, for prescribed variations in specimen length. By choosing suitable ramp parameters, different combinations of transient-length contractions were obtained (Table 1). Isometric contractions are special cases with no ramps.

Firstly, the muscle length was passively set as l_{ini}. After a certain time, at least 10 s, the muscle was isometrically stimulated for 150 ms before any length change, in order to give an almost maximum isometric force. Total stimulation time was 600 ms, during which the length regime was introduced; the time was limited in order to avoid fatigue effects. Passive forces were measured 1 s after the end of stimulation at the final length (l_{fin}), which was most often equal to the optimal length in present experiments.

The series of experiments can be divided into four sets according to the length variation in the stimulated state. In the 'Shortening' and 'Stretch' experiment sets, muscles were shortened or stretched from a certain length value with a certain velocity. For some of these experiments, the ramp was divided into two equal parts, and these parts were performed with a delay between them. 'Stretch-Shortening' experiments consist of active muscle stretch, followed by an active shortening, without a delay between the ramps. 'Long Shortening' experiments consisted of concentric contractions with a final length lower than optimal, $l_{\text{fin}} = -0.72\text{mm}$.

Ramp sizes (l_r) and ramp times (t_r) were chosen systematically to allow comparisons of steady-state active force modifications. These parameters are introduced in Table 1; all tested combinations were creating ramp velocities $6 \leq |l_r/t_r| \leq 24$ mm/s (corresponding to between $\sim$ 0.6 and $\sim$ 2.4 l_{opt}/s). Contractions for each muscle were therefore recorded, being the combinations of stretch and shortening ramps.

2.5. *Evaluation procedure*

The force-time histories for the isometric force development phases were fitted by exponential functions, through an in-house equal weights least-squares algorithm in Matlab (version R2006a, The MathWorks, Inc., Natick, MA, USA), with a view on the experiments as in Fig. 1, giving expressions of the form:

$$F(t) = F_r + (F_a - F_r) \cdot \exp(-1/\tau_r \cdot (t - t_0)), \tag{1}$$

where F_a, F_r, and $1/\tau_r$ were results from fitting for a phase starting at time t_0. The equation defines an exponential curve for F, starting at $F = F_a$ at time $t = t_0$, and with $F = F_r$ as the long term asymptote as $t \to \infty$. The redeveloped isometric force-time trace between end of last ramp and end of stimulation was considered.

TABLE 1. Parameters used in 'Shortening', 'Long Shortening', 'Stretch' and 'Stretch-Shortening' experiments, where l_r, t_r and v are ramp-size, ramp-time and ramp velocity, t_d is a delay time between two ramps, l_{fin} is a final muscle length, defined as a difference to individual optimal length. Experiments marked with asterisk were performed for SOL muscles only.

Experiment name	l_{r1}, [mm]	t_{r1}, [s]	$v_1=l_{r1}/t_{r1}$, [mm/s]	t_d [s]	l_{r2}, [mm]	t_{r2}, [s]	$v_2=l_{r2}/t_{r2}$, [mm/s]	l_{fin}, [mm]
ShoOne1	−0.36	0.06	−6	0	0	0	0	0
ShoOne2	−0.72	0.06	−12	0	0	0	0	0
ShoOne3	−0.36	0.12	−3	0	0	0	0	0
ShoOne4	−0.72	0.12	−6	0	0	0	0	0
ShoTwo1	−0.18	0.03	−6	0.12	−0.18	0.03	−6	0
ShoTwo2	−0.36	0.03	−12	0.12	−0.36	0.03	−12	0
ShoTwo3	−0.18	0.06	−3	0.12	−0.18	0.06	−3	0
ShoTwo4	−0.36	0.06	−6	0.12	−0.36	0.06	−6	0
ShoLong1	−2.16	0.36	−6	0	0	0	0	−0.72
ShoLong2	−1.98	0.33	−6	0	0	0	0	−0.72
ShoLong3	−1.80	0.30	−6	0	0	0	0	−0.72
ShoLong4	−1.62	0.27	−6	0	0	0	0	−0.72
ShoLong5	−1.44	0.24	−6	0	0	0	0	−0.72
ShoLong6	−1.26	0.21	−6	0	0	0	0	−0.72
StrOne1	0.18	0.06	3	0	0	0	0	0
StrOne2	0.18	0.12	1.5	0	0	0	0	0
StrOne3	0.36	0.12	3	0	0	0	0	0
StrOne4	0.09	0.03	3	0	0	0	0	0
StrOne5	0.09	0.06	1.5	0	0	0	0	0
StrOne6	0.09	0.12	0.75	0	0	0	0	0
StrTwo*	0.18	0.06	3	0.12	0.18	0.06	3	0
StrSho1	0.18	0.12	1.5	0	−0.18	0.06	−3	0
StrSho2	0.18	0.12	1.5	0	−0.36	0.06	−6	0
StrSho3	0.18	0.12	1.5	0	−0.72	0.06	−12	0
StrSho4*	0.36	0.12	3	0	−0.18	0.06	−3	0
StrSho5*	0.36	0.12	3	0	−0.36	0.06	−6	0
StrSho6*	0.36	0.12	3	0	−0.72	0.06	−12	0
StrSho7	0.18	0.06	3	0	−0.18	0.12	−1.5	0
StrSho8	0.18	0.06	3	0	−0.36	0.12	−3	0
StrSho9	0.18	0.06	3	0	−0.72	0.12	−6	0

A similar evaluation of force evolution was performed for initial isometric cases at lengths l_{fin}. Similarly as in Eq. (1), an isometric asymptotic force (F_o) and an exponential time constant (τ_o) were obtained.

The exponential fitting showed good agreement with experimental data for isometric force development and force redevelopment after ramps ($R^2 > 0.99$) (Hancock et al. 2004; Corr and Herzog 2005).

From the obtained values, the steady-state force modification was evaluated. In each experiment, the total force modification $F_{\text{mod,total}}$ was obtained as the difference between the asymptotic redeveloped isometric force following transient-length contractions and the asymptotic isometric force, Fig. 1, as:

$$F_{\text{mod,total}} = F_r - F_o = F_{\text{mod}} + F_{\text{mod,p}}. \tag{2}$$

The active modification of the muscular force F_{mod} was obtained by subtracting the change in passive force, $F_{\text{mod,p}}$, from the total force modification, $F_{\text{mod,total}}$. The passive forces were always measured 1 s after stimulation.

Mechanical work produced by the muscle during ramps was evaluated by integrating the force multiplied by ramp velocity, over the ramp period:

$$W = -\int_{l_{\text{ini}}}^{l_{\text{fin}}} F\, dl \equiv -\int_{t_{\text{ini}}}^{t_{\text{fin}}} F(t)\frac{dl}{dt}dt \tag{3}$$

giving positive work for shortening, negative for stretch. The integral was evaluated numerically through all recorded force values in the considered ramp intervals. Work from passive force during initial length setting to l_{ini} was not considered. In multi-ramp cases, the work was evaluated as the net value, considering positive and negative contributions.

3. Results

Examples of total force and length traces in SOL muscles, for stretch, shortening and stretch-shortening variations are shown in Fig. 2. The force was almost 90% of the maximal sustained output at initial length l_{ini} before ramps were introduced. During active shortening and stretch, force was rapidly decreasing or increasing, correspondingly. In tests with stretch and shortening in two steps, force reached an intermediate value during the delay between ramps. When ramps were completed, force approached a new steady-state value.

Figure 3 shows mean data of normalized active force modification after transient-length contractions of SOL (a) and EDL (b) muscles as functions of normalized mechanical work performed during the different ramps described in Table 1. Force modification, F_{mod}, was normalized by optimal force, F_{o}, to get a dimensionless value; mechanical work calculated as in Eq. (3) was divided by $F_{\text{o}}l_{\text{o}}$ to discard the unit. The positive and negative values of work relate to active shortening and stretch, respectively. Overall, the data points show a clear correlation between decreasing force and increasing mechanical work. The linear fits show that this correlation also exists within each set of experiments (shortening, long shortening, stretch, stretch shortening).

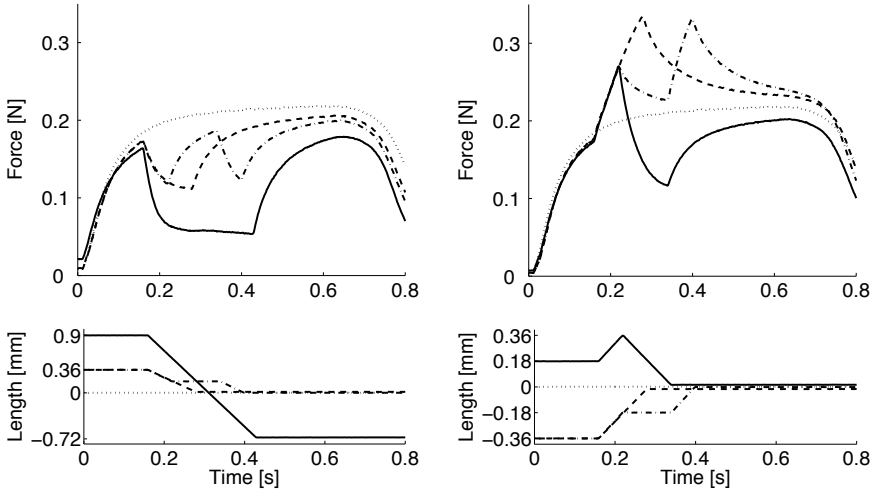

FIGURE 2. Examples of force-time traces of studied transient-length contractions on mouse SOL muscle. Dotted lines correspond to isometric contractions at optimal muscle length. Transient-length contractions: (a) ShoLong4 - solid line, ShoOne3 - dashed line, ShoTwo3 - dash-dot line. (b) StrSho8 - solid line, StrOne3 - dashed line, StrTwo2 - dash-dot line. Parameters of mentioned experiments are described in Table. 1.

As the EDL muscle is more vulnerable to stretch, active force was decreasing by almost 1% for each active stretching. Although we do not observe a significant force enhancement for EDL muscles, the relations between force modification and mechanical work are similar with the ones for SOL muscles, when the experimental loss is considered.

In Fig. 4 we specifically address a subset of shortening experiments. In these, shortening was induced with the same velocity and the same total length change, but either in one step or in two steps with a short isometric period in between. This isometric phase increased the force produced during the second half of shortening. Therefore, the mechanical work performed was always larger with two steps than with one step of shortening, and this was associated with markedly larger force depressions both in SOL (Fig. 4a) and EDL (Fig. 4b) muscles.

The modification in passive force show a pattern similar to that for active force; that is, a correlation between decreasing passive force and increasing mechanical work during the contraction both in SOL (Fig. 5a) and EDL (Fig. 5b) muscles. It should be noted, however, that the magnitude of passive force modification was only about one tenth of that for active force.

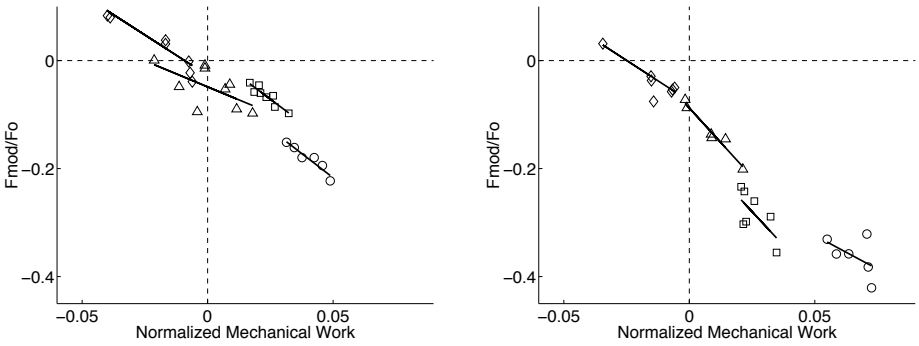

FIGURE 3. Steady-state force modification as a function of normalized mechanical work of mouse (a) SOL and (b) EDL muscles. Data points represent mean values for the groups presented in Table 1: Shortening - squares, Stretch - diamonds, Long Shortening - circles, Stretch-Shortening - triangles. Average value for group, maximum standard deviations for mechanical work are about 3%, for force modification are about 9% for both SOL and EDL.

4. Discussion

The motivation behind this study was to improve the predictive capacity of common Hill muscle models, where muscular force is described by only the current length after the transients in contractile component length have disappeared. The basic finding of the work is that a memory effect is present in muscular force production, as the steady-state isometric force is consistently modified by a preceding active shortening or stretch. This effect can be introduced in a Hill model. The results from the experiments show that the mechanical work produced by or on the muscle during the transient phase can be a good predictor for this force modification, valid for different length regimes.

Mechanical work, produced on or by the muscles during stretch and shortening, is a parameter which considers both direction magnitude and velocity of the ramp. The present results show that the mechanical work is negatively correlated with the force modification in all sets of experiments including shortening and stretches (Fig. 3). This suggests that the force depression with concentric contraction and the force enhancement with eccentric contraction are at least partially affected by a common mechanism. This is in contrast to the general idea that the force modification following shortening and stretches involves different mechanisms (Bullimore et al. 2007; Morgan 2007; Herzog et al. 2008). However it should be noted that the force enhancement observed with the present modest stretches was relatively small and that other mechanisms might become evident with more severe stretches.

Concentric contractions were performed in two different regimes. The muscles produced larger mechanical work after introducing a delay during the shortening ramp, as the force value was raised during the delay (see Fig. 2(a) and Fig. 4). The higher

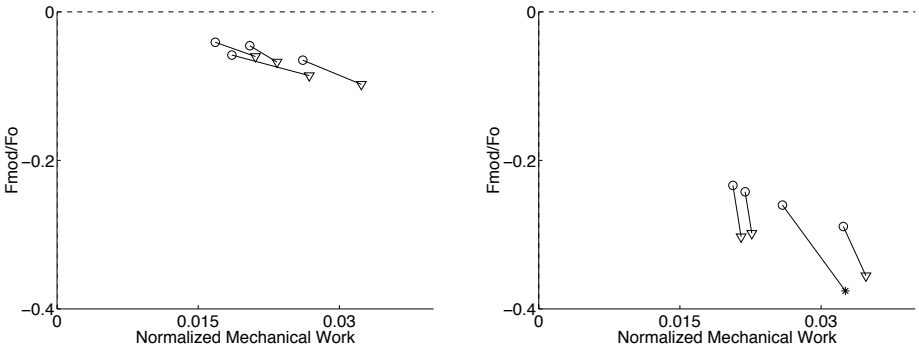

FIGURE 4. Steady-state force modification as a function of normalized mechanical work of mouse (a) SOL and (b) EDL muscles. Groups of experiments with one step Shortening - circles, two steps - triangles. Lines connect results from experiments with the same velocity and total length change. Average value for group, asterisk corresponds to group of just 3 specimens. Maximum standard deviations for mechanical work are about 1%, for force modification are about 3% and 9% for SOL and EDL, respectively.

force value at the start of the second half of the ramp makes the work quantity higher. Consistent with our hypothesis, this resulted in a larger force depression than for a single step shortening.

As stated above, the objective of the present study was to investigate the effect from a preceding transient contraction on the isometric force production. Focussing on the macroscopic transient behaviour, no experiments were thereby performed to directly investigate mechanisms underlying the active force modifications after length changes. However, some tentative mechanisms might be suggested. Cross-bridge kinetics was proposed by Marechal and Plaghki (1979) as a possible mechanism of force depression after shortening. They suggested that certain actin filaments were strained during shortening contractions and therefore unable to make normal cross-bridges. Results of our study and those from Leonard and Herzog (2005) support this theory, because work performed during shortening was a strong predictor of force depression but shortening velocity was not.

Edman et al. (1978) suggested that the tetanic force enhancement after a stretch is due to a parallel elastic element that is formed, reorganized or re-aligned during activation. This kind of mechanism might explain our finding of a similar relation between mechanical work and changes in passive and active force, albeit the changes were about ten times larger for active force (cf. Fig. 3 and Fig. 5).

That slope of the relation between the force modification, $F_{\mathrm{mod}}/F_{\mathrm{o}}$, and the normalized mechanical work, $W/(l_{\mathrm{o}} * F_{\mathrm{o}})$, is about 2 times steeper for EDL than for SOL

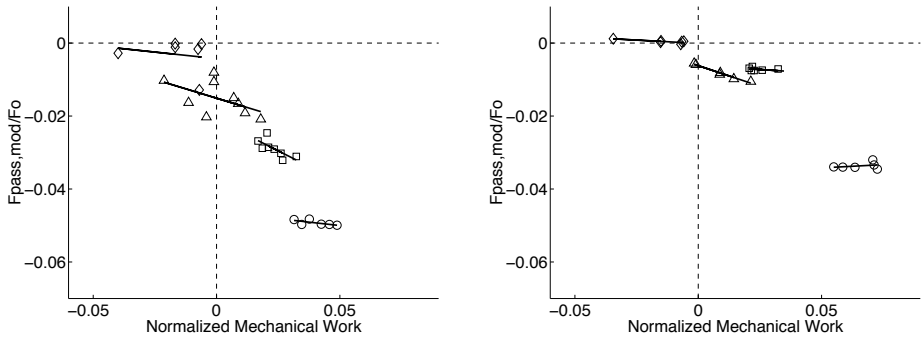

FIGURE 5. Passive force modification following contractions as a function of normalized mechanical work of mouse (a) SOL and (b) EDL muscles. Data points represent mean values for the groups presented in Table 1: Shortening - squares, Stretch - diamonds, Long Shortening - circles, Stretch-Shortening - triangles. Average value for group, maximum standard deviations for mechanical work are about 3%, for force modification are about 5% for both SOL and EDL.

(Fig. 3). This fits with the idea that the force modification is related to metabolic factors, because the rate of ATP consumption during contractions is markedly faster in EDL than in SOL muscles (Barclay et al. 1993) and the rate of cross-bridge cycling, and hence the rate of ATP consumption, is higher during shortening than under isometric conditions (Herzog et al. 2000). This would, for instance, lead to a more rapid breakdown of phosphocreatine during shortening, resulting in an increased concentration of phosphate ions, which tends to decrease isometric force production (Allen et al. 2008). Such an explanation is difficult to reconcile with the observation by Julian and Morgan (1979) and Abbott and Aubert (1952), that force depression can be decreased and even abolished by briefly interrupting the stimulation. Such behaviour is more easily explained by a theory based on shortening-induced non-uniform sarcomere lengths (Julian and Morgan 1979; Morgan 2007), where sarcomeres are re-organized by the brief interruption of stimulation. It is, however, difficult to see how this theory could explain the continuity in modification between stretch and shortening situations.

5. Conclusions

The study confirms presence of the active and passive force modification following contraction with various length changes. The results show that muscular force does not only depend on length l and length time differential $\dot{l}$. The steady-state force also takes into account the accumulated length history, as shown in transient-length contractions. Our results indicate that the mechanical work produced by or on the muscle during length variation is a good general predictor for the steady-state force modification induced by transient-length contractions.

Conflict of interest statement

There are no conflicts of interest present in the work.

Acknowledgements

The authors gratefully acknowledge technical support in preparing muscle specimens from Shi-Jin Zhang, and financial support from the Swedish Research Council. We also thank Jan Lännergren for construction of the mechanical apparatus.

References

Abbott, B., Aubert, X., 1952. The force exerted by active striated muscle during and after change of length. Journal of Physiology 117, 77–86.

Allen, D., Lamb, G., Westerblad, H., 2008. Skeletal muscle fatigue: cellular mechanisms. Physiological Reviews 88, 287–332.

Bagni, M., Cecchi, G., Colombini, B., 2005. Crossbridge properties investigated by fast ramp stretching of activated frog muscle fibres. Journal of Physiology 565(1), 261–268.

Bagni, M., Cecchi, G., Colombini, B., Colomo, F., 2002. A non-cross-bridge stiffness in activated frog muscle fibers. Biophysical Journal 82, 3118–3127.

Barclay, C. J., Constable, J. K., Gibbs, C. L., 1993. Energetics of fast- and slow-twitch muscles of the mouse. Journal of Physiology 472, 61–80.

Bullimore, S., Leonard, T., Rassier, D., Herzog, W., 2007. History-dependence of isometric muscle force: Effect of prior stretch or shortening amplitude. Journal of Biomechanics 40, 1518–1524.

Corr, D., Herzog, W., 2005. Force recovery after activated shortening in whole skeletal muscle: Transient and steady-state aspects of force depression. Journal of Applied Physiology 99(1), 252–260.

Edman, K.A., Elzinga, G., Noble, M.I., 1978. Enhancement of mechanical performance by stretch during tetanic contractions of vertebrate skeletal muscle fibres. Journal of Physiology 281, 139–155.

Eriksson, A., 2008. Optimization in target movement simulations. Computer Methods in Applied mechanics and Engineering 197(49-50), 4207–4215.

Forcinito, M., Epstein, M., Herzog, W., 1998. Can a rheological muscle model predict force depression/enhancement? Journal of Biomechanics 31(12), 1093–1099.

Günther, M., Schmitt, S., Wank, V., 2007. High-frequency oscillations as a consequence of neglected serial damping in hill-type muscle models. Biological Cybernetics 97(1), 63–79.

Hancock, W., Martin, D., Huntsman, L., 2004. Ca^{2+} and segment length dependence of isometric force kinetics in intact ferret cardiac muscle. Circulation research 73(4), 603–611.

Herzog, W., 2005. Force enhancement following stretch of activated muscle: Critical review and proposal for mechanisms. Medical and Biological Engineering and Computing 43(2), 173–180.

Herzog, W., Leonard, T., 1997. Depression of cat soleus forces following isokinetic shortening. Journal of Biomechanics 30(9), 865–872.

Herzog, W., Leonard, T., Joumaa, V., Mehta, A., 2008. Mysteries of muscle contraction. Journal of Applied Biomechanics 24(1), 1–13.

Herzog, W., Leonard, T., Wu, J., 2000. The relationship between force depression following shortening and mechanical work in skeletal muscle. Journal of Biomechanics 33(5), 659–668.

Joumaa, V., Rassier, D. E., Leonard, T. R., Herzog, W., 2008. The origin of passive force enhancement in skeletal muscle. American Journal of Physiology - Cell Physiology 294(1), C74–C78.

Julian, F., Morgan, D., 1979. The effect on tension of non-uniform distribution of length changes applied to frog muscle fibres. Journal of Physiology 293, 379–392.

Kaphle, M., Eriksson, A., 2008. Optimality in forward dynamics simulations. Journal of Biomechanics 41(6), 1213–1221.

Kosterina, N., Westerblad, H., Lännergren, J., Eriksson, A., 2008. Muscular force production after concentric contraction. Journal of Biomechanics 44(11), 2422–2429.

Lee, H., Herzog, W., 2003. Force depression following muscle shortening of voluntarily activated and electrically stimulated human adductor pollicis. Journal of Physiology 551, 993–1003.

Leonard, T., Herzog, W., 2005. Does the speed of shortening affect steady-state force depression in cat soleus muscle? Journal of Biomechanics 38(11), 2190–2197.

Lou, F., Curtin, N., Woledge, R., 1998. Contraction with shortening during stimulation or during relaxation: How do the energetic costs compare? Journal of Muscle Research and Cell Motility 19(7), 797–802.

Marechal, G., Plaghki, L., 1979. The deficit of the isometric tetanic tension redeveloped after a release of frog muscle at a constant velocity. Journal of General Physiology 73(4), 453–467.

Morgan, D., 2007. Can all residual force enhancement be explained by sarcomere non-uniformities? Journal of Physiology 578(2), 613–615.

Morgan, D., Whitehead, N., Wise, A., Gregory, J., Proske, U., 2000. Tension changes in the cat soleus muscle following slow stretch or shortening of the contracting muscle. Journal of Physiology 522(3), 503–513.

Rassier, D., Herzog, W., 2002. Force enhancement following an active stretch in skeletal muscle. Journal of Electromyography and Kinesiology 12(6), 471–477.

Schachar, R., Herzog, W., Leonard, T., 2002. Force enhancement above the initial isometric force on the descending limb of the force-length relationship. Journal of Biomechanics 35(10), 1299–1306.

Schachar, R., Herzog, W., Leonard, T., 2004. The effects of muscle stretching and shortening on isometric forces on the descending limb of the force-length relationship. Journal of Biomechanics 37(6), 917–926.

Sugi, H., Tsuchiya, T., 1988. Stiffness changes during enhancement and deficit of isometric force by slow length changes in frog skeletal muscle fibres. Journal of Physiology 407, 215–229.

Yamane, K., Nakamura, Y., 2007. Robot kinematics and dynamics for modeling the human body. Proceedings of International Symposium on Robotics Research, 77–88.

3

Paper 3

Impaired Myofibrillar Function in the Soleus Muscle of Mice With Collagen-Induced Arthritis

By Takashi Yamada[1,*], Nicolas Place[1,2], Natalia Kosterina[3], Therese Östberg[4,6], Shi-Jin Zhang[1], Cecilia Grundtman[4,5,6], Helena Erlandsson-Harris[4,6], Ingrid E. Lundberg[4,6], Birgitta Glenmark[6], Joseph D. Bruton[1], Håkan Westerblad[1]

[1] Department of Physiology and Pharmacology, Karolinska Institutet, Stockholm, Sweden
[2]University of Geneva, Geneva, Switzerland
[3]Department of Mechanics, Royal Institute of Technology, Stockholm, Sweden
[4]Karolinska University Hospital, Solna, Sweden
[5]Innsbruck Medical University, Innsbruck, Austria
[6]Karolinska Institutet, Stockholm, Sweden

Arthritis & Rheumatism
November 2009 (Vol. 60, Issue 11, Pages 3280–3289)

Objective Progressive muscle weakness is a common feature in patients with rheumatoid arthritis (RA). However, little is known about whether the intrinsic contractile properties are affected in RA. We investigated muscle contractility and myoplasmic free Ca^{2+} concentration ($[Ca^{2+}]_i$) in the soleus, a major postural muscle, in mice with collagen-induced arthritis (CIA).

Methods Muscle contractility and $[Ca^{2+}]_i$ were assessed in whole muscle and intact single fiber preparations, respectively. The underlying mechanisms of contractile dysfunction were assessed by investigating redox modifications using Western blotting and antibodies against nitric oxide synthase (NOS), superoxide dismutase (SOD), 3-nitrotyrosine (3-NT), carbonyl, malondialdehyde (MDA), and S-nitrosocysteine (SNO-Cys).

Results The tetanic force per cross-sectional area was markedly decreased in the soleus muscle of mice with CIA, and the change was not due to a decrease in the amplitude of $[Ca^{2+}]_i$ transients. The reduction in force production was accompanied by slowing of the twitch contraction and relaxation and a decrease in the maximum shortening velocity. Immunoblot analyses showed a marked increase in neuronal NOS expression but not in inducible or endothelial NOS expression, which, together with the observed decrease in SOD2 expression, favors peroxynitrite formation. These changes were accompanied by increased 3-NT, carbonyl, and MDA adducts content in myofibrillar proteins from the muscles of mice with CIA. Moreover, there was a significant increase in SNO-Cys content in myosin heavy-chain and troponin I myofibrillar proteins from the soleus muscle of mice with CIA.

Conclusion These findings show impaired contractile function in the soleus muscle of mice with CIA and suggest that this abnormality is due to peroxynitrite-induced modifications in myofibrillar proteins.

1. Introduction

Patients with rheumatoid arthritis (RA) frequently suffer from impaired muscle function, which limits daily activities and decreases the quality of life (1). Despite the fact that muscle histopathology is often normal in RA patients, with no evidence of infiltrating inflammatory cells (2), a 25-50% reduction of muscle strength has been reported in up to two-thirds of patients (3). Decreased muscle strength is generally associated with a loss of muscle mass (2). However, little is known about whether the muscle fibers' intrinsic contractile properties are affected in RA. In one study of the relationship between muscle weakness and muscle wasting in patients with RA, it was found that the muscle weakness was more marked than muscle atrophy (4), suggesting a loss of intrinsic contractile performance.

Significant skeletal muscle weakness also appears to develop in a variety of inflammatory related conditions, including chronic heart failure (5-7), sepsis (8), and chronic infection (9). Although the basis of muscle dysfunction in inflammatory disease is multifactorial, there is good evidence for a major role for an intrinsic impairment of the contractile apparatus (10). In some studies, impaired contractility has been associated with an altered intracellular Ca^{2+} transient (11,12). However, many other studies have reported depressed contractility even in the skinned fiber preparation (6,13), suggesting that a significant component of the contractile dysfunction arises due to abnormalities of the contractile apparatus. Several previous reports have suggested that the alterations in myofibrillar functions in inflammatory disease may be directly related to the redox modifications of the key myofibrillar proteins, myosin heavy chain (MyHC) (5,7,14), actin (5), and tropomyosin (5).

Recent evidence indicates that most of the cytotoxicity attributed to excessive NO production is due to the peroxynitrite anion, the product of the diffusion-controlled reaction of NO with the superoxide radical (15,16). A number of potentially harmful modifications is produced by peroxynitrite-derived radicals, including nitration of accessible tyrosine residues to form 3-nitrotyrosine (3-NT), S-nitrosylation of cysteine residues to form S-nitrosocysteine (SNO-Cys), formation of protein carbonyls, and peroxidation of unsaturated fatty-acid-containing phospholipids (15). Of these modifications, the formation of 3-NT is a major peroxynitrite-mediated protein modification that is different from any modification mediated by reactive oxygen species (15). Increased levels of 3-NT are found in the joints of RA patients (17) and an RA animal model (18). Intriguingly, accumulation of 3-NT has been associated with reduced skeletal muscle force production in pathological conditions (8). Furthermore, experiments on skinned muscle fibers showed that exogenous peroxynitrite has a strong inhibitory effect on maximal Ca^{2+}-activated force (19). Thus, modifications of myofibrillar proteins caused by peroxynitrite-derived radicals could be a mechanism underlying the contractile dysfunctions associated with RA.

One widely used animal model of RA is collagen-induced arthritis (CIA), which displays many of the pathological characteristics of human RA, including similar patterns of synovitis, pannus formation, erosion of cartilage and bone, fibrosis, and loss

of joint function (20). The susceptibility to both human RA and murine CIA is associated with genes encoding major histocompatibility complex (MHC) class II molecules (21). In both RA and CIA there is an increase in nitric oxide (NO) generated by NO synthase (NOS) (16) and activation of multiple inflammatory signaling cascades with the ensuing release of bioactive circulating molecules, such as cytokines (e.g. tumor necrosis factor α [TNF]-α and interleukin-1β [IL-1β] (22). Moreover, treatment with anti-TNF-α antibody has been shown to reduce the disease severity in both RA and CIA (23). Interestingly, application of TNF-α results in impaired myofibrillar function and decreased force production associated with increased intracellular oxidant activity (24).

RA patients show significantly greater postural sway (25) and slower walking speeds (26). These problems are likely to be related to dysfunction of postural muscles such as the soleus muscle, which is important in stabilization of the ankle joint at rest and during walking. In this study we used CIA mice as a model for acute RA and studied the contractile function of soleus muscles. Our results show impaired contractile function in soleus muscles of CIA mice, which we suggest is due to contractile protein modifications induced by peroxynitrite-derived radicals.

2. Materials and methods

2.1. *Induction and evaluation of CIA*

Female DBA/1 mice, weighing 18-22 grams, were supplied by Taconic (Lille Skensved, Denmark). Mice were housed 5 per cage, with free access to food and water in a 12-hour light/dark cycle.

Type II collagen (CII) was obtained from bovine nasal cartilage and mixed in a collagen emulsion (27). A preparation of 100 μg of CII and 300 μg of Mycobacterium tuberculosis in 0.1 ml of emulsion was injected subcutaneously into the base of the tail of the DBA/1 mice. On day 28, the mice received a booster injection of CII in Freund's incomplete adjuvant (100 μg subcutaneously). Control mice were injected with 0.1 ml of saline on both occasions.

Mice were observed daily for the development of erythema and swelling of the metatarsophalangeal and ankle joints. Individual paws were scored for inflammation on a scale of 0-3, as follows: 0 = normal, 1 = 1 joint affected, 2 = 2 joints affected, and 3 = whole paw affected. Mice were killed by rapid neck disarticulation when the inflammation score for a single hind limb had reached the maximum (score of 3), which occurred a mean $\pm$ SEM 16$\pm$1 days (n = 8) after the second injection. This resembles an acute phase of severe RA in humans. The soleus muscle from the limbs of saline-treated control mice and from the limbs with an inflammation score of 3 in mice with CIA were excised; in some experiments, we also excised fast-twitch extensor digitorum longus (EDL) muscles. All experimental procedures were approved by the Stockholm North Ethics Committee.

2.2. *Measurements of force and shortening velocity*

Intact soleus muscles were mounted between a force transducer (Dual-Mode Muscle Lever System; Aurora Scientific, Toronto, Ontario, Canada) and an adjustable holder,

and superfused with Tyrode solution supplemented with 0.1% fetal calf serum, bubbled with 5% CO_2/95% O_2, and kept at 30°C. Stainless-steel hooks were tied to the tendons as close as possible to the ends of the muscle fibers. Muscles were stimulated with supramaximal current pulses of 0.5 msec. Muscles were monitored during contraction, with the use of a microscope with a graticule fitted to a 12.5x-magnification lens. No stretching or slippage of the tendons in the soleus muscles of control mice or mice with CIA was observed during contraction. The muscle length was adjusted to the length (L_0) that yielded maximum tetanic force.

The time to peak force and half-relaxation time of the twitch were measured. The force-frequency relationship was determined by evoking tetani at different frequencies (10-120 Hz, 600 msec long) at 1-minute intervals. In some experiments, the force-frequency relationship was also determined in the EDL muscle.

In the soleus muscle, the shortening velocity at zero load (V_0) was measured with slack tests (28). Rapid releases of at least 5 different amplitudes were applied during tetani of 1-minute intervals. The release amplitudes were plotted against the time needed to take up the slack, and a straight line was fitted to the data points. The V_0 was then obtained by dividing the slope of this fitted line by L_0.

Muscle weight was measured after these experiments. Force was normalized to the cross-sectional area, calculated as the muscle weight divided by L_0 and the density of the muscle (1,056 kg/m^3) (14).

2.3. *Measurement of myoplasmic free Ca^{2+} concentration ($[Ca^{2+}]_i$)*

Intact single fibers were dissected from the soleus muscle, mounted at optimum length in a stimulation chamber, and microinjected with the Ca^{2+} indicator indo-1 (Molecular Probes, Eugene, OR). Force-$[Ca^{2+}]_i$ curves were generated by plotting the mean force of whole soleus muscle against the mean $[Ca^{2+}]_i$ at different frequencies (29, 30).

2.4. *Preparation of muscle samples*

Muscle samples were fractionated into myofibrillar and cytosolic fractions (31). Samples were homogenized in pyrophosphate buffer with a motor-driven glass homogenizer and then centrifuged at 1000 g for 10 minutes. The supernatant was removed (designated the cytosolic fraction). The pellet was then washed 4 times with 10-volume low-salt buffer followed by 1 wash with low-salt buffer containing 0.02% (volume/volume) Triton X-100 and 1 wash with 0.02% (weight/volume) sodium deoxycholate. The pellet was then washed twice more in low-salt buffer and subsequently suspended in pyrophosphate buffer (designated the myofibrillar fraction). Protein concentrations of muscle fractions were measured using the Bradford technique (32).

2.5. *Determination of MyHC and actin content in myofibrillar proteins*

To separate the myofibrillar proteins, sodium dodecyl sulfate-polyacrylamide gel electrophoresis (SDS-PAGE) was performed using a 4-12% Bis-Tris gel (Invitrogen, Carlsbad, CA). Aliquots of myofibril extracts containing 5 μg of protein were subjected to electrophoresis and stained with SimplyBlue Safestain (Invitrogen). Images of

the gels were acquired using the GelDoc imaging system (Bio-Rad, Philadelphia, PA). The relative content of MyHC or actin in total myofibrillar proteins was evaluated densitometrically using ImageJ (National Institutes of Health, Bethesda, MD; http://www.rsb.info.nih.gov/).

2.6. *Separation of MyHC isoforms*

Using a 6% polyacrylamide slab gel, electrophoresis was performed (14). Aliquots of the extracts containing 0.5 μg of myofibrillar protein were applied to the gel. Electrophoresis was run at 4°C for 48 hours at 160V. Gels were silver-stained, and images of the gels were acquired using the GelDoc imaging system. The percent distribution of various isoforms was densitometrically evaluated with ImageJ.

2.7. *Immunoblotting*

Immunoblotting was performed using anti-3-NT (1:1000; Cayman Chemical, Ann Arbor, MI), anti-2,4-dinitrophenylhydrazone (1:150, Oxyblot kit; Chemicon International, Temecula, CA), antimalondialdehyde (anti-MDA) (1:500; Academy Bio-Medical, Houston, TX), anti-SNO-Cys (1:1000; Sigma, St. Louis, MO), anti-neuronal NOS (anti-nNOS), anti-endothelial NOS (anti-eNOS) and anti-inducible NOS (anti-iNOS) (1:1000; BD Biosciences, Lexington, KY), anti-copper/zinc superoxide dismutase (anti-SOD1) (1:1000; Abcam, Cambridge, UK), anti-manganese SOD (anti-SOD2) (1:1000; Upstate Biotechnology, Lake Placid, NY), anti-troponin I (1:1000; Millipore, Billerica, MA), anti-dihydropyridine receptor (1:500; Abcam), and anti-actin (1:1000; Sigma).

The immunoblots for redox modification were performed on unstimulated muscle samples, to avoid the complication of changes that could result from contractile activity. Aliquots of the fractionated proteins (10 μg of myofibrillar protein or 20 μg of cytosolic protein) were subjected to SDS-PAGE (4-12% or 12% Bis-Tris gels; Invitrogen). Proteins were transferred onto polyvinylidene difluoride membranes. Membranes were blocked in 5% (w/v) nonfat milk with Tris buffered saline containing 0.05% (v/v) Tween 20, followed by incubation overnight at 4°C with a primary antibody made up in 5% (w/v) nonfat milk. Membranes were then washed and incubated for 1 hour at 22°C with a secondary antibody (donkey anti-rabbit or donkey anti-mouse, 1:5000; Bio-Rad). Immunoreactive bands were visualized using enhanced chemiluminescence (SuperSignal; Pierce, Rockford, IL). The redox modification was assessed with densitometry, involving measurement of the total density in a box covering the width and length of each lane, with results analyzed using ImageJ. In addition, for SNO-Cys, the density of MyHC and troponin I was measured.

2.8. *Statistical analysis*

Data are presented as the mean $\pm$ SEM. Student's unpaired t-tests were used to establish significant differences between control and CIA muscles. Two-way repeated-measures analysis of variance (ANOVA) was used when comparing repeated measurements in 2 groups. If the ANOVA showed a significant difference between groups, a

Bonferroni post hoc test was performed. P values less than 0.05 were considered significant.

3. Results

3.1. *Body and muscle weights*

After the mice were killed, the body and muscle weights of the mice were determined. The body weights of the mice with CIA were significantly lower than those of the control group (mean ± SEM 17.1 ± 0.5 gm versus 20.0 ± 0.4 gm [n = 6-8 per group]; $P < 0.001$). In addition, the soleus muscle weights were also lower in the mice with CIA compared with controls (3.1 ± 0.2 mg versus 4.3 ± 0.4 mg [n = 6-8 per group]; $P < 0.01$). However, there was no significant difference in the normalized soleus muscle weight (determined as the ratio of muscle weight to body weight) between mice with CIA and control mice (0.18 ± 0.01 mg/gm versus 0.21 ± 0.02 mg/gm; $P > 0.05$). Similar results were obtained for the EDL muscles, in which the EDL muscle weights were significantly lower in mice with CIA than in control mice (5.3 ± 0.3 mg versus 6.5 ± 0.3 mg [n = 6 per group]; $P < 0.05$), whereas there was no difference in the normalized EDL muscle weight between the 2 groups (0.31 ± 0.02 mg/gm versus 0.32 ± 0.01 mg/gm; $P > 0.05$).

3.2. *Contractile speed of CIA soleus muscles*

There was no significant difference in the specific twitch force of the soleus muscle between mice with CIA and control mice (mean ± SEM 117 ± 12 kN/m^2 versus 143 ± 17 kN/m^2 [n = 6-7 per group]; $P > 0.05$). In contrast, time to peak tension (44 ± 2 msec versus 35 ± 3 msec [n = 6-7 per group]; $P < 0.05$) and half-relaxation time of the twitch contraction (58 ± 4 msec versus 34 ± 2 msec [n = 6-7 per group]; $P < 0.001$) were significantly increased in CIA soleus muscles compared with control soleus muscles.

V_0 was assessed by slack tests (Figures 1A-C). Consistent with the slowed twitch characteristics, V_0 showed a significant decrease in CIA muscles compared with control muscles (4.5 ± 0.2 L_0/second versus 5.6 ± 0.4 L_0/second [n = 6-7 per group]; $P < 0.05$).

The intercept on the y-axis in Figure 1C reflects the series elasticity of the muscles (33). The elasticity of the soleus muscle in mice with CIA (0.57 ± 0.06 mm) was not different from that in control mice (0.75 ± 0.05 mm). This, together with the fact that visual inspection revealed no stretching or slippage of the tendons, showed that the changes in contractile function between CIA and control muscles observed under our experimental conditions were not related to altered tendon properties.

3.3. *Intrinsic contractile properties of CIA soleus muscles*

There was a marked reduction in the specific tetanic force in CIA soleus muscles at stimulation frequencies from 30 Hz to 120 Hz (at 30 Hz, $P < 0.01$ versus controls; at 50-120 Hz, $P < 0.001$ versus controls) (Figure 2A). We observed a similar picture in the EDL muscles from mice with CIA, with specific forces being significantly lower

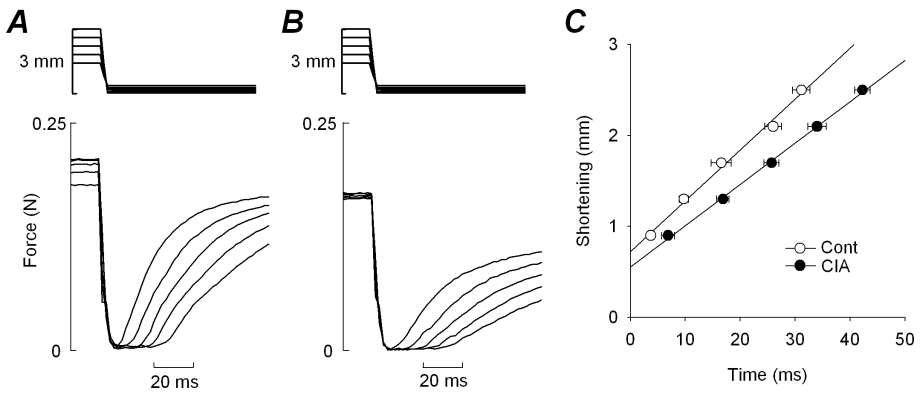

FIGURE 1. Shortening velocity at zero load (V_0) in mouse soleus muscle, as measured by the slack test. **A** and **B**, Changes in muscle length (top) and muscle force (bottom) during application of 5 consecutive tetani with rapid releases, in soleus muscles from control (Cont) mice (**A**) and mice with collagen-induced arthritis (CIA) (**B**). The initial 40 msec of force redevelopment was fitted by a single exponential function. The time value at zero force in each fitted curve was used in measurements of the time to take up the slack. **C**, Amplitude of the shortening step plotted against the time to take up the slack. Data points were fitted by a straight line, and the slope of this line was divided by the optimal length to obtain the V_0.

in the CIA muscles than in the control muscles at 20-150-Hz stimulation ($P < 0.05$) and being $\sim$35% lower than in control muscles at 100 Hz (237 ± 20 kN/m^2 versus 364 ± 30 kN/m^2 [n = 5-7 per group]). Thus, the changes in muscle weight and force production observed in mice with CIA were similar in the soleus and EDL muscles, despite major differences in the composition of the fiber type (i.e., mixed fiber types [as described below] versus fast-twitch fibers) and in the activation pattern (mostly tonic versus phasic activation) (34). No further experiments were performed on the EDL muscle.

The maximal force of the soleus muscle was assessed by producing 100 Hz tetani in the presence of caffeine (100 μM), which is a widely used stimulator of the Ca^{2+} release channels of sarcoplasmic reticulum (SR) (35). Caffeine was applied for 3 minutes before production of the tetanus. The caffeine-stimulated tetanus was markedly lower in CIA soleus muscles than in control soleus muscles (228 ± 21 kN/m^2 versus 357 ± 23 kN/m^2 [n = 7-8 per group]; $P < 0.01$), which implies that impaired myofibrillar function, reduced Ca^{2+} release, and/or reduced total SR Ca^{2+} content could account for the defects in specific force production in the CIA soleus muscle.

To determine the site of excitation-contraction coupling failure in CIA soleus muscle, we measured the $[Ca^{2+}]_i$ using the Ca^{2+} indicator indo-1. The results showed a significantly higher tetanic $[Ca^{2+}]_i$ in CIA soleus fibers at high stimulation frequencies (at 100 Hz, $P < 0.01$ versus controls; at 120 Hz, $P < 0.001$ versus controls) (Figure

2B). The resting $[Ca^{2+}]_i$ was similar between control muscle fibers and CIA muscle fibers (101 $\pm$ 10 nM versus 102 $\pm$ 18 nM). The time taken for the tetanic $[Ca^{2+}]_i$ to decay by 90% from its final plateau value was 234 $\pm$ 37 msec in control muscle fibers and 198 $\pm$ 28 msec in CIA muscle fibers ($P > 0.05$). Thus, the force depression and slowed twitch kinetics in CIA soleus muscle cannot be ascribed to abnormal SR Ca^{2+} release or reuptake or to decreased Ca^{2+} content in the SR.

Force-$[Ca^{2+}]_i$ curves were constructed from the mean data (Figure 2C). Analyses of these curves showed that the calculated maximum Ca^{2+}-activated force (Pmax) was reduced by $\sim$40% in CIA soleus muscles relative to control soleus muscles (mean 234 kN/m^2 versus 374 kN/m^2). In contrast, there was no difference in $[Ca^{2+}]_i$ at 50% of Pmax (Ca_{50}) between CIA and control muscles (0.26 μM in both groups) or in the steepness of the relationship (1.85 versus 2.29). Thus, the marked force depression in the CIA soleus muscle was due mainly to the impaired ability of the cross-bridge to generate force.

3.4. *MyHC and actin content*

The decreased force production in the CIA soleus muscle could result from a decreased amount of contractile proteins. We therefore assessed the expression levels of MyHC and actin. Figure 3A shows a typical expression pattern of these myofibrillar proteins in control and CIA muscles. There was a small, but statistically significant, reduction ($\sim$7%) in the MyHC content in CIA muscles as compared with control muscles (Figure 3B). In contrast, there was no difference in actin content between the 2 groups. Thus, a minor part of the force deficit might be attributed to a reduction in contractile protein levels.

3.5. *Expression of MyHC isoforms*

The soleus muscle in DBA mice is composed of both slow- and fast-twitch fibers. The MyHC-I, MyHC-IIa, and MyHC-IId/x isoforms, but not the MyHC-IIb isoform, were observed in both control mice and mice with CIA (Figure 3C). There were no significant differences in the distribution of the MyHC isoforms between the 2 groups (Figure 3D). Thus, the altered contractile properties, including the decreased V_0, in CIA soleus muscle, were not due to changes in the expression of different MyHC isoforms.

3.6. *Expression levels of NOS and SOD*

Posttranslational modifications of proteins, such as oxidative and nitrosative modifications, have been implicated in the intrinsic contractile dysfunction of skeletal muscle in inflammatory diseases (10). We therefore investigated whether the defects in contractile properties were accompanied by changes in the redox status in the CIA soleus muscle. There was a significant increase in the expression of nNOS, but not eNOS, in CIA muscles compared with control muscles (Figures 4A and B). The iNOS isoform was not detected in either group.

The expression of SOD2 was significantly reduced by ∼20% in CIA muscles compared with control muscles (Figures 4A and C). There was no difference in SOD1 expression between the 2 groups (Figure 4C).

3.7. *Redox modifications in myofibrillar proteins*

Peroxynitrite is a strong oxidant that is formed in vivo via the diffusion-limited reaction between NO and the superoxide anion (15). The findings of altered NOS and SOD expression suggest that accelerated production of peroxynitrite has occurred, since decreased expression of SOD2 could result in an increased steady-state concentration of superoxide, and the overproduction of NO via nNOS further favors the formation of peroxynitrite (15). To assess the involvement of peroxynitrite in impaired contractile function in the CIA soleus muscle, myofibrillar extracts were analyzed for redox modifications, using specific antibodies.

Of note, 3-NT is considered to be a major end product of peroxynitrite-derived radical interaction with proteins. The soleus muscles from mice with CIA showed significantly higher levels of total 3-NT content than did control soleus muscles (Figures 5A and D).

In addition to the modifications of tyrosine residues, peroxynitrite-derived radicals can produce protein carbonyls (36) and lipid peroxidation (15). The total carbonyl content was increased in CIA soleus muscles compared with control soleus muscles (Figures 5B and D).

The presence of MDA-protein adducts is an indicator of lipid peroxidation (Figure 5C). The soleus muscles from mice with CIA showed higher levels of total MDA-protein adducts than did control soleus muscles (Figure 5D).

Among the protein modifications induced by redox stress, structural alterations in cysteine residues are most strongly implicated in muscle function (37). Previous studies have demonstrated that the reaction of peroxynitrite-derived radicals with cysteine could result in the formation of SNO-Cys (38). In the present study, there was a significant increase in total SNO-Cys content in CIA muscles compared with control muscles (Figures 6A and B). Careful inspection of the detected bands showed that MyHC, the most abundant contractile protein in the myofibrils, had higher SNO-Cys content in CIA muscles compared with control muscles (Figures 6A and B). Moreover, there was a marked increase in SNO-Cys content in the regulatory contractile protein troponin I in CIA muscles compared with control muscles (Figures 6C and D).

4. Discussion

In the present study, we showed a marked decrease in muscle force per cross-sectional area in the postural soleus muscle of mice with CIA, which is a commonly used model for investigating factors contributing to RA in humans (20-23, 27). The reduction in force production was accompanied by the slowing of force development and relaxation and a decreased V_0. Measurements of $[Ca^{2+}]_i$ in intact single fibers indicated

that impaired cross-bridge function, rather than alterations in SR Ca^{2+} handling, is responsible for the contractile dysfunctions in CIA soleus muscle. Moreover, CIA muscles displayed higher redox modifications in myofibrillar proteins, which are most likely the consequence of increased peroxynitrite production. Overall, these results suggest a deleterious effect of peroxynitrite-derived radicals on cross-bridge function in the soleus muscle of mice with CIA.

The marked depression in isometric forces, even after forces were normalized to the cross-sectional area, indicates that intrinsic contractile defects are responsible for CIA-induced loss of muscle strength. Decreased force production in skeletal muscle can be caused by reduced Ca^{2+} release from the SR. However, the force deficits in CIA soleus muscles were accompanied by an increased, rather than decreased, tetanic $[Ca^{2+}]_i$. The rate of tetanic $[Ca^{2+}]_i$ decay was not different between CIA and control muscles, which indicates that the increased tetanic $[Ca^{2+}]_i$ in CIA muscles was due to an effect on SR Ca^{2+} release, rather than uptake. It is conceivable that increased production of NO results in an increased amplitude of Ca^{2+} transients, given that NO has been shown to regulate SR Ca^{2+} release channel function by nitrosylation of cysteine residues of this protein (39).

When reduced SR Ca^{2+} release is excluded as a possible mechanism of decreased muscle force, the decrease in force in CIA muscles could, in principle, be attributed to the reduced ability of cross-bridges to generate force and/or decreased myofibrillar Ca^{2+} sensitivity (40). To distinguish between these 2 possibilities, force-$[Ca^{2+}]_i$ curves were constructed. Ca50, which describes myofibrillar Ca^{2+} sensitivity (41), was not different between the 2 groups. In contrast, Pmax, which represents the maximum Ca^{2+}-activated force, was markedly depressed in CIA muscles. Thus, the force depression in CIA muscles was caused by a reduction in the maximum force-generating capacity of the cross-bridges. This interpretation is further reinforced by our observation that the reduction in maximum tetanic force production in CIA muscles could not be overcome by application of caffeine, which is well known to substantially increase tetanic $[Ca^{2+}]_i$ (42).

Over the past decade, accumulating evidence indicates that redox stress is one of several mechanisms involved in skeletal muscle dysfunction (10). Furthermore, decreased force production and the deleterious effects of peroxynitrite on muscle function have been associated with many pathologic conditions (8, 43). Exposure of skinned muscle fiber to peroxynitrite donors has been shown to cause a marked decline in maximal Ca^{2+}-activated force (19). Our observations of increased total 3-NT content, which is a widely used marker of protein modifications induced by peroxynitrite-derived radicals (15), are consistent with these previous findings and suggest that acceleration of peroxynitrite formation could play a crucial role in the development of myofibrillar dysfunction in the CIA soleus muscle.

In addition to the nitration of tyrosine residues, the other protein modifications observed in this study might also be induced by an increased rate of peroxynitrite production (15). Cysteine modification is most strongly implicated in contractile dysfunction of skeletal muscle, in that it alters protein structure and the availability of regulatory sites (37). We observed increased SNO-Cys content in both MyHC and

troponin I in CIA soleus muscles. The oxidation or chemical modification of 2 highly reactive cysteines of myosin S1 is a well-established mechanism for the strong inhibition of actomyosin ATPase (mATPase) activity (44). Furthermore, experiments on the purified troponin subunit showed that the troponin complex reconstituted with oxidized troponin I had markedly reduced mATPase activity, which could be restored by the reducing agent dithiothreitol (45).

Slowing of twitch contractile function was also a prominent feature in the CIA soleus muscles. V_0 reflects the cycling rate of the cross-bridge, which is determined primarily by the mATPase activity. Thus, a decreased V_0 indicates a reduction in mATPase activity in CIA soleus muscle. Experiments on skinned muscle fibers showed that an exogenous NO donor had inhibitory effects on mATPase activity and V_0 (46). Taken together, these findings suggest that the decreased mATPase activity observed in our study accounts for the impaired cross-bridge kinetics affecting the generation of force in CIA soleus muscles.

Three types of NOS and several different splice isoforms have been identified in skeletal muscle (16). Constitutively expressed nNOS and eNOS are activated by the interaction with Ca^{2+}/calmodulin, whereas iNOS is Ca^{2+}/calmodulin-insensitive. Although the NOS activity in skeletal muscle is normally dominated by nNOS, increased levels of NO in inflammatory states are traditionally thought to result from increased expression of iNOS, which is transcriptionally up-regulated by proinflammatory cytokines (16). Our results showing no detectable iNOS in either group but, instead, a marked increase in nNOS expression in CIA soleus muscles are not surprising, because it was clearly demonstrated, in rat gastrocnemius muscle, that iNOS protein expression peaked 12 hours after endotoxin injection and disappeared within 24 hours, whereas nNOS expression increased progressively over 24 hours (43). Interestingly, it has been demonstrated that nNOS, rather than iNOS, is primarily responsible for 3-NT formation in the quadriceps femoris muscles of patients with chronic obstructive pulmonary disease (47). Thus, these findings suggest an important pathologic role of sustained elevation of the nNOS level in skeletal muscle.

Little is known about the changes in antioxidant defenses in the skeletal muscles of patients with RA. Our results suggest that these are reduced, given that the expression of SOD2 was significantly decreased in the soleus muscles of mice with CIA. The precise mechanism for the decrease in SOD2 content is unclear. However, it is conceivable that reduced expression and activity of SOD2 may represent a peroxynitrite-dependent nitration of tyrosine residues of this enzyme, given that protein nitration has been shown to increase the susceptibility of breakdown by the proteaosome (48). Our finding suggests that, regardless of the underlying mechanism, decreased levels of SOD2 in CIA soleus muscles will lead to an increased steady-state concentration of superoxide in mitochondria, forming a positive loop for enhancing peroxynitrite formation in the presence of excessive NO production.

The present study results in female DBA/1 mice indicate that arthritis causes intrinsic contractile defects in the soleus muscle; specifically, the ability of cross-bridges to generate force is impaired. The increased levels of nNOS and tyrosine nitration in myofibrillar proteins suggest that peroxynitrite-derived radicals are responsible, at

least in part, for this impairment. A previous study showed that treatment with a metalloporphyrin, which has peroxynitrite-scavenging activity, ameliorates septic contractile dysfunction in the diaphragms of rats (49). Interestingly, it has been reported that peroxynitrite scavenging markedly reduces both arthritis incidence and severity in murine CIA (50), but further studies are required to reveal whether this treatment also improves muscle function.

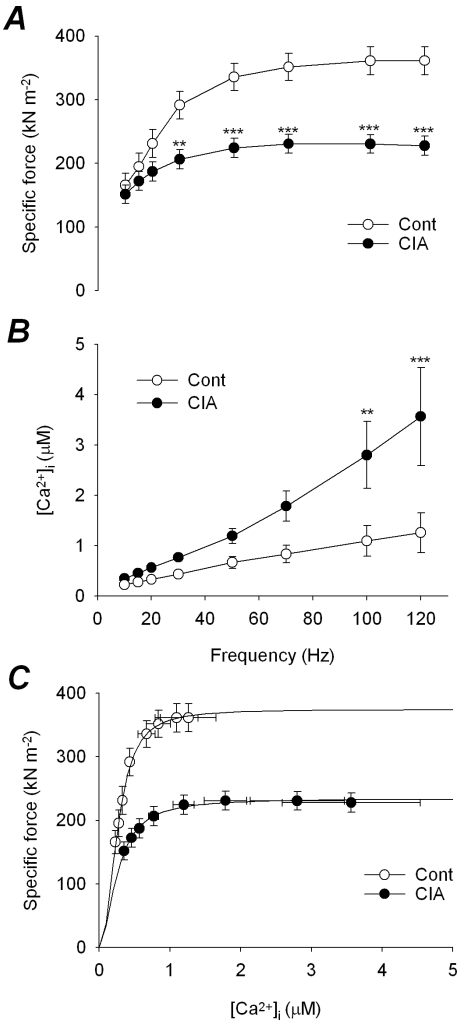

FIGURE 2. Decreased muscle force production due to impaired cross-bridge function in CIA soleus muscles. **A**, Force-frequency relationship in control and CIA soleus muscles. **B**, Myoplasmic free Ca^{2+} concentration ($[Ca^{2+}]_i$)-frequency relationship in control and CIA soleus muscle fibers. **C**, Force-$[Ca^{2+}]_i$ curves, generated by plotting the mean muscle force against the mean $[Ca^{2+}]_i$ at different frequencies. Bars show the mean $\pm$ SEM results from 6-8 muscles per group. ** = $P < 0.01$; *** = $P < 0.001$ versus controls. See Figure 1 for other definitions.

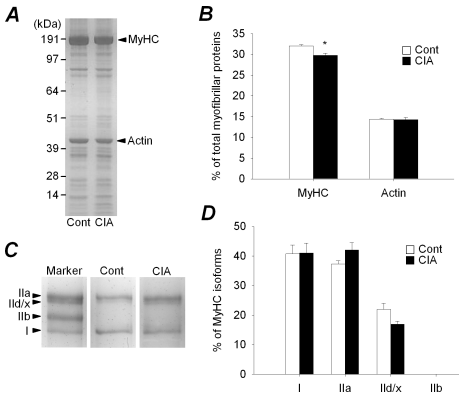

FIGURE 3. Decrease in myosin heavy-chain (MyHC) content, but no changes in MyHC isoform expression in CIA soleus muscles. **A**, Expression levels of the myofibrillar proteins MyHC and actin were assessed in control and CIA soleus muscles by SimplyBlue Safestain. **B**, The percentage distribution of MyHC and actin content in total myofibrillar proteins was compared between control and CIA soleus muscles. **C**, Fast-MyHC isoforms IIa, IId/x, and IIb and slow-MyHC isoform I were electrophoretically separated, and their expression levels were assessed in control and CIA soleus muscles. **D**, The percentage distribution of the 4 MyHC isoforms was compared between control and CIA soleus muscles. Bars in **B** and **D** show the mean and SEM results from 3-4 muscles per group. * = $P < 0.05$ versus controls. See Figure 1 for other definitions.

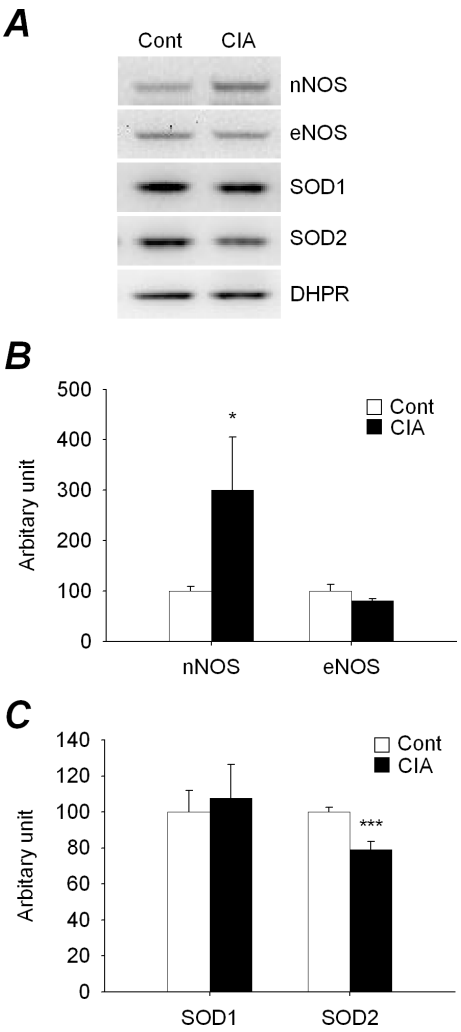

FIGURE 4. Alterations in the metabolism of reactive nitrogen and reactive oxygen species in CIA soleus muscles. **A**, The levels of nitric oxide synthase (NOS) and superoxide dismutase (SOD) isoforms in control and CIA soleus muscles were determined by Western blotting. The inducible NOS isoform was not detected in either group. **B** and **C**, The levels of NOS isoforms (**B**) and SOD isoforms (**C**) were quantified, with results normalized to the dihydropyridine receptor (DHPR) content. Bars show the mean and SEM results from 5-10 muscles per group. * = $P < 0.05$; *** = $P < 0.001$ versus controls. nNOS = neuronal NOS; eNOS = endothelial NOS; SOD1 = copper/zinc SOD; SOD2 = manganese SOD (see Figure 1 for other definitions).

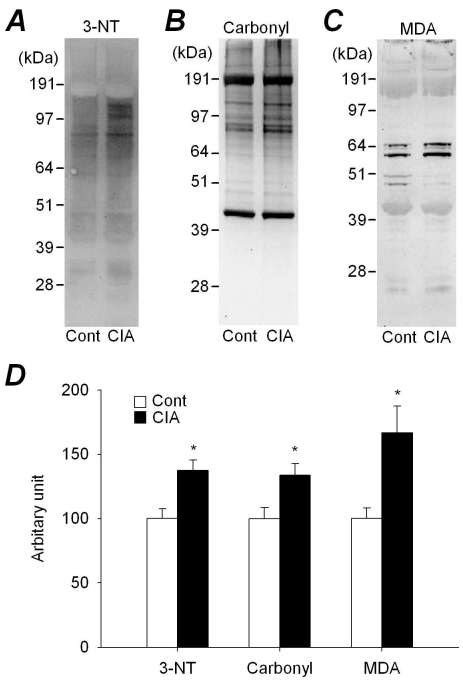

FIGURE 5. Increased total 3-nitrotyrosine (3-NT), carbonyl, and malondialdehyde (MDA)-protein adducts content in myofibrillar proteins from collagen-induced arthritis (CIA) soleus muscles. The levels of 3-NT (**A**), carbonyl (**B**), and MDA-protein adducts (**C**) were assessed in myofibrillar proteins from control (Cont) and CIA soleus muscles by Western blotting, and results were quantified as arbitrary units normalized to actin content (**D**). Densitometry was used to measure the total density of each lane. Bars show the mean and SEM results from 3-4 muscles per group. * = $P < 0.05$ versus controls.

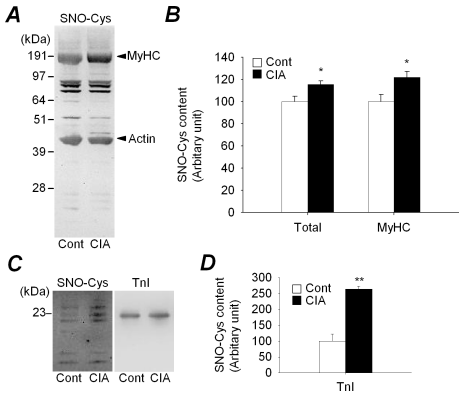

FIGURE 6. Increased S-nitrosocysteine (SNO-Cys) content in myosin heavy-chain (MyHC), troponin I (TnI), and other myofibrillar proteins from CIA soleus muscles. **A**, Representative Western blots illustrating the levels of SNO-Cys in myofibrillar proteins from control and CIA soleus muscles. The densities of all bands in a box covering each lane and the MyHC band were densitometrically measured. **B**, Quantification of the levels of SNO-Cys in total myofibrillar proteins and in MyHC in CIA and control soleus muscles, with results normalized to actin content. **C**, The same membrane as used in the experiment shown in **A**, developed for a longer time to reveal the less abundant low molecular weight bands reacting with anti-SNO-Cys antibody. Membranes were then stripped and reprobed with anti-troponin I antibody. **D**, Quantification of the Western blotting results shown in **C**, with the density of the SNO-Cys band at ~23-kd protein normalized to the content of total troponin I. Bars in **B** and **D** show the mean and SEM results from 4 muscles per group. * = $P < 0.05$; ** = $P < 0.01$ versus controls. See Figure 5 for other definitions.

References

1. Sokka T, Häkkinen A, Kautiainen H, Maillefert JF, Tolaza S, Hansen J, et al. Physical inactivity in patients with rheumatoid arthritis: data from twenty-one countries in a cross-sectional, international study. Arthritis Rheum 2008;59:42-50.
2. Lundberg IE, Nader GA. Molecular effects of exercise in patients with inflammatory rheumatic disease. Nat Clin Pract Rheumatol 2008;4:597-604.
3. Stenström CH, Minor MA. Evidence for the benefit of aerobic and strengthening exercise in rheumatoid arthritis. Arthritis Rheum. 2003;49:428-434.
4. Helliwell PS, Jackson S. Relationship between weakness and muscle wasting in rheumatoid arthritis. Ann Rheum Dis 1994;53:726-8.
5. Dalla Libera L, Ravara B, Gobbo V, Danieli Betto D, Germinario E, Angelini A, et al. Skeletal muscle myofibrillar protein oxidation in heart failure and the protective effect of Carvedilol. J Mol Cell Cardiol 2005;38:803-7.
6. Szentesi P, Bekedam MA, van Beek-Harmsen BJ, van der Laarse WJ, Zaremba R, Boonstra A, et al. Depression of force production and ATPase activity in different types of human skeletal muscle fibers from patients with chronic heart failure. J Appl Physiol 2005;99:2189-95.
7. Coirault C, Guellich A, Barbry T, Samuel JL, Riou B, Lecarpentier Y. Oxidative stress of myosin contributes to skeletal muscle dysfunction in rats with chronic heart failure. Am J Physiol 2007;292:H1009-17.
8. Lanone S, Mebazaa A, Heymes C, Henin D, Poderoso JJ, Panis Y, et al. Muscular contractile failure in septic patients: role of the inducible nitric oxide synthase pathway. Am J Respir Crit Care Med 2000;162:2308-15.
9. Drew JS, Farkas GA, Pearson RD, Rochester DF. Effects of a chronic wasting infection on skeletal muscle size and contractile properties. J Appl Physiol 1988;64:460-5.
10. Supinski GS, Callahan LA. Free radical-mediated skeletal muscle dysfunction in inflammatory conditions. J Appl Physiol 2007;102:2056-63.
11. Ward CW, Reiken S, Marks AR, Marty I, Vassort G, Lacampagne A. Defects in ryanodine receptor calcium release in skeletal muscle from post-myocardial infarct rats. FASEB J 2003;17:1517-9.
12. Wehrens XH, Lehnart SE, Reiken S, van der Nagel R, Morales R, Sun J, et al. Enhancing calstabin binding to ryanodine receptors improves cardiac and skeletal muscle function in heart failure. Proc Natl Acad Sci USA 2005;102:9607-12.
13. Supinski G, Nethery D, Nosek TM, Callahan LA, Stofan D, DiMarco A. Endotoxin administration alters the force vs. pCa relationship of skeletal muscle fibers. Am J Physiol 2000;278:R891-6.
14. Yamada T, Mishima T, Sakamoto M, Sugiyama M, Matsunaga S, Wada M. Oxidation of myosin heavy chain and reduction in force production in hyperthyroid rat soleus. J Appl Physiol 2006;100:1520-1526.
15. Szabo C, Ischiropoulos H, Radi R. Peroxynitrite: biochemistry, pathophysiology and development of therapeutics. Nat Rev Drug Discov 2007;6:662-80.
16. Pacher P, Beckman JS, Liaudet L. Nitric oxide and peroxynitrite in health and disease. Physiol Rev 2007;87:315-424.

17. Sandhu JK, Robertson S, Birnboim HC, Goldstein R. Distribution of protein nitrotyrosine in synovial tissues of patients with rheumatoid arthritis and osteoarthritis. J Rheumatol 2003;30:1173-81.
18. Cuzzocrea S, McDonald MC, Mota-Filipe H, Mazzon E, Costantino G, Britti D, et al. Beneficial effects of tempol, a membrane-permeable radical scavenger, in a rodent model of collagen-induced arthritis. Arthritis Rheum 2000;43:320-8.
19. Supinski G, Stofan D, Callahan LA, Nethery D, Nosek TM, DiMarco A. Peroxynitrite induces contractile dysfunction and lipid peroxidation in the diaphragm. J Appl Physiol 1999;87:783-91.
20. Williams RO. Collagen-induced arthritis as a model for rheumatoid arthritis. Methods Mol Med 2004;98:207-16.
21. Campbell IK, Hamilton JA, Wicks IP. Collagen-induced arthritis in C57BL/6 (H-2b) mice: new insights into an important disease model of rheumatoid arthritis. Eur J Immunol 2000;30:1568-75.
22. Marinova-Mutafchieva L, Williams RO, Mason LJ, Mauri C, Feldmann M, Maini RN. Dynamics of proinflammatory cytokine expression in the joints of mice with collagen-induced arthritis (CIA). Clin Exp Immunol 1997;107:507-12.
23. Feldmann M, Brennan FM, Williams RO, Woody JN, Maini RN. The transfer of a laboratory based hypothesis to a clinically useful therapy: the development of anti-TNF therapy of rheumatoid arthritis. Best Pract Res Clin Rheumatol 2004; 18:59-80.
24. Reid MB, Lännergren J, Westerblad H. Respiratory and limb muscle weakness induced by tumor necrosis factor-alpha: involvement of muscle myofilaments. Am J Respir Crit Care Med 2002;166:479-84.
25. Ekdahl C. Muscle function in rheumatoid arthritis. Assessment and training. Scand J Rheumatol Suppl 1990;86:9-61.
26. Häkkinen A, Kautiainen H, Hannonen P, Ylinen J, Mäkinen H, Sokka T. Muscle strength, pain, and disease activity explain individual subdimensions of the Health Assessment Questionnaire disability index, especially in women with rheumatoid arthritis. Ann Rheum Dis 2006;65:30-4.
27. Kokkola R, Li J, Sundberg E, Aveberger AC, Palmblad K, Yang H, et al. Successful treatment of collagen-induced arthritis in mice and rats by targeting extracellular high mobility group box chromosomal protein 1 activity. Arthritis Rheum 2003;48:2052-8.
28. Lännergren J. The force-velocity relation of isolated twitch and slow muscle fibres of Xenopus laevis. J Physiol 1978;283:501-21.
29. Bruton J, Tavi P, Aydin J, Westerblad H, Lännergren J. Mitochondrial and myoplasmic [Ca2+] in single fibres from mouse limb muscles during repeated tetanic contractions. J Physiol 2003;551:179-90.
30. Andrade FH, Reid MB, Allen DG, Westerblad H. Effect of hydrogen peroxide and dithiothreitol on contractile function of single skeletal muscle fibres from the mouse. J Physiol 1998;509:565-75.
31. Fagan JM, Sleczka BG, Sohar I. Quantitation of oxidative damage to tissue proteins. Int J Biochem Cell Biol 1999; 31:751-7.
32. Bradford MM. A rapid and sensitive method for the quantitation of microgram quantities of protein utilizing the principle of protein-dye binding. Anal Biochem 1976;72:248-54.
33. Edman KA. The velocity of unloaded shortening and its relation to sarcomere length and isometric force in vertebrate muscle fibres. J Physiol 1979;291:143-59.
34. Hennig R, Lomo T. Firing patterns of motor units in normal rats. Nature 1985; 314:164-6.

35. Allen DG, Westerblad H. The effects of caffeine on intracellular calcium, force and the rate of relaxation of mouse skeletal muscle. J Physiol 1995;487:331-42.
36. Ischiropoulos H, al-Mehdi AB. Peroxynitrite-mediated oxidative protein modifications. FEBS Lett 1995;364:279-82.
37. Ferreira LF, Reid MB. Muscle-derived ROS and thiol regulation in muscle fatigue. J Appl Physiol 2008;104:853-60.
38. Alvarez B, Radi R. Peroxynitrite reactivity with amino acids and proteins. Amino Acids 2003;25:295-311.
39. Stamler JS, Sun QA, Hess DT. A SNO storm in skeletal muscle. Cell 2008;133:33-5.
40. Allen DG, Lännergren J, Westerblad H. Muscle cell function during prolonged activity: cellular mechanisms of fatigue. Exp Physiol 1995;80:497-527.
41. Westerblad H, Allen DG. Changes of myoplasmic calcium concentration during fatigue in single mouse muscle fibers. J Gen Physiol 1991;98:615-35.
42. Fryer MW, Neering IR. Actions of caffeine on fast- and slow-twitch muscles of the rat. J Physiol 1989;416:435-54.
43. El-Dwairi Q, Comtois A, Guo Y, Hussain SN. Endotoxin-induced skeletal muscle contractile dysfunction: contribution of nitric oxide synthases. Am J Physiol 1998;274:C770-9.
44. Tiago T, Simao S, Aureliano M, Martin-Romero FJ, Gutierrez-Merino C. Inhibition of skeletal muscle S1-myosin ATPase by peroxynitrite. Biochemistry 2006;45:3794-804.
45. Horwitz J, Bullard B, Mercola D. Interaction of troponin subunits. The interaction between the inhibitory and tropomyosin-binding subunits. J Biol Chem 1979;254:350-5.
46. Perkins WJ, Han YS, Sieck GC. Skeletal muscle force and actomyosin ATPase activity reduced by nitric oxide donor. J Appl Physiol 1997;83:1326-32.
47. Barreiro E, Gea J, Corominas JM, Hussain SN. Nitric oxide synthases and protein oxidation in the quadriceps femoris of patients with chronic obstructive pulmonary disease. Am J Respir Cell Mol Biol 2003;29:771-8.
48. Souza JM, Choi I, Chen Q, Weisse M, Daikhin E, Yudkoff M, et al. Proteolytic degradation of tyrosine nitrated proteins. Arch Biochem Biophys 2000;380:360-6.
49. Nin N, Cassina A, Boggia J, Alfonso E, Botti H, Peluffo G, et al. Septic diaphragmatic dysfunction is prevented by Mn(III)porphyrin therapy and inducible nitric oxide synthase inhibition. Intensive Care Med 2004;30:2271-8.
50. Mabley JG, Liaudet L, Pacher P, Southan GJ, Groves JT, Salzman AL, et al. Part II: beneficial effects of the peroxynitrite decomposition catalyst FP15 in murine models of arthritis and colitis. Mol Med 2002;8:581-90.

Paper 4

4

History effect and timing of force production introduced in a skeletal muscle model

By Natalia Kosterina[1], Håkan Westerblad[2] and Anders Eriksson[1]

[1] Department of Mechanics, Royal Institute of Technology, SE-100 44 Stockholm, Sweden
[2] Department of Physiology and Pharmacology, Karolinska Institutet, Stockholm, Sweden

Biomechanics and Modeling in Mechanobiology
Accepted 8 December 2011

Skeletal muscle modelling requires a detailed description of muscular force production. We have performed series of experiments on mouse skeletal muscles to give a basis for an improved description of the muscular force production. Our previous work introduced a force modification in isometric phases, which was based on the work performed by or on the muscle during transient length-varying contractions. Here, state-space diagrams were used to investigate the timing aspects of the force production. These show a dominant exponential nature of the force development in isometric phases of the contractions, reached after a non-exponential phase, assumed as an activation or deactivation stage, not further analysed here. The time constants of the exponential functions describing isometric force redevelopment after length variations appear to be related to the one for an initial isometric contraction, but depending on the previous history. The timing of force production calculated from the state-space diagrams were in agreement with the generally accepted muscle properties, thereby demonstrating the reliability of the method. A macroscopic muscular model consisting of a contractile element (CE), parallel and series elastic elements (PEE, SEE) was developed. The parameters from the experiment analysis, particularly the force modification after non-isometric contractions and the time constants, were reproduced by the simulations. The relation between time constants introduced in a mechanistic model and the measured macro scale timings is discussed.

Keywords: Muscular force; Length variations; State-space diagrams; Time constant; Muscle model; Hill-type; Force modification

1. Introduction

Previous work by the authors focused on the isometric force modifications taking place after transient-length muscular contractions, commonly denoted as force depression following concentric contractions and force enhancement following eccentric contractions (Kosterina et al. 2008, 2009). These studies were based on introduction of systematic length regimes during contraction in experiments on mouse *soleus* ('SOL') and *extensor digitorum longus* ('EDL') muscles. It was concluded that the work produced by the muscle during shortening, and on the muscle during stretch, was a good

predictor for this force modification when focusing on a macroscopic description of the muscle force production, rather than on a phenomenological description of the inner mechanisms (Abbott and Aubert 1952; Marechal and Plaghki 1979; Sugi and Tsuchiya 1988; Lou et al. 1998; Schachar et al. 2004; Bagni et al. 2005; Morgan 2007). The description thus aimed at a model for numerical simulations of whole-body systems, which can consider the history effects in the force producing capacity.

For the active isometric force immediately continuing a transient-length contraction, the description of a force modification is focussed on an asymptotic, i.e., a theoretical long-term steady-state force value. This was compared to the asymptotic force for an initial isometric contraction, where the same length was held constant from the start of stimulation. Such values were evaluated from the force-time trace by curve-fitting (Kosterina et al. 2009). With experimental length variations according to Fig. 1, the curve fitting considered the isometric phases before and after a length variation. A good numerical fit was generally obtained with an exponential functions of the form:

$$F(t) = F_\infty + (F_a - F_\infty) \cdot e^{-(t-t_a)/\tau} \tag{1}$$

where the force F at a time t goes from a value F_a at a time t_a to a steady-state asymptotic value F_∞ through an exponential function with a time constant τ (Hancock et al. 2004; Corr and Herzog 2005). The conclusion from Kosterina et al. (2008) was that the time constant τ_r for an isometric phase following shortening was – for practical purposes and on the macro scale – well predicted by the one, τ_o, for an initial isometric contraction.

The result from our previous papers, Kosterina et al. (2008, 2009), is thereby that the transient force production in an isometric phase of a contraction following a length variation can be well predicted by the introduction of a force modification, considering the history through the work quantity, and the initial time constant, being a typical parameter for a muscle individual. The force modification, positive or negative, is here seen as a difference between the isometric forces obtainable at initial and at post-ramp isometric contractions at the corresponding length. Example force-time and length-time traces for one SOL muscle individual for isometric, stretch, shortening, stretch-shortening and two-steps shortening experiments are presented in Fig. 1.

Here, the further mathematical analysis of the force-time traces takes the experience from fitting Eq. (1) to isometric phases as inspiration. From a mechanical viewpoint, the contents of the equation would indicate the presence of a viscous damper in series with the force generator in the muscle. This can be seen by identifying the equation as an evolution process, where the time differential of the force is described by:

$$\dot{F}(t) \equiv \frac{d\,F}{dt} = \frac{1}{\tau}\,(F_\infty - F(t)) \tag{2}$$

where F_∞ is the asymptotic force, and the superposed dot denotes a time differential, i.e., the slope of the time trace. The expression emphasizes that the force value is constantly approaching the asymptotic value, in each time interval reducing the distance by the same ratio.

A common way to consider an evolution expression like the one in Eq. (2), an autonomous differential equation, is through the state-space (Thompson and Stewart

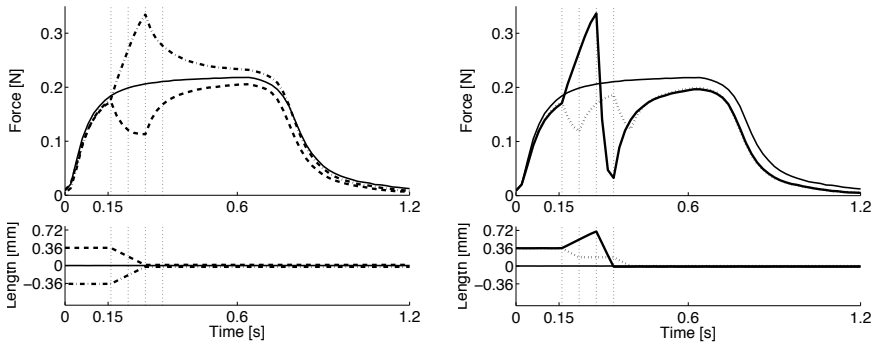

FIGURE 1. Examples of force-time traces on mouse SOL muscles. Thin solid lines correspond to isometric contractions. Transient-length contractions: (a) dash-dot line - stretching and dashed line - shortening by 0.36 mm in 0.12 s, (b) dotted line - two-step shortening by 0.18 mm in 0.06 s each with 0.12 s delay between them, thick solid line - stretch-shortening cycle. All experiments end at the optimal length of the muscle. Time t=0 denotes the stimulation start, Length=0 the individual optimal length.

1986; Jeffrey 1990; Jordan and Smith 1999), where $F(t)$ and $\dot{F}(t)$ are seen as the axes in a plane diagram, and where an expression of the form in Eq. (2) will come out as a straight line, with a slope of $-\frac{1}{\tau}$, and coming to $\dot{F} = 0$ for $F = F_\infty$. Utilization of this technique for description of the macro muscular behaviour is the main content of the present paper. We,however, would like to point to the fact that this macro timing is phenomenologically an aggregate of several internal time constants, and not immediately comparable to other time constants used in interpolation or modelling of muscle experiments.

The state-space visualization of the experimental time-data will thus reveal if the measured quantity, here muscular force, is realistically described by a function like the one in Eq. (1). Straight lines in the diagram will confirm this assumption for a phase of the interval, whereas curved lines will correspond to phases, where either the behaviour is not exponential, or the asymptotic value is not a constant attractor (Jeffrey 1990). It is already here noted, that the non-isometric parts of the force-trace should not be straight lines, as the changing length will in itself implicate differences in isometric force.

There is always a time span before the force takes the path of exponential development or redevelopment after stimulation and destimulation, respectively. These time intervals obviously correspond to some aspects of activation of the muscle, but in order to not confuse previous definitions of this term (Stephenson and Williams 1982; Stein et al. 1982), we will here use a terminology not related to internal aspects of muscle action. The present analysis thus defines periods to reach maximum and

minimum (i.e. the maximal negative) rates of force time derivative. We will denote them $t_{\triangle}$ and $t_{\triangledown}$. The time-stamps of the points in the diagram indicate the different phases of behaviour. In particular, the time-stamps of the end points of the straight lines in the diagram carry a meaning with respect to force time differential extremum.

A skeletal muscle model described by Günther et al. (2007) was considered as a basis for our simulations. The model was adopted for mouse SOL and EDL muscles. A so called history effect, emergent after active shortening and stretch (Abbott and Aubert 1952; Herzog and Leonard 1997), was introduced in the model in order to improve the numerical muscular force description. Previous attempts to include a history effect in muscle models used dependence of the force modification on ramp parameters such as amplitude and velocity, Edman (1979); Marechal and Plaghki (1979); Meijer et al. (1998). Our previous study has shown linear relations between the force modification and mechanical work produced during stretch and shortening, Kosterina et al. (2008, 2009); this is also supported by Herzog et al. (2000); McGowan et al. (2010). The need for reasonably accurate macro level muscular models, considering the timing, is emphasized by studies on optimal human movements, Pettersson et al. (2010).

The present paper will discuss the analysis of muscle contraction experiments performed, by means of the state-space view, aiming at a macroscopic interpretation of the force production in the isometric phases of contractions. These findings were introduced in the rheological skeletal muscle model presented in this study. A brief review of the experiments is given in Section 2, which also describes the mathematical analysis procedure and the numerical muscle modelling aspects. The results are given in Section 3, and discussed in Section 4.

2. Materials and methods

2.1. *Mouse muscle experiments*

The present work is built upon a set of transient-length experiments on dissected mouse SOL and EDL muscles, (Kosterina et al. 2009). The maximum admissible decrease in optimal force before discarding a specimen was set to 10%. The experiment series contained a total of 11 SOL and 14 EDL muscles. As each muscle was only used in a subset of experiments, the final results for each experiment are based on results from $\mathrm{n} = 5 - 6$ muscles. In each experiment the length was systematically varied during full tetanic stimulation of the muscle. The forces and the lengths were recorded for processing. Full experimental details are given in the reference, as are main characteristic data of the muscles investigated.

2.2. *Data processing*

Force and length data were recorded at $500\,\mathrm{Hz}$ during the experiments. The noise level in the data was low, hardly visible in the time traces of the quantities. As, however, for the present purposes the time differentials of the force data were needed, a filtering of the force data was performed. This filtering was defined by a second-order Butterworth lowpass recursive filter with a cutoff frequency of 60 Hz, performed in

Matlab (version R2010a, The MathWorks, Inc., Natick, MA, USA). The force differential was then evaluated in the midpoints of the time steps recorded, through a central difference approximation; corresponding force values were the averages between the neighboring points:

$$t_{i+1/2} = \frac{1}{2}\left(t_i + t_{i+1}\right) \tag{3}$$

$$F_{i+1/2} = \frac{1}{2}\left(F_i + F_{i+1}\right) \tag{4}$$

$$\dot{F}_{i+1/2} = \frac{1}{\Delta t}\left(F_{i+1} - F_i\right) \tag{5}$$

where the indices refer to experimental time $t_i = i \cdot \Delta t = i \cdot 0.002\,[\mathrm{s}]$ since start of the stimulation.

2.3. *State-space analysis*

All the experiments were after filtering plotted in the state-space diagrams, with $F(t)$ as ordinate and $\dot{F}(t)$ as abscissa. The borderlines between the different isometric and isokinetic parts of the curves were marked, and each such segment treated separately. As examples, the state-space diagrams of some of the experiments are given in Figs. 2–5, with the time stamps at interesting points.

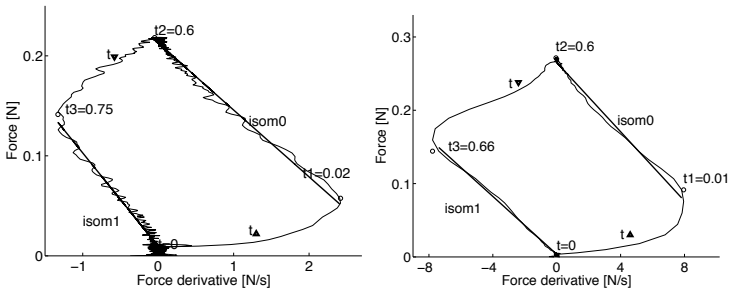

(a) (b)

FIGURE 2. State-space plot of example isometric test performed on mouse SOL (a) and EDL (b) muscles, showing the relation between current force and force time differential values over experimental time. Time $t_0 = 0$ denotes start of stimulation, the force time differential, $\dot{F}(t)$, increases during $t_\triangle$ until reaching a maximum value at time t_1. Then the force, $F(t)$, rises exponentially ('isom0') and reaches a steady-state value when the $\dot{F}(t)$ drops to zero. After the stimulation terminates at time t_2, force and force derivative start to decrease. $\dot{F}(t)$ drops to its minimum value during $t_\triangledown$ (until time t_3), then the force decays exponentially to its passive level ('isom1').

It is obvious from Figs. 2–5 that the start and end of stimulation cause non-straight lines corresponding to a preparation for isometric active and passive phases of force development and decay. In the figures, time stamps are marked where the assumed

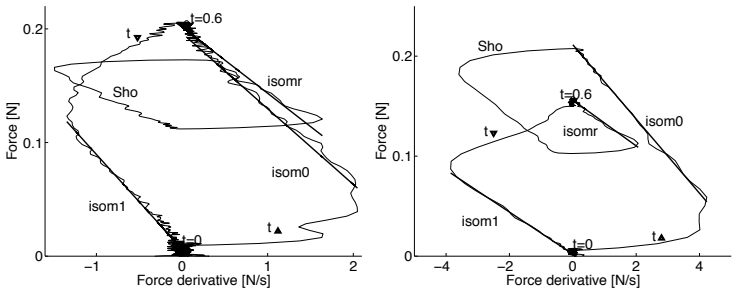

FIGURE 3. State-space plot of example shortening test performed on mouse SOL (a) and EDL (b) muscles, showing the relation between current force and force time differential values over experimental time. Time $t = 0$ denotes start of stimulation, stimulation is ended at $t = 0.6$ s. The straight lines are regression fits of the isometric phases of muscle contractions: 'isom0' - initial force development, 'isomr' - force redevelopment after shortening, 'isom1' - force decay after destimulation. 'Sho' denotes the active shortening phase.

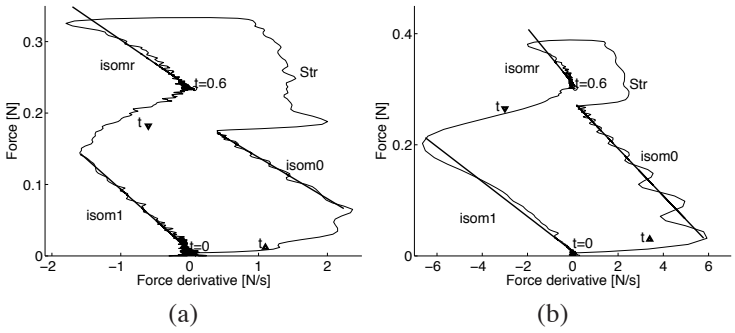

FIGURE 4. State-space plot of example stretch test performed on mouse SOL (a) and EDL (b) muscles, showing the relation between current force and force time differential values over experimental time. Time $t = 0$ denotes start of stimulation, stimulation is ended at $t = 0.6$ s. The straight lines are regression fits of the isometric phases of muscle contractions: 'isom0' - initial force development, 'isomr' - force redevelopment after stretching, 'isom1' - force decay after destimulation. 'Str' denotes the active stretch phase.

straight lines start. These points were defined as maximum and minimum values of the force time differential, $\dot{F}(t)$, reached from start and end of stimulation on a relevant time interval. Times $t_{\triangle}$ and $t_{\triangledown}$ for each experiment denote the intervals of this rise and drop of force rate.

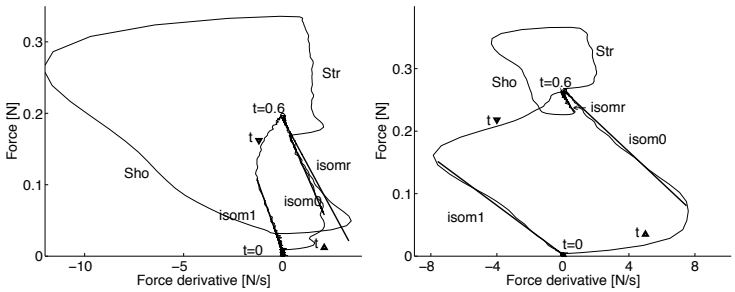

FIGURE 5. State-space plot of example stretch-shortening test performed on mouse SOL (a) and EDL (b) muscles, showing the relation between current force and force time differential values over experimental time. Time $t = 0$ denotes start of stimulation, stimulation is ended at $t = 0.6$ s. The straight lines are regression fits of the isometric phases of muscle contractions: 'isom0' - initial force development, 'isomr' - force redevelopment after stretch-shortening ramp, 'isom1' - force decay after destimulation. 'Str' and 'Sho' denote the active stretch and shortening phases correspondingly.

When the maximum rate of force rise was reached, an exponential isometric force development began. This phase appeared as a straight line on the state-space diagram (Fig. 2). Change of length or activation regime leads to clear changes in the curve. A phase of force redevelopment after active lengthening or shortening was identified using time stamps, and this turned out as a straight line (Figs. 3–5). Passive force deactivation was detected using the time stamps, and also appeared as a straight line.

Having defined these time instances, the time constants for the straight lines of all isometric phases can be evaluated from the straight-line fitting. The time constants can be assumed to be valid for isometric, fully-active or fully passive phases. We denote by τ_0 the time constant for an active initial isometric case, by τ_r^-, τ_r^+ and $\tau_r^\pm$ the one for active recovery after shortening, stretch and stretch-shortening cycle, and by τ_1 the one for passive force loss.

As will be shown below, the time constants τ_r^-, τ_r^+ and $\tau_r^\pm$ for the active phases of the experiments are related to the initial time constant, τ_0, for a specific muscle individual.

2.4. *Modelling*

Simulation of muscular force generation was based on work done by Günther et al. (2007) and van Soest and Bobbert (1993) and was implemented in Matlab. A muscle-tendon complex was represented as a contractile element (CE) in parallel with an elastic element (PEE) and connected to a series elastic element (SEE), Fig. 6. Both elastic elements contain a damping components (D_{PE}, D_{SE}) in order to avoid high frequency oscillations which might occur in impact (Günther et al. 2007; Rode et al.

2009b). In our work, force modification component (Mod) is added in parallel to both CE and SEE.

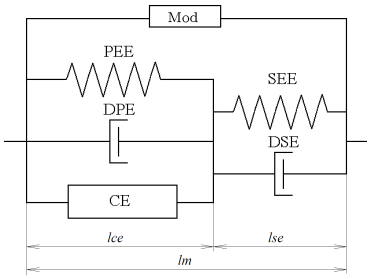

FIGURE 6. Schematic representation of the muscular model. The muscle-tendon model consists of two main components: the contractile element (CE) with parallel damped elastic element (PEE, D_{PE}), both of the same length, and the serial damped elastic element (SEE, D_{SE}). In total they form a whole muscle of length l_m, the sum of l_{CE} and l_{SE}. Force modification element (Mod) is placed parallel to CE and SE components.

The activation dynamics of a muscle is modelled as described by Ebashi and Endo (1968) and Hatze (1977), where the isometric force F_{CE} is scaled by the activation q, which in turn represents the Ca^{2+}-concentration of the muscle, Günther et al. (2007). The muscle deactivation after stimulation termination differs from the activation dynamics, therefore β_q coefficient was defined as a ratio of τ_0 to τ_1 (Eq. 1 in Günther et al. (2007)). The force-length bell-curve fitting gave four parameters, ΔW_{asc}, ΔW_{des}, $\nu_{\text{CE,asc}}$ and $\nu_{\text{CE,des}}$, describing the isometric force as a function of CE length (Eq. 5 in Günther et al. (2007)).

When stimulation and muscle length regimes are defined, contraction dynamics takes part. An equation for the contractile element velocity was derived by van Soest and Bobbert (1993)

$$\dot{l}_{CE} = \dot{l}_{CE}(l_m, l_{CE}, q) \tag{6}$$

as a function of the muscle length, CE length and activation q from the Hill equation, Hill (1938). The Hill parameters in the equation are dependent on current CE length, l_{CE}, and activation, q, as in Günther et al. (2007) and also Gordon et al. (1966); Julian and Morgan (1979); van Soest and Bobbert (1993). The concentric contractions were extrapolated into the eccentric region avoiding discontinuity on the boundary (Günther et al. 2007). The forces produced by CE with PE should be balanced with SE force. Considering damped PEE and SEE, the force equilibrium is

$$\begin{aligned} F_{CE}(l_{CE}, \dot{l}_{CE}, q) + F_{PEE}(l_{CE}) + d_{PE} * \dot{l}_{CE} = \\ F_{SEE}(l_{SE}) + d_{SE}(F_{CE}) * \dot{l}_{SE}. \end{aligned} \tag{7}$$

We solved the equation at each time instance by a secant method, giving the CE length velocity, $\dot{l}_{CE}$. The series and parallel elastic elements both have non-linear properties (Table 1). The series damping is force-dependent, the parallel damping is constant, scaled to the optimal force, F_0, to reflect individual parameters.

The history effect described in Kosterina et al. (2008, 2009) has been introduced in the model. Mechanical work, w, performed by and on the muscle was calculated for all transient phases from the beginning of stimulation. The force modifications evaluated were fitted with a straight line, and the history coefficient, K_{hist}, was defined as the slope of the line, seen as a parameter for the muscle individual. Negative work during stretch-shortening contractions was not taken into account for SOL muscles due to the ability of active shortening to suppress effects from force enhancement invoked by preceding lengthening, Herzog and Leonard (2000); Lee et al. (2001). The force modification, $F_{mod} = K_{hist} \cdot w$, was in the model added to the total force from Eq. 7 (Fig. 6).

In order to adopt the model for the mouse muscles, 20 parameters had to be varied and tested. The anatomical muscle length when generating the optimal force was equated to $l_{m,0}$. The optimal force, F_0, and the rates of force development and fall, τ_0 and τ_1, were extracted from the isometric contractions, Sections 2.2 and 2.3. These four parameters are the only individual characteristics. The remaining parameters were possible to keep invariable for SOL muscles, as model predictions were not significantly improved by modifying these. In order to achieve a good fit for EDL muscle contractions, more parameters must be varied for each specimen, but the higher variability in results leads to difficulties.

The optimal CE and SE lengths, $l_{CE,0}$ and $l_{SE,0}$, were always defined as 60% and 40% of the total length $l_{m,0}$, representing the ratio between the lengths of fibers and tendons with connective tissue.

3. Results

The time constants of isometric force redevelopment after non-isometric contractions are given in Table 2. The time constants of isometric force redeveloping, τ_r, are different from the initial timings, τ_0. But these time constants are similar inside the sets of experiments, as can be seen from the standard deviations for τ_r^-, τ_r^+ and $\tau_r^\pm$. A coefficient characterizing the type of non-isometric contraction, k, can be used to define the time constant, τ_r, of isometric force redevelopment as follows:

$$\tau_r = k \cdot \tau_0. \tag{8}$$

The multiplier k is presented in Table 2. The time constants for passive force loss, τ_1, appeared to be higher than the ones for active force development, τ_0, for SOL, and lower for EDL (Table 2, the last line).

For isometric contractions, the times of pre-isometric force rate rise, $t_\triangle$, were 0.037 ± 0.012 s for SOL and 0.012 ± 0.005 s for EDL muscles. The times of pre-isometric force rate fall, $t_\triangledown$, were 0.170 ± 0.021 s for SOL and 0.054 ± 0.006 s for EDL muscles. We can see that the EDL muscles are about three times faster than the SOL in activation and deactivation.

TABLE 1. Parameters of a SOL muscle-tendon model for an adult male NMRI mouse used in the simulations. Some of the parameters kept as in Günther et al. (2007) (Gün), others were obtained from the experiments (Exp) or simulation fitting (Fit).

	Constants and values				Source
Individual parameters	l_m (m)	F_0 (N)	τ_0 (s)	τ_1 (s)	
(typical values)	0.011	0.210	0.063	0.052	Exp
General parameters	$l_{CE} = l_{PE}$	l_{SE}	β_q	$K_{hist}(m^{-1})$	
	$0.6 \cdot l_m$	$0.4 \cdot l_m$	τ_0/τ_1	-3	Fit, Exp
Isometric force	ΔW_{asc}	ΔW_{des}	$\nu_{CE,asc}$	$\nu_{CE,des}$	
$F_{isom}(l_{CE})$	0.39	0.3	2.7	2	Exp, Fit
Contraction dymanics	$A_{rel,0}$	$B_{rel,0}$ (1/s)	$\mathcal{S}_{ecc}$	$\mathcal{F}_{ecc}$	
(concentric, eccentric)	0.1	1	2	1.8	Fit,Gün
Parallel elastic element	$\mathcal{L}_{PEE,0}$	ν_{PEE}	$\mathcal{F}_{PEE}$	d_{PE}(Ns/m)	
(nonlinear), damping	0.9	2.5	1	$6 \cdot F_0$	Gün,Fit
Series elastic element	$\Delta U_{SEE,nll}$	$\Delta U_{SEE,l}$	$\Delta F_{SEE,0}$(N)		
(nonlinear)	0.1825	0.073	$2 \cdot F_0$		Gün
Series damping	d_{SE}(Ns/m)	D_{SE}	R_{SE}		
(force-dependent)	6	0.3	0.01		Gün

The stretch and shortening ramps were applied when the isometric force had almost reached a steady value. Therefore, it was possible to measure the time $t_\triangle$, for different initial muscle lengths. It has been noticed that a lengthened muscle reaches the maximum rate of rise faster than a shortened one. The time, $t_\triangle$, depends on the muscle length, Fig. 7, for both fast and slow twitch muscles, though this occurrence is not pronounced for EDL.

The force rate fall, $t_\triangledown$, depends on the length history, Fig. 8, Table 3. For SOL muscles, this time after active shortening and stretch-shortening cycle is almost the same as after an isometric contraction, while deactivation after active stretch is twice as long. For EDL muscles, the fall of the force rate to a minimum value after an isometric contraction happens up to three times faster than after a non-isometric contraction.

The numerical muscle model has been described as a combination of contractile, elastic and damping elements, Siebert et al. (2008), Fig. 6. The set of equations used in the model was taken from Günther et al. (2007). Six parameters were obtained from the experimental force-time traces. Each of 20 other parameters was varied in order to fit the simulation output with the experimental data (Table 1). If variation did not improve the force prediction, the parameters were kept as in Günther et al. (2007). Simulation of the force during isometric, shortening, stretch and stretch-shortening contractions for a SOL muscle from experiments is plotted in Fig. 9.

TABLE 2. The time constants of isometric force redevelopment after non-isometric contractions and their ratios with the initial time constant. The time constants were calculated from a linear approximation of the $F(t) - \dot{F}(t)$ curve on isometric phases and averaged on all experiments in the corresponding set, and for n $= 5 - 6$ SOL and n $= 5$ EDL muscles. The results are given as mean $\pm$ standard deviation, [s].

Experiments	SOL		EDL	
Isometric (rise)	τ_0 0.076 ± 0.018	$-$	τ_0 0.035 ± 0.007	$-$
Shortening	τ_r^- 0.046 ± 0.008	τ_r^-/τ_0 0.685 ± 0.112	τ_r^- 0.027 ± 0.004	τ_r^-/τ_0 0.929 ± 0.129
Lengthening (negative)	τ_r^+ 0.052 ± 0.009	τ_r^+/τ_0 0.721 ± 0.113	τ_r^+ 0.087 ± 0.014	τ_r^+/τ_0 2.342 ± 0.369
Lengthening- -Shortening	$\tau_r^\pm$ 0.064 ± 0.006	$\tau_r^\pm/\tau_0$ 0.775 ± 0.088	$\tau_r^\pm$ 0.039 ± 0.005	$\tau_r^\pm/\tau_0$ 1.086 ± 0.155
Isometric (fall)	τ_1 0.100 ± 0.025	τ_1/τ_0 1.335 ± 0.258	τ_1 0.024 ± 0.003	τ_1/τ_0 0.709 ± 0.121

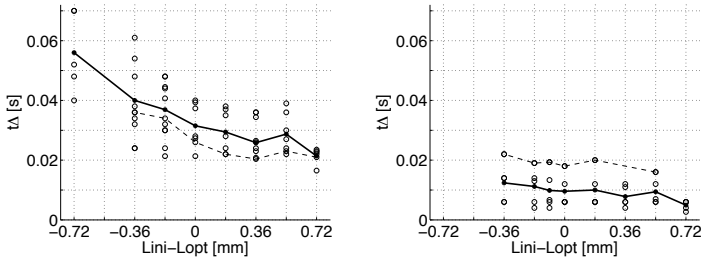

FIGURE 7. Times of the force rate rise, $t_\triangle$, at different muscle lengths, l_{ini}, compared to optimal length, l_{opt},. The nodes of the thick solid line relate to a mean $t_\triangle$ time value of all experiments started at the corresponding length, l_{ini}, for n$= 5 - 6$ SOL (a) and EDL (b) muscles. The circles correspond to an individual muscles (mean values for isometric force development at each length), the dashed line connects the individual values for a specific muscle.

The timing constants, τ, were obtained for the total force development while in the model only the CE force component is described by the exponential function. The serial elastic element, that takes 40% of the muscle length, slows down isometric development of the total force, F_m, and speeds up isometric force fall. The time

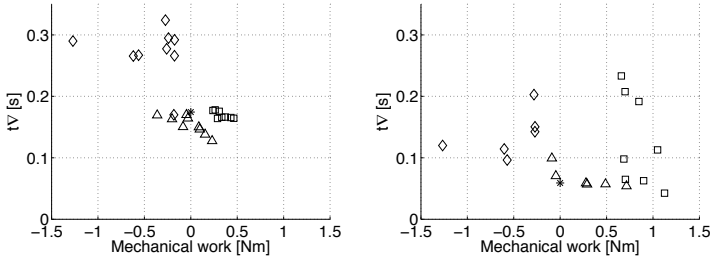

(a) (b)

FIGURE 8. Times of the force rate drop, t_∇, as a function of performed mechanical work. Results from n $= 5 - 6$ SOL (a) and n $= 5$ EDL (b) muscles are presented as mean values: Shortening - squares, Lengthening - diamonds, Lengthening-Shortening - triangles. Average value of t_∇ after an isometric contraction is marked as asterisk.

TABLE 3. Times of the force rate drop after stimulation termination, t_∇, following isometric and non-isometric contractions. Results from n $= 5 - 6$ SOL and n $= 5$ EDL muscles are given as mean $\pm$ standard deviation, [s].

Experiments	SOL	EDL
Isometric	0.170 ± 0.021	0.054 ± 0.006
Shortening	0.170 ± 0.014	0.132 ± 0.081
Lengthening	0.293 ± 0.059	0.138 ± 0.055
Lengthening-Shortening	0.154 ± 0.020	0.066 ± 0.021

constant in the model was found to be approximately 40% longer that the experimental time constants for a good fit. Similar modifications were done for force fall during deactivation. The resulting fitting is shown on the force-time plots and the state-space diagrams (Fig. 9–10). The timing constants $\tau_{0,sim}$ calculated from the state-space plots for the simulated force appeared as 0.067 ± 0.012s, this is about 80% of the experimental values τ_0. The timing constants $\tau_{r,sim}$ are between 60% and 140% of the experimental values τ_r. The best fit was reached for the concentric contractions.

4. Discussion

The study was motivated by an intention to improve the predictive capacity of available macroscopic transient muscle models such as the common Hill-type models. The main objective was to evaluate an accurate description of the muscular force during various regimes and to apply these findings to reproduce the muscular force generation.

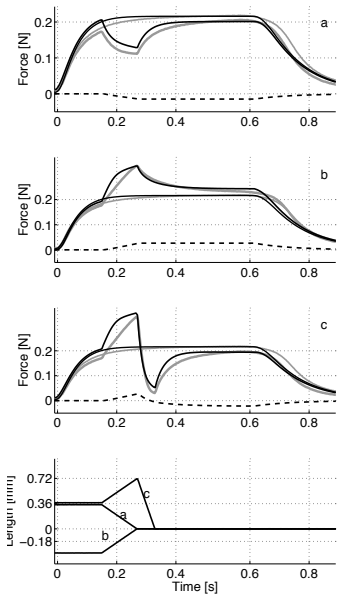

FIGURE 9. Simulations (black) and experiments (grey) of non-isometric contractions: shortening (a), stretching (b) and stretch-shortening (c), in each case compared to isometric contraction at the final length. Force modification is plotted as dashed line. The length regime is plotted below the force curves. SOL muscle.

To create a basis for a numerical muscle model, the timing aspects of the force production should be described. An exponential fitting of the force-time traces is generally used (Hancock et al. 2004; Corr and Herzog 2005). The state-space diagrams show linear relations between the muscular force and the force time differential during isometric force development. This observation confirms the admissibility of the exponential nature of the muscular force development (Stein et al. 1982), noting that the exponential phase is not reached immediately in all contexts.

The time constants characterizing the macroscopic force development at a constant muscle length were calculated from the state-space diagrams. These constants appeared approximately two times longer for SOL than for EDL muscles (Table 2). This is expected due to the different fibre compositions of these muscles, and is consistent with previous work (Luff 1981; Ranatunga 1982; Stein et al. 1982; Brooks and Faulkner 1988).

It has been noticed that the force after non-isometric phases also follows an exponential function, Table 2. The time constants related to isometric force redevelopment following different length variations differ from the initial time constants by about

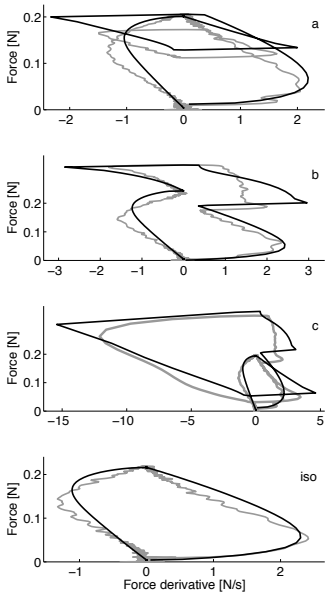

FIGURE 10. Sample state-space plots of simulations of isometric contraction (iso) and non-isometric contractions: shortening (a), stretching (b) and stretch-shortening (c), black lines. Experimental values are plotted with grey lines. SOL muscle.

30% only. We suggest that this difference is not significant and can without major inaccuracies be neglected in a muscle model for full body modelling. This similarity makes easy the extraction of timing constant for the force recovery using the time constant of initial isometric force development. It is prominent that the time constant for the EDL muscle force redevelopment after lengthening is more than double the initial one. We assume that the slower force recovery occurs due to vulnerability of fast muscle fibres to an active stretch, but not due to muscle damage, since verification tests have been performed to control the isometric force level (Kosterina et al. 2009).

Passive force loss following destimulation and deactivation of the muscles can also be described by an exponential function of time (τ_1). These findings give a more accurate description of the transient muscular force variation, and can be applied in the skeletal muscle model.

The state-space description allows an evaluation of times for the muscle force rate rise and fall. Here, these are defined as the times between a change in the stimulation (0/100%) and the time when the muscular force enters an exponential development curve, i.e. the straight lines in the state-space diagram. As noted above, these time

intervals can be related to activation aspects of muscle, but we see them as mathematical constants not to be compared to previously used terms or to be related to specific internal mechanisms, however, it seems obvious that the macro timing aspects are dependent on a set of internal events, each with its own time-scale..

The $t_{\triangle}$ and $t_{\triangledown}$ times of the muscle contractions have been used as indicators of motor unit recruitment (Fang and Mortimer 1991). This is presumably based on the size principle, implying that small and slow motor units are recruited at low force levels, and, that gradually larger and faster motor units are recruited with the force increasing (Henneman et al. 1965; Zajac and Faden 1985). Meanwhile, Savelberg (2000) has shown that the fiber composition in a muscle also affects the rise and relaxation times, and our study confirmed this observation.

It can be noticed from Figs. 2–5 that the relations between the force and the force time differential after destimulation become linear after a drop of force from the steady value by approximately 50%. This validates Stein et al. (1982), who showed that the force decays exponentially after falling to a force value of one-half to two-thirds of the peak. This, in essence, also agrees with the concept of half-relaxation times, evaluated from experiments, and used as a measure for de-activation timing.

Regarding the modelling part, we achieved a fairly good similarity between the experimental and the simulation traces. The timings calculated from the state-space diagrams were used to evaluate the time constants in the model, noting that the time constants are defined in different ways, depending on context, terminology, and modelling assumptions. A non-isometric phase of the contractions was fairly well simulated for shortening mode and less well for stretch mode due to a notable spread in the results for active lengthening and pecuilarity of eccentric contractions. However, a specific mechanism of eccentric force simulation based on a recruitable elastic titin spring was proposed (Till et al. 2008; Rode et al. 2009a).

An interesting observation is that the force redevelopment during the post-stretch and the post-shortening period in the muscle model can be perfectly fitted to an exponential function, even though the total force is a solution for the equilibrium equation and is not founded upon an exponential function. Therefore we affirm correctness of the principal model by Günther et al. (2007) and reaffirm the relevance of Hill's equation. As we can see from Table 1, many of the parameters used by Günther et al. (2007) were kept unchanged, even though the model was used for the simulation of a different type of muscles, and for another species. Many more experiments would be needed to verify differences in these constants.

The force modification following non-isometric contractions remarkably improved the force description. Although different mechanisms are believed to cause force depression and force enhancement, these phenomena were reasonably well described by a simple formula based on previous observations (Kosterina et al. 2009). Force modification after stretch-shortening contractions has not been thoroughly investigated yet and a mathematical description may vary between different settings. Findings of Herzog and Leonard (2000); Lee et al. (2001) show that the effect of force enhancement disappears with the following shortening, though this contradicts another observation

(Bullimore et al. 2008). The SOL and EDL mouse muscles show different force modification after sretch-shortening cycles (Kosterina et al. (2009), Fig.3). Therefore we did not count the negative work during stretch-shortening cycles for SOL muscles in the history-based force modification. The muscle model can be used in movement simulations, for cases where the history effect on the resulting movements is interesting.

5. Conclusions

The experimental analysis allowed us to evaluate the time constants of the exponential functions describing isometric force redevelopment after non-isometric contractions. The time constants calculated from the state-space diagrams were in agreement with generally accepted muscle properties, thereby demonstrating the reliability of the method, and the presence of activation modification timing.

The numerical muscle model based on Günther et al. (2007), was adapted for SOL mouse muscles. The history effect and the timings obtained from the state-space diagrams gave better simulation results for SOL mouse muscles in a variety of length regimes.

Acknowledgements

The authors gratefully acknowledge technical support in preparing muscle specimens from Shi-Jin Zhang, and financial support from the Swedish Research Council. We also thank Jan Lännergren for construction of the mechanical apparatus.

References

Abbott, B., Aubert, X., 1952. The force exerted by active striated muscle during and after change of length. Journal of Physiology 117, 77–86.

Bagni, M., Cecchi, G., Colombini, B., 2005. Crossbridge properties investigated by fast ramp stretching of activated frog muscle fibres. Journal of Physiology 565(1), 261–268.

Brooks, S., Faulkner, J., 1988. Contractile properties of skeletal muscles from young, adult and aged mice. Journal of Physiology 404, 71–82.

Bullimore, S., MacIntosh, B., Herzog, W., 2008. Is a parallel elastic element responsible for the enhancement of steady-state muscle force following active stretch? Journal of Experimental Biology 211, 3001–3008.

Corr, D., Herzog, W., 2005. Force recovery after activated shortening in whole skeletal muscle: Transient and steady-state aspects of force depression. Journal of Applied Physiology 99(1), 252–260.

Ebashi, S., Endo, M., 1968. Calcium ion and muscle contraction. Progress in Biophysics and Molecular Biology 18, 123–166.

Edman, K., 1979. The velocity of unloaded shortening and its relation to sarcomere length and isometric force in vertebrate muscle fibres. Journal of Physiology 291, 143–159.

Fang, Z.-P., Mortimer, J., 1991. A method to effect physiological recruitment order in electrically activated muscle. IEEE Transactions on Biomedical Engineering 38(2), 175–179.

Gordon, A., Huxley, A., Julian, F., 1966. The variation in isometric tension with sarcomere length in vertebrate muscle fibers. Journal of Physiology 184, 170–192.

Günther, M., Schmitt, S., Wank, V., 2007. High-frequency oscillations as a consequence of neglected serial damping in Hill-type muscle models. Biological Cybernetics 97(1), 63–79.

Hancock, W., Martin, D., Huntsman, L., 2004. Ca^{2+} and segment length dependence of isometric force kinetics in intact ferret cardiac muscle. Circulation Research 73(4), 603–611.

Hatze, H., 1977. A myocybernetic control model of skeletal muscle. Biological Cybernetics 25(2), 103–119.

Henneman, E., Somjen, G., Carpenter, D., 1965. Functional significance of cell size in spinal motoneurons. Journal of Neurophysiology 28(3), 560–580.

Herzog, W., Leonard, T., 1997. Depression of cat soleus forces following isokinetic shortening. Journal of Biomechanics 30(9), 865–872.

Herzog, W., Leonard, T., 2000. The history dependence of force production in mammalian skeletal muscle following stretch-shortening and shortening-stretch cycles. Journal of Biomechanics 33, 531–542.

Herzog, W., Leonard, T., Wu, J., 2000. The relationship between force depression following shortening and mechanical work in skeletal muscle. Journal of Biomechanics 33(5), 659–668.

Hill, A., 1938. The heat of shortening and the dynamic constants of muscle. Proceedings of the Royal Society of London 126, 136–195.

Jeffrey, A., 1990. Linear algebra and ordinary differential equations. Blackwell Scientific Publications, England.

Jordan, D., Smith, P., 1999. Nonlinear ordinary differential equations: an introduction to dynamical systems, 3rd Edition. Oxford University Press Inc., New York.

Julian, F., Morgan, D., 1979. The effect on tension of non-uniform distribution of length changes applied to frog muscle fibres. Journal of Physiology 293, 379–392.

Kosterina, N., Westerblad, H., Eriksson, A., 2009. Mechanical work as predictor of force enhancement and force depression. Journal of Biomechanics 42(11), 1628–1634.

Kosterina, N., Westerblad, H., Lännergren, J., Eriksson, A., 2008. Muscular force production after concentric contraction. Journal of Biomechanics 44(11), 2422–2429.

Lee, H., Herzog, W., Leonard, T., 2001. Effects of cyclic changes in muscle length on force production in in situ cat soleus. Journal of Biomechanics 34, 979–987.

Lou, F., Curtin, N., Woledge, R., 1998. Contraction with shortening during stimulation or during relaxation: How do the energetic costs compare? Journal of Muscle Research and Cell Motility 19(7), 797–802.

Luff, A., 1981. Dynamic properties of the inferior rectus, extensor digitorum longus, diaphragm and soleus muscles of the mouse. Journal of Physiology 313, 161–171.

Marechal, G., Plaghki, L., 1979. The deficit of the isometric tetanic tension redeveloped after a release of frog muscle at a constant velocity. Journal of General Physiology 73(4), 453–467.

McGowan, C. P., Neptune, R. R., Herzog, W., 2010. A phenomenological model and validation of shortening-induced force depression during muscle contractions. Journal of Biomechanics 43(3), 449–454.

Meijer, K., Grootenboer, H., Koopman, H., Van Der Linden, B., Huijing, P., 1998. A Hill type model of rat medial gastrocnemius muscle that accounts for shortening history effects. Journal of Biomechanics 31(6), 555–563.

Morgan, D., 2007. Can all residual force enhancement be explained by sarcomere non-uniformities? Journal of Physiology 578(2), 613–615.

Pettersson, R., Nordmark, A., Eriksson, A., 2010. Free-time optimization of targeted movements based on temporal FE approximation. Proceedings CST2010, Valencia.

Ranatunga, K., 1982. Temperature-dependence of shortening velocity and rate of isometric tension development in rat skeletal muscle. Journal of Physiology 329, 465–483.

Rode, C., Siebert, T., Blickhan, R., 2009a. Titin-induced force enhancement and force depression: A 'sticky-spring' mechanism in muscle contractions? Journal of Theoretical Biology 259(2), 350–360.

Rode, C., Siebert, T., Herzog, W., Blickhan, R., 2009b. The effects of parallel and series elastic components on estimated active cat soleus muscle force. Journal of Mechanics in Medicine and Biology 9(1), 105–122.

Savelberg, H., 2000. Rise and relaxation times of twitches and tetani in submaximally recruited, mixed muscle: A computer model. In: Herzog, W. (Ed.), Skeletal muscle mechanics: from mechanisms to function. Wiley, New York, pp. 225–240.

Schachar, R., Herzog, W., Leonard, T., 2004. The effects of muscle stretching and shortening on isometric forces on the descending limb of the force-length relationship. Journal of Biomechanics 37(6), 917–926.

Siebert, T., Rode, C., Herzog, W., Till, O., Blickhan, R., 2008. Nonlinearities make a difference: comparison of two common Hill-type models with real muscle. Biological Cybernetics 98, 133–143.

Stein, R., Gordon, T., Shrive, J., 1982. Temperature dependence of mammalian muscle contractions and atpase activities. Biophysical Journal 40(2), 97–107.

Stephenson, D., Williams, D., 1982. Effects of sarcomere length on the forceâĂŤpca relation in fast- and slow-twitch skinned muscle fibres from the rat. Journal of Physiology 333, 637–653.

Sugi, H., Tsuchiya, T., 1988. Stiffness changes during enhancement and deficit of isometric force by slow length changes in frog skeletal muscle fibres. Journal of Physiology 407, 215–229.

Thompson, J., Stewart, H., 1986. Nonlinear dynamics and chaos, 1st Edition. Wiley, England.

Till, O., Siebert, T., Rode, C., Blickhan, R., 2008. Characterization of isovelocity extension of activated muscle: A hill-type model for eccentric contractions and a method for parameter determination. Journal of Theoretical Biology 255(2), 176–187.

van Soest, A., Bobbert, M., 1993. The contribution of muscle properties in the control of explosive movements. Biological Cybernetics 69(3), 195–204.

Zajac, F., Faden, J., 1985. Relationship among recruitment order, axonal conduction velocity, and muscle-unit properties of type-identified motor units in cat plantaris muscle. Journal of Neurophysiology 53(5), 1303–1322.

Paper 5

5

Force enhancement and force depression in a modified muscle model used for muscle activation prediction

By Natalia Kosterina, Ruoli Wang, Anders Eriksson and Lanie Gutierrez-Farewik

Department of Mechanics
Royal Institute of Technology
SE-100 44 Stockholm, Sweden

Journal of Biomechanics
Submitted 18 April 2012

This article presents a skeletal muscle model force for modification applied to dynamic simulations of musculoskeletal system motion. Force depression and force enhancement induced by active muscle shortening and lengthening, respectively, represent muscle history effects. A muscle model depending on the preceding contractile events together with the current parameters was developed for OpenSim software, and applied in simulations of standing heel-raise and squat movements. Muscle activations were computed using joint kinematics and ground reaction forces recorded from the motion capture of seven individuals. In the muscle-actuated simulations, a modification was applied to the computed activation, and was compared to the measured electromyography data. For the studied movements, the history gives a small but visible effect to the muscular force trace. The muscle model modification improves the existing muscle models and gives more accurate description of underlying forces in musculoskeletal system movement simulation.

Keywords: Muscle model; Force modification; Musculoskeletal system; Heel-raise; Squat; Electromyography

1. Introduction

Musculoskeletal modelling is widely used for motion analysis and movement prediction. The existing muscle models are limited due to complexity of the underlying processes and gaps in knowledge. Based on previous research (Kosterina et al. 2008, 2009, 2011) we have suggested improvements to a common muscle model by adding a history dependence during active length variations. Residual force enhancement (FE) induced by active stretching and force depression (FD) induced by active shortening are complex phenomena, but can be relatively well predicted by a simple formula as these history effects can be described by the mechanical work accumulated or performed during the movements (Kosterina et al. 2008, 2009). History effects have mostly been studied *in vitro*, (Abbott and Aubert 1952; Marechal and Plaghki 1979;

Sugi and Tsuchiya 1988; Herzog and Leonard 1997; Lou et al. 1998; Morgan et al. 2000; Lee and Herzog 2003).

A study on voluntary contractions of large human muscles *in vivo* has shown that the activation reduces along with FE after stretch contractions (Seiberl et al. 2012), which shows that the motor control system can adjust according to the history effect. Activation modification was observed along with the force modification in the intact muscle contraction, (Hahn et al. 2007; Altenburg et al. 2008). Both components of the history effect are essential although the results diverge (Pinniger and Cresswell 2007; Tilp et al. 2009; Seiberl et al. 2012). Finding a balance between force and activation modifications during voluntary contractions will be a development in muscle history description. Regarding the quantitative significance of FD and FE, these phenomena have been suggested to lead to alterations in the neural stimulation and changes in metabolic cost of contractions rather than producing smaller or larger forces (Seiberl et al. 2012).

An accurate muscle model is an essential factor for reliable musculoskeletal system simulation of dynamic tasks. The main characteristics of the muscles during contractions are length and force. These have an important role in the mechanics of muscle behaviour. Ultrasonography and magnetic resonance imaging allow fairly accurate estimations of muscle length (Maganaris 2001), and the musculotendon complex length can be estimated from anatomical and joint kinematic data (Fukunaga et al. 2001). However, measurements of muscle forces *in vivo* are invasive and limited to superficial structures such as Achilles' tendon (Finni et al. 1998) and intact tendons (Schuind et al. 1992). To estimate muscle force, the torque can be measured (Lee et al. 1999; Hahn et al. 2007; Altenburg et al. 2008) and the load sharing problem solved, though the solution will depend on the optimisation design and criteria.

Due to these limitations, a muscle model is generally validated by comparing calculated muscle activation with the recorded electromyography signal (EMG), instead of investigating the muscle force itself. Thelen et al. (2003) proposed an equation describing how muscle force and activation are related:

$$F = \left(A \cdot F_{\mathrm{lv}}(l, \dot{l}) + F_{\mathrm{passive}}(l) \right) \cdot \cos(\alpha), \tag{1}$$

where F is a steady-state muscle force, A the activation, F_{lv} the active force-length-velocity surface, F_{passive} the passive force, α the pennation angle at the steady-state muscle length l for a given muscle, and $\dot{l}$ denotes time derivative of length.

Muscle activation, A, can be calculated for an existing muscle model using experimental data by solving A from F under given l, $\dot{l}$ and muscle architecture. This is the procedure used in e.g. OpenSim (Delp et al. 2007) when necessary muscular forces are decided from motion capture registration. The inverse calculation of activations from kinematics and external forces implicitly assumes Eq. (1) as the relation from A to F, disregarding history, but noting that the F forces are required for dynamic equilibrium.

A correction of the forces based on history effects from the calculated activation according to the muscle force modification formula (Kosterina et al. 2009):

$$F' = F + dF_{\mathrm{mod}}, \tag{2}$$

would, however, not satisfy dynamic equilibrium and lead to incorrect movements with these activations. In order to match registered movements, a modified activation inducing force F can be computed according to:

$$A_{\mathrm{mod}} = \left(\frac{F_{\mathrm{mod}}}{\cos(\alpha)} - F_{\mathrm{passive}}(l) \right) \cdot \frac{1}{F_{\mathrm{lv}}(l, \dot{l})}, \tag{3}$$

where $F_{\mathrm{mod}} = F - dF_{\mathrm{mod}}$ is the force devoid of history component. The chain of calculations is shown in Fig. 1. Our hypothesis is that introducing history effect in a musculoskeletal system improves the inverse dynamic analysis of movements which is based on an activation-to-force description according to Eq. (1), and activation A_{mod} conforms to EMG data better than the OpenSim output A.

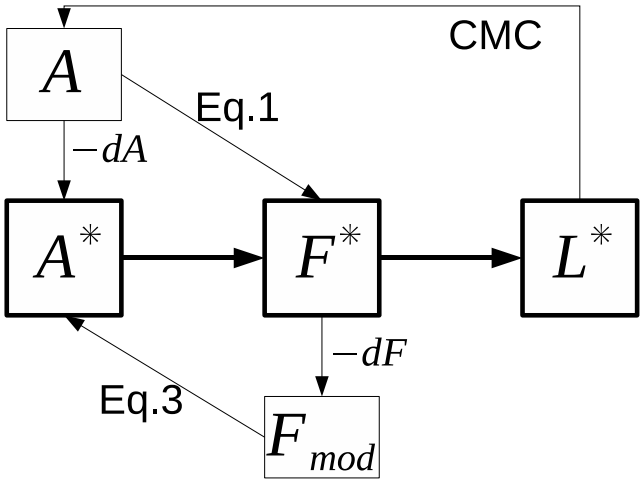

FIGURE 1. Schematic diagram of muscle parameters interaction. Initiated in the brain, the activation signals A^* pass through motor neurons to the muscle and cause a series of chemical reactions which in turn generate muscle contractile forces F^* leading to body movement represented by L^*. When modelling musculo-skeletal system motion, muscle excitations A are inversely calculated, e.g. using CMC, to satisfy an equilibrium for forces F^* and kinematics L^*. Equation (1) connecting A and F^* does not include muscle history. To improve the model and approach the real values A^*, modifications dA can be calculated by extracting force modification $F^* - dF$ and applying Eq. (3).

The present article introduces a method to refine musculoskeletal system modelling by implementing the force history effect in a muscle model in the open-source

software OpenSim which allows dynamic simulations of movement of musculoskeletal structures. A series of experiments on human movement was conducted to test the effects of this modified muscle model.

The work is based on the validity of necessary approximation in Eq. (3), disregarding the fact that also the modification should be A-scaled.

2. Methods

Seven healthy adults, 6 females and 1 male (age 29 ± 3 years, weight 56.1 ± 6.9 kg, height 1.63 ± 0.04 m) participated in this study. The subjects participated with informed consent; they were physically active, but none of them participated in any competitive exercise training. The protocol of this study was approved by the local Ethics Committee.

2.1. *Experimental setup*

A maximum voluntary isometric contraction (MVIC) test was performed for EMG scaling. The subjects sat upright in an isometric dynamometer chair, the hip, knee and ankle were fixed at 90, 60 and 90 deg (neutral), respectively (Örtqvist et al. 2007). The calf and the foot were tightly fastened to restrict joint motion. The isometric condition was defined as a fixed-end contraction where the muscle-tendon complex was held at constant length. Surface EMG signals (Motion Laboratory System, Baton Rouge, LA) were recorded for the subjects for the rectus femoris (RecFem), tibialis anterior (TibAnt), medial head of the gastrocnemius muscle (MedGas) and soleus (Sol) bilaterally according to the SENIAM protocol (www.seniam.org).

A series of tasks was chosen to place a high load on the five mentioned muscles. The participants performed a dynamic task after the MVIC test: 3 cycles of standing heel-raise (rise up and down on toes) with a 3 second delay in the upper position, and 3 cycles of squats. The subjects were examined using an 8–camera motion capture system (Vicon MX40, Oxford, UK) and two force-plates (Kister, Winterthur, Switzerland). Sixty-four reflective markers (9mm) were placed bilaterally on bony landmarks based on a conventional full-body marker set (Vicon Plug-in-Gait), plus a multi-segment foot model marker set (Stebbins et al. 2006).

One subject performed an additional analysis of squats both slow and quick, and both with and without an additional load of 40 kg, held at the shoulders.

2.2. *Data processing*

During experiments, EMG was sampled at 1000Hz. Data were filtered using a bidirectional second order Butterworth filter with a cutoff frequency of 3Hz in Matlab (version R2011a, The MathWorks, Natick, USA). EMG for each muscle was normalized from zero to one based on the minimum and maximum values for that muscle during the MVIC and the performed movements.

2.3. *Musculoskeletal model*

A generic musculoskeletal model with 14 segments, 23 degrees-of-freedom and 96 musculotendon actuators was used to generate the simulation in OpenSim 2.4 (Delp

et al. 2007). The head, arms, and torso were modeled as a single rigid body which articulated with the pelvis via a ball-and-socket back joint. Each hip was modeled as a ball-and-socket joint, each knee as a hinge joint, each ankle, subtalar and metatarsophalangeal joint as a revolute joint (Delp et al. 1990; Anderson and Pandy 1999).

A subject-specific simulation of heel-raise and squat was generated. The model was scaled to each subject based on the experimental marker set placed on anatomical landmarks. The inverse kinematics algorithms solved for joint kinematics that minimised the differences between experimental marker and virtual markers positions. Dynamic inconsistency between the measured ground reaction forces and the kinematics was resolved by applying small external forces and torques (i.e. residuals) to the torso and making small adjustments to the model mass properties and kinematics (Delp et al. 2007). Constraints on muscle excitation were pre-defined based on the EMG records, primarily for maintaining the load-sharing between synergetic muscles. The range of the excitation was outlined as filtered normalized EMG signal $\pm 10\%$ of its maximum value. Computed muscle control (CMC) (Thelen et al. 2003) with the pre-defined constraints on muscle excitation was used to find a set of actuator excitations, A, implicitly using the $A-F$ relation of Eq. (1). The constraints are required to track the kinematics and to be generally consistent with experimental EMG patterns. Static optimization was used in CMC to determine the muscle forces and to minimize a cost function at every timestep t for the set of N muscles:

$$J(t) = \sum_{i=1}^{N} V_{\mathrm{i}} \left[A_{\mathrm{i}}\left(t\right)\right]^2,$$

where V_{i} is the volume of muscle i and $A_{\mathrm{i}}(t)$ is the activation of muscle i (Happee 1994; Thelen and Anderson 2006).

2.4. *Muscle model modification*

The muscle force modification in Eq. (2) during and after non-isometric contractions is expressed with a simple formula:

$$dF_{\mathrm{mod}} = K_{\mathrm{hist}} \cdot W \cdot A, \tag{4}$$

where K_{hist} is the history coefficient, and W is the mechanical work performed by and on the muscle during the dynamic movement (described by the sign of W). The force modification described by Kosterina et al. (2009) was studied for fully active muscle. We scaled the force modification to muscle excitation A in order to eliminate the history effect when the muscle is destimulated (Julian and Morgan 1979; Morgan et al. 2000). The modified activation was calculated according to Eq. (3) and appeared as:

$$A_{\mathrm{mod}} = A - dA_{\mathrm{mod}} = A - \frac{dF_{\mathrm{mod}}}{\cos(\alpha) \cdot F_{\mathrm{lv}}}, \tag{5}$$

Due to lack of information about the history coefficient for human muscles, and considering $K_{\mathrm{hist}} = -3\mathrm{m}^{-1}$ and $-4\mathrm{m}^{-1}$ for mouse extensor digitorum longus and soleus, respectively, we employed the value $K_{\mathrm{hist}} = -10\mathrm{m}^{-1}$ in order to test the benefit of implementing the muscle force modification. The mechanical work was

evaluated by a numerical integration over the event of the force multiplied by shortening velocity:

$$W = \sum F \cdot \dot{l} \cdot \Delta t, \tag{6}$$

where F and $\dot{l}$ are quantities in the time series of intervals Δt.

The new functionality was added to the general OpenSim software using an application programming interface (API). A plug-in was written in C++ using dynamically linked libraries to calculate F_{mod} and A_{mod} using built-in classes and objects. The plug-in was then used in the graphical user interface for simulated dynamical motions.

2.5. *Data analysis*

To test the accuracy of the muscle model modification we compared simulated quantities to experimental data. EMG data was compared to both muscle activation (A) and modified activation (A_{mod}). The differences between the datasets (EMG - A and EMG - A_{mod}) were calculated. The square root of the mean squared values was extracted (RMSE). The RMSE quantity was calculated for every attempt, then mean and standard deviations for the groups of individual attempts were computed for both squat and heel-raise movements.

3. Results

Heel-raise and squat data were analysed. Due to technical problems, squat data for two of the tested subjects could not be analysed, so the results are based on n=7 subjects for heel-raise and n=5 subjects for squat. Two pairs of muscles with the highest normalized forces during the specified movements were chosen. These muscles during a heel-raise were MedGas and Sol, and during squat TibAnt and RecFem.

The muscle excitations during a heel-raise and a squat are plotted along with the EMG signal in Figures 2(a), 4(a). The error measures RMSE between EMG and A, EMG and A_{mod} are presented in Figures 2(b), 4(b). The modified activation A_{mod} was closer to the EMG signal than the OpenSim output A for MedGas, Sol and TibAnt muscles but not for RecFem.

The muscle force F (calculated with A and Eq. (1)) was plotted along with the modified muscle force $F' = F + dF_{\mathrm{mod}}$, Figure 3. The force modification appeared negative or positive depending on the preceding muscle length variation. Quantitatively, modulus of the modification is up to 15% of the force value.

Different conditions of squat performance were compared in a pilot-study. A subject was asked to squat slowly and quickly, then do the same with two 20 kg loads held at the shoulders. Force traces for RecFem muscles are presented on Figure 5. EMG signal, activation and force modification appeared larger for quick and loaded squats than for slow and unloaded, correspondingly. The results from the additional motion analysis illustrate that force modification is practically non-existent in slow motion with low loads, but present when motion is both loaded and fast.

The plug-in used for additional analysis, i.e. for calculating of modified muscle activation and force, takes approximately 10% of time used by CMC analysis.

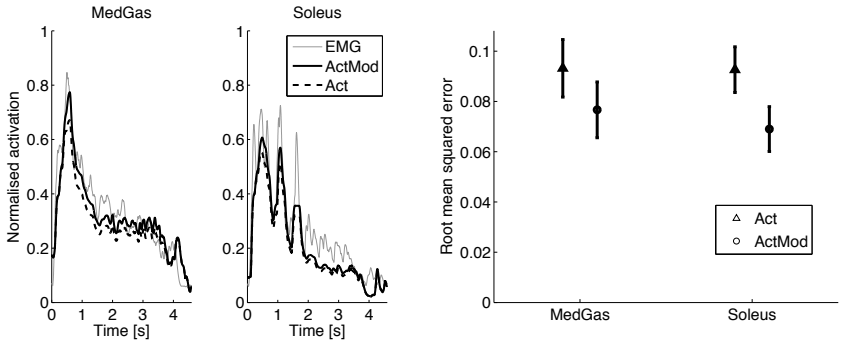

FIGURE 2. Simulation of muscle excitation compared to EMG signal during one heel-raise cycle with ≈ 3 seconds delay in the upper position. The results are given for MedGas and Sol muscles. (a) Example of normalised EMG signal - *thin grey line*, muscle activation - *dashed black line*, modified muscle activation - *solid thick black line*. (b) Root mean squared residuals between muscle activation and EMG signal (*triangles*) and modified muscle activation and EMG signal (*circles*), mean$\pm$std, n=7.

4. Discussion

The main consequence of this study is the improvement of a skeletal muscle model by adding the history effect to the muscle activation using the possibility to add new functionality to the open-source software OpenSim. The modified activation was closer to experimentally observed activation in 3 out of 4 studied muscles.

The major function of the muscle is to transform an electrical signal into length variation through contractile force generation, Figure 1(a). CMC (Thelen and Anderson 2006) allows to compute activation which results in force F, which in turn can be modified by adding a history component dF_{mod}, Eq. (4). However, force $F + dF_{\mathrm{mod}}$ would lead to a new movement, so activation modification was introduced instead. Muscle memory has mainly been investigated in electrically stimulated muscles *in vitro*, therefore modification of activation have not been described in detail. Recent studies of voluntary contractions of human muscles (Altenburg et al. 2008; Seiberl et al. 2012) have shown presence of activation modification along with the force modification. Considering muscle history phenomena, the brain adjusts the signal according to a desired motion. Thus muscle activation decreases to lower metabolic cost after lengthening and increases to compensate for a reduced force after shortening.

In our study, CMC analysis was used to evaluate the set of muscular forces necessary for reproducing recorded movements, therefore we assume $F \approx F^*$ and only consider activation modification $-dA_{\mathrm{mod}}$, Eq. (5), Figure 1. In fact, both modifications of activation and force must be included and future studies should be aimed at defining a correlation between dA and dF. These could be represented in a new

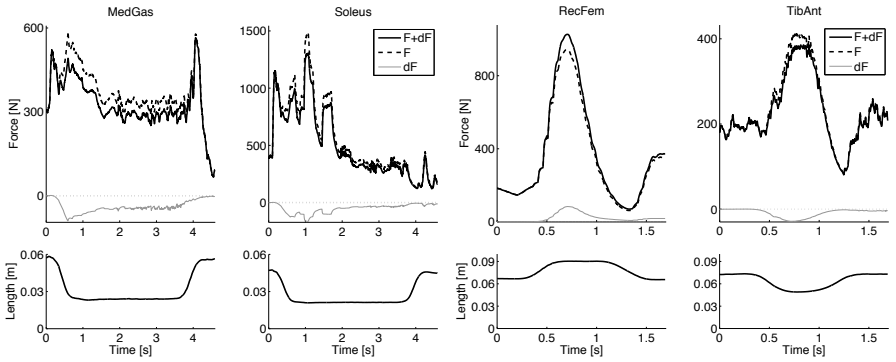

(a) (b)

FIGURE 3. Simulation of muscle force (*dashed black line*) and modified muscle force (*solid black line*) are plotted above, traces of normalized muscle length plotted below. (a) Example of heel-raise cycle with $\approx$ 3 seconds delay in the upper position, the results are given for MedGas and Sol muscles. (b) Example of squat, the results are given for RecFem and TibAnt muscles. The force modification (*grey line*) is negative during shortening-stretch cycles (MedGas, Sol, TibAnt) and positive during stretch-shortening cycle (RecFem).

formula giving a more accurate description for skeletal muscle model:

$$F + (1 - c) \cdot dF_{\mathrm{mod}} = \Big((A - c \cdot dA_{\mathrm{mod}}) \cdot F_{\mathrm{lv}}(l, \dot{l}) + F_{\mathrm{passive}}(l) \Big) \cdot \cos(\alpha), \quad (7)$$

where $c \in [0, 1]$ defines a balance between dF_{mod}, Eq. (4), and dA_{mod}, Eq. (5), induced by active muscle length variations and motor control. In the current study we assumed that $c = 1$, i.e. the brain has full control of the force generation and adjusts the activation level so that the force is not influenced by the length variations. An example of $c = 0$ is when the central nervous system does not consider the history effect, for instance when *in vitro* stimulation at a constant activation is performed. Refering to study by Seiberl et al. (2012) wherein both activation and force were modified after active stretch, we speculate that coefficient c might possess any value between 0 and 1 depending on the extent to which the brain predicts and responds to the active muscle length variation leading to the history effect.

For computing the force modification, there is one constant needed, K_{hist}, Eq. (4). In our previous study, we derived a value of the history coefficient for tested mouse muscles, but there are no data for human muscles. The amount of FD and FE in most published studies has been associated with the shortening magnitude, (Abbott and Aubert 1952; Herzog and Leonard 1997; Lou et al. 1998; Schachar et al. 2004; Bullimore et al. 2007) or speed of shortening (Marechal and Plaghki 1979; Sugi and Tsuchiya 1988; Herzog and Leonard 1997; Morgan et al. 2000; Lee and Herzog 2003). However, a strong association between FD/FE and the mechanical work performed by

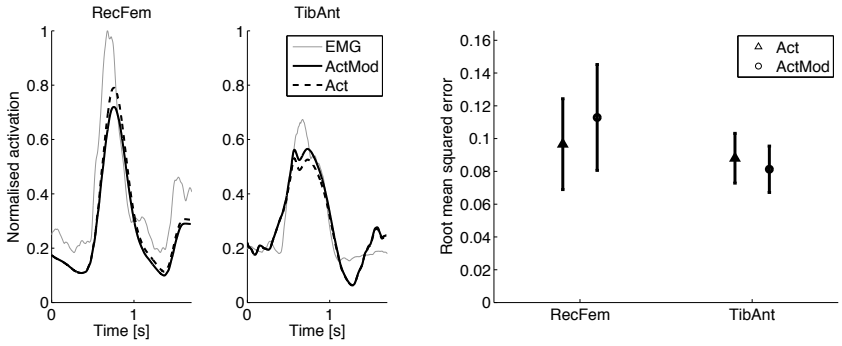

FIGURE 4. Simulation of muscle excitation compared to EMG signal during one squat. The results are given for TibAnt and RecFem muscles. (a) Example of EMG signal - *thin grey line*, muscle activation - *dashed black line*, modified muscle activation - *solid thick black line*. (b) Root mean squared residuals between muscle activation and EMG signal (*triangles*) and modified muscle activation and EMG signal (*circles*), mean$\pm$std, n=5.

and on the muscle has been identified (Josephson and Stokes 1999; Herzog et al. 2000; Kosterina et al. 2008, 2009). Assuming that force modification is linearly related with $W \cdot A$, we tested different values of the scaling coefficient and decided upon $K_{\mathrm{hist}} = -10\mathrm{m}^{-1}$. The decision is based on the amount of force modification which lies in a range between -30 and 20% of maximum isometric force, MVIC (Ruiter et al. 1998; Lee and Herzog 2003), and the tested movements do not actually demand a substantial effort. A more correct value for K_{hist} in human muscle demands further work and may differ for different muscles. This parameter can be obtained from *in vitro* experiments, and most likely will be a muscle-specific characteristic but not necessarily person-specific (Kosterina et al. 2008, 2009).

The modified excitation A_{mod} matches measured EMG signal better than A for Sol and MedGas during a heel-raise (Figure 2) and TibAnt during a squat, but not for RecFem (Figure 4). The inconstancy of the error tendencies (Figures 2(b), 4(b)) is probably due to the optimization procedure in OpenSim. A closer look at the muscle activation A in Figures 2(a), 4(a) shows that its peak is always below the EMG peak. For this reason, A_{mod} after stretch is inferior to A. Stronger control constraints for muscle excitations based on EMG signal might invalidate this remark but the intention was to give more freedom for the activation and see the trend of the modification. It is also noted that the optimization of load-sharing in OpenSim presently does not consider the history effect, which is not a negligible source of error.

The muscle force was plotted with probable modified forces, the results show that dF_{mod} increases force for RecFem but decreases for MedGas, Sol and TibAnt, Figure 3. The diversity is explained by muscle length variations during the movement. In the studied motions Sol, MedGas and TibAnt muscles perform shortening-stretch

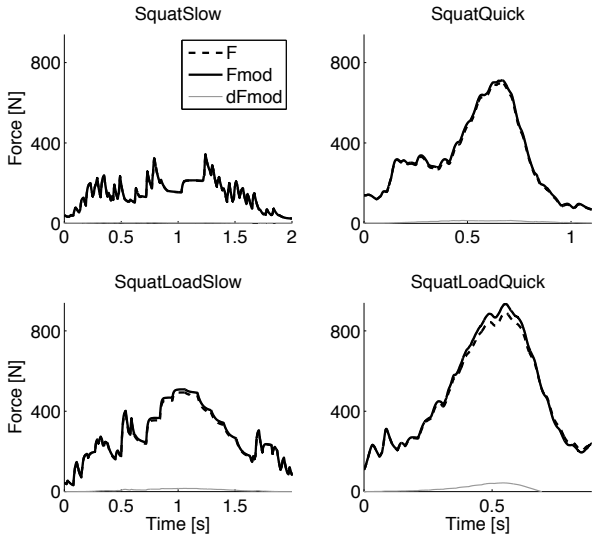

FIGURE 5. Simulation of RecFem muscle force during one squat cycle. Muscle force F - *dashed black line*, modified muscle force F_{mod} - *solid black line*, force modification dF_{mod} - *grey line*.

cycles, while RecFem muscle does the opposite: it first stretches and then shortens. Force modification reflects this variation: muscle shortening induces FD, and muscle lengthening induces FE; $dF_{\mathrm{mod}} \geq 0$ during stretch-shortening and $dF_{\mathrm{mod}} \leq 0$ during shortening-stretch contraction. The modification tends to change the force in the expected direction, but the technique does not allow us to measure muscle forces and validate the improvement. Moreover, Eq. (7) should be used in inverse dynamics and CMC analysis in OpenSim.

The force modification introduced in musculoskeletal modelling may be most relevant in sport and impact biomechanics since the effect of muscle history increases with speed of motion and load. While the magnitude of force modification was somewhat low in the tested motions, the additional analysis was included to illustrate that force modification may be negligible in slow, unloaded movements, but non-negligible in fast motions with high loads. This may have important implications in, for instance, sports or collision simulations.

5. Conclusions

Skeletal muscle model modification representing muscle force depression induced by active shortening and force enhancement induced by active lengthening was introduced in simulations of musculoskeletal system motion by a simple formula. Though current techniques do not enable us to validate the result fully, the supplement improved description of skeletal muscle force and showed the importance of the modification in demanding tasks.

Conflict of interest statement

No authors had any proprietary, financial, professional or other personal conflicts of interest that may have influenced this study.

Acknowledgements

The authors gratefully acknowledge financial support from the Swedish Research Council.

References

Abbott, B., Aubert, X., 1952. The force exerted by active striated muscle during and after change of length. Journal of Physiology 117, 77–86.

Altenburg, T., Ruiter, C. D., Verdijk, P., Mechelen, W. V., Haan, A. D., 2008. Vastus lateralis surface and single motor unit emg following submaximal shortening and lengthening contractions. Applied Physiology, Nutrition, and Metabolism 33(6), 1086–1095.

Anderson, F., Pandy, M., 1999. A dynamic optimization solution for vertical jumping in three dimensions. Computer Methods in Biomechanics and Biomedical Engineering 2(3), 201–231.

Bullimore, S., Leonard, T., Rassier, D., Herzog, W., 2007. History-dependence of isometric muscle force: Effect of prior stretch or shortening amplitude. Journal of Biomechanics 40, 1518–1524.

Delp, S., Anderson, F., Arnold, A., Loan, P., Habib, A., John, C., Thelen, E. G. D., 2007. Opensim: open-source software to create and analyze dynamic simulations of movement. IEEE Transactions on Biomedical Engineering 54(11), 1940–1950.

Delp, S., Loan, J., Hoy, M., Zajac, F., Topp, E., Rosen, J., 1990. An interactive graphics-based model of the lower extremity to study orthopaedic surgical procedures. IEEE Transactions on Biomedical Engineering 37(8), 757–767.

Finni, T., Komi, P. V., Lukkariniemi, J., 1998. Achilles tendon loading during walking: application of a novel optic fiber technique. European Journal of Applied Physiology and Occupational Physiology 77(3), 289–291.

Fukunaga, T., Kubo, K., Kawakami, Y., Fukashiro, S., Kanehisa, H., Maganaris, C., 2001. In vivo behaviour of human muscle tendon during walking. Proceedings of the Royal Society of London 268, 229–233.

Hahn, D., Seiberl, W., Schwirtz, A., 2007. Force enhancement during and following muscle stretch of maximal voluntarily activated human quadriceps femoris. European Journal of Applied Physiology 100(6), 701–709.

Happee, R., 1994. Inverse dynamic optimization including muscular dynamics, a new simulation method applied to goal directed movements. Journal of Biomechanics 27(7), 953–960.

Herzog, W., Leonard, T., 1997. Depression of cat soleus forces following isokinetic shortening. Journal of Biomechanics 30(9), 865–872.

Herzog, W., Leonard, T., Wu, J., 2000. The relationship between force depression following shortening and mechanical work in skeletal muscle. Journal of Biomechanics 33(5), 659–668.

Josephson, R., Stokes, D., 1999. Work-dependent deactivation of a crustacean muscle. Journal of Experimental Biology 202(18), 2551–2565.

Julian, F., Morgan, D., 1979. The effect on tension of non-uniform distribution of length changes applied to frog muscle fibres. Journal of Physiology 293, 379–392.

Kosterina, N., Westerblad, H., Eriksson, A., 2009. Mechanical work as predictor of force enhancement and force depression. Journal of Biomechanics 42(11), 1628–1634.

Kosterina, N., Westerblad, H., Eriksson, A., 2011. History effect and timing of force production introduced in a skeletal muscle model. Biomechanics and Modeling in Mechanobiology.DOI: 10.1007/s10237-011-0364-5.

Kosterina, N., Westerblad, H., Lännergren, J., Eriksson, A., 2008. Muscular force production after concentric contraction. Journal of Biomechanics 41(11), 2422–2429.

Lee, H., Herzog, W., 2003. Force depression following muscle shortening of voluntarily activated and electrically stimulated human adductor pollicis. Journal of Physiology 551, 993–1003.

Lee, H.-D., Suter, E., Herzog, W., 1999. Force depression in human quadriceps femoris following voluntary shortening contractions. Journal of Applied Physiology 87(5), 1651–1655.

Lou, F., Curtin, N., Woledge, R., 1998. Contraction with shortening during stimulation or during relaxation: How do the energetic costs compare? Journal of Muscle Research and Cell Motility 19(7), 797–802.

Maganaris, C., 2001. Force–length characteristics of in vivo human skeletal muscle. Acta Physiologica Scandinavica 172(4), 279–285.

Marechal, G., Plaghki, L., 1979. The deficit of the isometric tetanic tension redeveloped after a release of frog muscle at a constant velocity. Journal of General Physiology 73(4), 453–467.

Morgan, D., Whitehead, N., Wise, A., Gregory, J., Proske, U., 2000. Tension changes in the cat soleus muscle following slow stretch or shortening of the contracting muscle. Journal of Physiology 522(3), 503–513.

Örtqvist, M., Gutierrez-Farewik, E., Farewik, M., Jansson, A., Bartonek, Å., Broström, E., 2007. Reliability of a new instrument for measuring plantarflexor muscle strength. Archives of Physical Medicine and Rehabilitation 88(9), 1164–1170.

Pinniger, G., Cresswell, A., 2007. Residual force enhancement after lengthening is present during submaximal plantar flexion and dorsiflexion actions in humans. Journal of Applied Physiology 102(1), 18–25.

Ruiter, C. D., Haan, A. D., Jones, D., Sargeant, A., 1998. Shortening-induced force depression in human adductor pollicis muscle. The Journal of Physiology 507(2), 583–591.

Schachar, R., Herzog, W., Leonard, T., 2004. The effects of muscle stretching and shortening on isometric forces on the descending limb of the force-length relationship. Journal of Biomechanics 37(6), 917–926.

Schuind, F., Garcia-Elias, M., Cooney, W., An, K.-N., 1992. Flexor tendon forces: In vivo measurements. The Journal of Hand Surgery 17(2), 291–298.

Seiberl, W., Hahn, D., Herzog, W., Schwirtz, A., 2012. Feedback controlled force enhancement and activation reduction of voluntarily activated quadriceps femoris during sub-maximal muscle action. Journal of Electromyography and Kinesiology 22, 117–123.

Stebbins, J., Harrington, M., Thompson, N., Zavatsky, A., Theologis, T., 2006. Repeatability of a model for measuring multi-segment foot kinematics in children. Gait Posture 23(4), 401–410.

Sugi, H., Tsuchiya, T., 1988. Stiffness changes during enhancement and deficit of isometric force by slow length changes in frog skeletal muscle fibres. Journal of Physiology 407, 215–229.

Thelen, D., Anderson, F., 2006. Using computed muscle control to generate forward dynamic simulations of human walking from experimental data. Journal of Biomechanics 39, 1107–1115.

Thelen, D., Anderson, F., Delp, S., 2003. Generating dynamic simulations of movement using computed muscle control. Journal of Biomechanics 36, 321–328.

Tilp, M., Steib, S., Herzog, W., 2009. Force-time history effects in voluntary contractions of human tibialis anterior. European Journal of Applied Physiology 106(2), 159–66.